Theses and Dissertations--Pharmacology and Nutritional Sciences

Pharmacology and Nutritional Sciences

2018

THE PREBIOTIC INULIN BENEFICIALLY MODULATES THE GUT-BRAIN AXIS BY ENHANCING METABOLISM IN AN APOE4 MOUSE MODEL

Jared D. Hoffman
University of Kentucky, jdho253@g.uky.edu
Author ORCID Identifier:
https://orcid.org/0000-0002-9424-3526
Digital Object Identifier: https://doi.org/10.13023/etd.2018.405

THE PREBIOTIC INULIN BENEFICIALLY MODULATES THE
GUT-BRAIN AXIS BY ENHANCING METABOLISM IN AN APOE4
MOUSE MODEL

_____

DISSERTATION
_____

A dissertation submitted in partial fulfillment of the
requirements for the degree of Doctor of Philosophy in the
College of Medicine at the University of Kentucky

By
Jared David Hoffman

Lexington, Kentucky

Director: Dr. Ai-Ling Lin, Professor of Nutritional Sciences
Co-Director: Dr. Ming Gong, Professor of Nutritional
Sciences

Lexington, Kentucky

2018

ABSTRACT OF DISSERTATION

THE PREBIOTIC INULIN BENEFICIALLY MODULATES THE GUT-BRAIN AXIS
BY ENHANCING METABOLISM IN AN APOE4 MOUSE MODEL

Alzheimer's disease (AD) is the most common form of dementia and a growing disease burden that has seen pharmacological interventions primarily fail. Instead, it has been suggested that preventative measures such as a healthy diet may be the best way in preventing AD. Prebiotics are one such potential measure and are fermented into metabolites by the gut microbiota and acting as gut-brain axis components, beneficially impact the brain. However, the impact of prebiotics in AD prevention is unknown. Here we show that the prebiotic inulin increased multiple gut-brain axis components such as scyllo-inositol and short chain fatty acids in the gut, periphery, and in the case of scyllo-inositol, the brain. We found in E3FAD and E4FAD mice fed either a prebiotic or control diet for 4-months, that the consumption of the prebiotic inulin can beneficially alter the gut microbiota, modulate metabolic function, and dramatically increase scyllo-inositol in the brain. This suggests that the consumption of prebiotics can beneficially impact the brain by enhancing metabolism, helping to decrease AD risk factors.

KEYWORDS: Alzheimer's Disease, APOE4, Gut Microbiota, Gut-Brain Axis, Prebiotic Inulin, Amyloid β

<div style="text-align: right">

Jared David Hoffman

October 23, 2018

</div>
Date

THE PREBIOTIC INULIN BENEFICIALLY MODULATES THE GUT-BRAIN
AXIS BY ENHANCING METABOLISM IN AN APOE4 MOUSE MODEL

By

Jared David Hoffman

<div style="text-align:right">

Dr. Ai-Ling Lin
Co-Director of Dissertation

Dr. Ming Gong
Co-Director of Dissertation

Dr. Howard Glauert
Director of Graduate Studies

October 9th, 2018
Date

</div>

ACKNOWLEDGMENTS

thank God for all the opportunities and blessings I have been given. "I can do all things through Christ who strengthens me." Phillipians 4:13.

Lastly, I would like to thank and acknowledge my funding sources during my time here: Graduate School Academic Year Fellowship, Kentucky Opportunity Fellowship Award, and the NIH T32 Fellowship. Without this funding, I would have been unable to do the amazing research that I was able to.

TABLE OF CONTENTS

LIST OF FIGURES

LIST OF TABLES

Chapter 1   Background

1.1   Dissertation Overview

Alzheimer's disease (AD) is the most common form of dementia with age being the greatest risk factor but with certain genetic differences also dramatically increasing one's risk of developing this disease. These include having the Apolipoprotein 4 (APOE4) allele and Familial Alzheimer's Disease (FAD) gene mutations. Recently, the gut-brain axis, or bi-directional communication between gut microbiota and brain, has become a topic of intense investigation. Indeed, the gut microbiome, or the trillions of bacteria in the gut, can be modulated to improve one's health, including that of brain health. One way to modulate the gut microbiome is by the ingestion of prebiotics, the non-digestible carbohydrates in certain foods that promote the growth of beneficial bacteria. One such prebiotic is inulin, a prominently studied prebiotic found in chicory root and other vegetables. We will test the hypothesis that modulating the gut microbiome with the prebiotic inulin will potentially prevent AD-like symptoms.

1.2   Alzheimer's Disease: Overview

AD is a chronic neurological disorder originating in the hippocampus and frontal and temporal lobes and characterized by a progressive decline in one's mental capabilities and cognition [1]. AD is the most common form of dementia with advanced age being the greatest risk factor [2]. As such, AD has become a growing health concern for society as the prevalence of this disease has concurred with the increasing age of the baby boomer population. Indeed, it is

anticipated that the population greater than 65 years of age will double between the years 2010 to 2050, according to the U.S. Census Bureau [3]. This is quite worrisome as the incidence of AD increases exponentially after the age of 65, and increases even more after the age of 90 [4]. With pharmacological interventions primarily failing, new preventive measures need to be utilized to prevent and delay the onset of this disease in those susceptible to AD [5]. Indeed, a recent study has indicated that preventative measures such as exercising, eating a healthful diet, and cognitive training may be an effective way to prevent AD [6].

AD has two primary hallmarks. These are the formation of amyloid β (Aβ) plaques and neurofibrillary tangles (NFTs), or hyper phosphorylated tau. Usually, Aβ deposition precedes the formation of NFTs with accumulation beginning in the isocortical areas of the brain followed by the limbic and allocortical structures and lastly, progressing to the subcortical structures and cerebellar cortex [7]. Further, Aβ is a 36-43 amino acid peptide cleaved from amyloid precursor protein (APP) by the successive cleavage of β- and γ-secretases [7]. These form intermediate soluble oligomers and insoluble β-sheet pleated amyloid fibrils that are the primary components of extracellular Aβ plaques. These plaques may be diffuse, amorphous wisps of amyloid without a central core not associated with AD, or dense-core plaques, composed of a dense Thioflavin-S-(ThioS-) positive core and are associated with the progression of AD. Dystrophic neuritis and activated microglial cells and astrocytes also usually surround dense-core

plaques and are most pronounced in the cerebral cortex and hippocampus of the brain [7].

The second hallmark, tau, is an intracellular microtubule protein that supports axonal transport via stabilization of microtubules. However, in AD, tau is hyper phosphorylated and aggregates, forming NFTs. NFTs originate in the medial temporal lobes and hippocampus with eventual spread to the neocortex [7]. They have a spatiotemporal progression that is associated with the severity of cognitive decline. Though generally thought of as the intracellular hallmark, these tangles can become extracellular when neurons die. Aside from these two primary AD hallmarks, other notable characteristics of AD include neuronal and synapse loss and cognitive decline, ultimately leading to dementia [7].

The single greatest risk factor for AD is increased age [8]. However, other risk factors include high blood pressure, hypercholesterolemia, Type-2 diabetes (T2D), and the female gender. After the age of 75, females exhibit a 2-fold greater risk of AD compared to men, perhaps due to lack of estrogen [8]. However, the greatest genetic risk factor that increases one's risk of developing AD is the apolipoprotein E4 (APOE4) allele, while other genetic risk factors include the Familial Alzheimer's Disease (FAD) genetic mutations [8].

1.2.1 Genetic Risk Factors

Genetic risk factors for AD include the FAD mutations. These are mutations in the APP, presenilin 1 (PSEN1), and/or presenilin 2 (PSEN2) genes that lead to early onset Familial Alzheimer's Disease [9]. These mutations cause

increased cleavage by γ-secretase and formation of the 42 amino acid Aβ isoform, which aggregates more readily than the 40 amino acid form. As a clinical diagnostic marker, the 42/40 amino acid ratio of Aβ can predict the age of onset of AD [10].

The greatest genetic risk factor towards AD is the APOE4 allele. APOE is a class of proteins essential for the transport and catabolism of triglyceride-rich lipoprotein among certain cells and tissues. In fact, APOE is primarily synthesized and secreted in the liver but is also produced in the brain, adrenal glands, testis, and skin. It has a strong affinity for lipids and phospholipids and may become lipidated through interactions with the cell surface or secretory vesicles [11]. APOE has three isoforms in humans: APOE2, protective against AD, APOE3, neutral towards AD, and APOE4, increases one's risk of developing AD. Notably, the allele frequencies vary considerably in the human population. APOE3 is the most common at 77%, followed by APOE4 at 15%, and APOE2 at 8% of the population. Intriguingly, APOE2 and APOE4 only vary from APOE3 by a single amino acid substitution in this 299-amino acid protein. Indeed, APOE2 contains a cysteine at 112 and 158, APOE3 contains a cysteine at 112 and an arginine at 118, and APOE4 contains arginine at both 112 and 158 [12]. However, this substitution has a profound effect on the individual towards the development of AD, cerebral amyloid angiopathy, amyloid deposition in blood vessels, and recovery from cerebral trauma [11].

1.2.2 APOE4 Risk Factors

Despite APOE4 and APOE3 only being different by a single amino acid, APOE4 can increase one's risk of developing AD dependently and independently of Aβ. Dependently of Aβ, APOE4 may increase AD risk because of the differences in the affinity for Aβ due its lipid-binding domain [13]. This lipid-binding domain is located on the C-terminus of APOE, whereas the N-terminus houses the amino acid differences between APOE3 and APOE4. This suggests the C- and N-terminus regions interact affecting what APOE3 and APOE4 preferentially bind, including the isoform differences displayed when binding to the Aβ peptide. Indeed, APOE4 binds more rapidly to Aβ and even appears to enhance zinc- and copper-induced Aβ aggregation compared to APOE3 [14]. However, this binding of APOE4 to Aβ may depend upon its lipidation state including whether or not it is purified, lipid-poor, reconstituted with HDL lipids, or originated from astrocytes, cerebral spinal fluid (CSF), or serum. In general, it is also thought that APOE4 is less lipidated than APOE3 with an increased chance of being in an intermediate molten globule state, an unstable form [15]. This would provide less surface area for Aβ to interact with. Further confirming this in one study using mice, soluble APOE4/Aβ complex levels were decreased and had less stability compared to APOE3. It was also discovered that oligomerized Aβ was increased in APOE4 mice compared to APOE3 mice [16]. However, the APOE4 may not only complex with Aβ more effectively than APOE3, as previously mentioned, but also appears to decrease Aβ clearance from the brain, leading to increased plaque formation [11]. Overall, it appears the APOE4/Aβ

complex is less lipidated and stable than that of APOE3 *in vitro,* potentially

increasing oligomerized Aβ levels but decreasing Aβ clearance and thus,

increasing the risk of AD.

Aβ-independent mechanisms by which APOE4 increases one's risk of AD

include inducing synaptic and cholinergic deficits, behavior dysfunction, and

impairment of GABAergic interneurons. However, the primary cause of APOE4

related AD deficits might be via fragmentation from proteolytic cleavage that may

originally be prompted by brain stressors or injury [11]. Indeed, APOE4 is more

susceptible to proteolytic cleavage than APOE3 [17]. These carboxyl-terminal-

truncated fragments enter the cell, wreaking havoc on organelles including that

of tau and other cytoskeletal components. They have even been demonstrated

in vitro to increase the formation of neurofibrillary tangles and appear to lead to

mitochondrial dysfunction. Our lab has previously demonstrated in APOE4

mouse models that cerebral glucose metabolism is decreased [18] and these

truncated fragments may be one potential cause of this in APOE4 allele carrier.

Another notable experiment in human studies found that APOE4 allele carriers

had decreased cerebral blood flow (CBF) before AD-like symptoms occurred

[19]. One reason this may potentially occur was explained in a study

demonstrating that APOE4 leads to increased blood brain barrier (BBB)

permeability via activation of the Cyclophilin A (CypA)-Nuclear Factor-κ-B

(NFκB)-Metalloproteinase 9 (MMP-9) pathway in pericytes in the BBB [20]. The

APOE4 allele promotes this inflammatory pathway by inhibiting low-density

lipoprotein receptor-related protein 1 (LRP1) function, which maintains CypA

levels. In contrast, APOE3 normally stimulates LRP-1 activity. Thus, APOE4

increases the pathway in which MMP-9 leads to tight junction barrier degradation

via decreased protein expression of ZO-1, occludin, and claudin, basement

membrane degradation, increased BBB permeability, and decreased CBF [20].

Collectively, the APOE4 allele can increase one's AD risk through mechanisms

dependent and independent of Aβ.

1.2.3   APOE4 on Host Metabolism

Carriers of the APOE4 allele also appear to have an altered metabolism.

Indeed, APOE4 allele preferentially binds to large very low-density lipoprotein

cholesterol (VLDL) particles and the APOE genotypes account for interindividual

differences in lipid and lipoprotein levels [21]. The allele is even associated with

a less desirable lipid profile that includes increased low-density lipoprotein

cholesterol (LDL-C) levels and risk for coronary heart disease [22]. The APOE4

allele also appears to play a role in glucose metabolism where APOE4 carriers

have decreased cerebral metabolic rate of glucose, even in young adults [23]. In

an AD mouse model utilizing the APOE4 allele, mitochondrial dysfunction began

as early as 3-months in the mice [24]. Further in an AD mouse model utilizing the

APOE4 allele and a mutation in APP, the APOE4 mice had greater impairment

of insulin signaling compared to the APOE3 mice [25]. Another study even

suggested that the APOE4 allele may interact with the insulin receptor less than

that of the APOE3 allele [26]. Next, other alterations in the brain have also been

found such as in one study by Johnson et al. that found APOE4 mice to have

alterations in hippocampal metabolites involved in purine, glutamate, glycerophospholipid (GPL), and pentose phosphate pathway metabolism [27]. Collectively, the APOE4 allele appears to lead to mitochondrial dysfunction and deleterious alterations in glucose and lipid metabolism.

1.2.4 APOE Mouse Models

One of the more effective ways of understanding the isoform effects caused by the APOE4 and APOE3 alleles on AD pathology is by using APOE transgenic mouse models [28]. In their history, APOE knock out models were initially utilized in an attempt to understand the effect of APOE in the brain. However, due to the differences in mouse and human APOE, this had severe shortcomings for translating these studies to humans. Indeed, the homology of mouse and human APOE is only 70%. Thus, to expand this research, mouse models that expressed APOE specifically in glia or neurons through heterologous promoters were utilized. These include glial fibrillar acidic protein (GFAP, GFAP-APOE) and neuron-specific enolase (NSE, NSE-APOE). Unfortunately, heterologous promoters are not as well-regulated as endogenous promoters for a few reasons: protein expression and copy number of the transgene is not as well controlled, and evidence suggests glia, not neurons, primarily express APOE. Thus, mouse models using knock-in, or target replacement (TR), of human APOE utilizing endogenous promoters for expression of APOE were generated. APOE-TR models have glial cells that express human APOE at physiological levels, replacing mouse APOE, a huge

advantage over previous models. Next, APOE-deficient and APOE-TR models were crossed with those that express human FAD mutations, including mutations in APP and/or PS1, with the goal of examining the effects of various human APOE isoforms on Aβ deposition [28]. The human FAD models are generally designated Aβ-Tg and include PDAPP (APP^{V717F}), J9 (PS1^{M146V,L286V}, APP^{V717F}), and 5xFAD (APP^{K670N,M671L,I716V,V717I}, PS1^{M146V,L286V}), the latter having a more rapid onset of AD pathology than the two former. Typically, Aβ-Tg models develop plaque formation by 6-months of age; however, 5xFAD mice develop plaques by 2-months of age. When target replacement human APOE3 or APOE4 is added to 5xFAD mice (EFAD), plaque formation is delayed by 4 months. Due to this delay in plaque deposition, the EFAD model offers an easier and more tractable ability to analyze plaque accumulation in the presence of human APOE alleles and the progression thereof. The EFAD model is also advantageous for studying markers related to AD, analyzing Aβ plaque formation via regional and temporal comparisons in the brain, and using interventions that may be more translatable to humans than previously mentioned AD mouse models [28].

The mouse model that is the focus of this dissertation is the EFAD mouse model (E3FAD and E4FAD) that utilizes mice with the C57BL/6 background that are a cross of transgenic mice that overexpress human Aβ via 5 FAD (5xFAD) mutations and mice that express either the target replacement human APOE3 or APOE4 gene. This recent model was developed by Dr. Mary Jo LaDu in 2012 [29]. The first study featuring this model described the synergistic effects of

APOE4 and Aβ. In mice with FAD mutations, amyloid deposits develop as early as 2-months of age [30]. However, the addition of APOE4 delayed amyloid deposition [31]. This holds true in this E4FAD model as the mice in this study demonstrated changes in Aβ buildup starting between 2- to 6-months of age, with E4FAD have greater total Aβ levels and Aβ42 compared to E3FAD mice. Specifically, total Aβ42 was greater in the hippocampus and cortex of APOE4 mice compared to APOE3 but levels remained the same in the cerebellum. Next, E4FAD mice had significantly greater plaque deposition than E3FAD mice in the frontal cortex and subiculum at 4-months of age and in the frontal cortex at 6-months of age. Interestingly, the E4FAD mice had significantly greater amounts of dense-core plaques while the E3FAD mice had more diffuse plaques. APOE4 levels were significantly lower than APOE3 in the cerebellum at 4-months of age, the cortex at 2-, 4-, and 6-months of age, and the hippocampus at 2- and 4-months of age. Overall, APOE levels were greatest in the cortex and hippocampus, regions susceptible to Aβ deposition, and lowest in the cerebellum, a brain region resistant to Aβ, with APOE4 levels lower than APOE3 in each brain region at each time point. Quite importantly, soluble Aβ42 and soluble oligomeric Aβ levels, both associated with AD progression, were higher in the APOE4 mice compared to the APOE3 mice at 6-months of age. Based on these findings, the authors concluded that in the E4FAD mice, the decreased total APOE4 but increased Aβ42 levels is indicative that APOE4 promotes Aβ accumulation in the hippocampus and cortex. However, this is due to the function of APOE4, not the quantity thereof [29].

Other studies using the EFAD transgenic mice have found additional genotype effects. Rodriguez et al. found that E4FAD mice have more prominent plaques via Aβ staining than the E3FAD mice along with more dense plaques in the subiculum. Interestingly, the E4FAD mice had much greater cortical levels of IL-1β, a proinflammatory cytokine, in the cortex compared to E3FAD mice. E4FAD mice also exhibited increased measures of microglia reactivity and dystrophy in the cortex along with a genotype effect on the number of microglial cells surroundings plaques. Further, E4FAD mice had significantly greater average microglial cells surrounding plaques compared to APOE3. Collectively, this study showed that E4FAD mice have increased microglial and cytokine activation compared to E3FAD mice [32].

EFAD mice have displayed genotype differences in cognition. Liu et al. demonstrated that female E4FAD mice at 2-, 4-, and 6-months of age displayed an intensified age-dependent decline in the Morris water maze test compared to E3FAD mice, indicative of diminishing long-term reference memory, spatial learning, and working memory. The E4FAD also demonstrated an age-dependent decline in the Y-maze, unlike the E3FAD mice, indicative of decaying spatial recognition memory. Similar to other aforementioned studies, the total APOE levels were decreased in E4FAD mice compared to E3FAD. Next, the E4FAD mice in this study also have reduced post-synaptic protein levels, N-methyl-D-aspartate receptor (NMDAR) levels, and brain-derived neurotropic factor (BDNF) levels at 6-months of age, which likely contribute to the cognitive deficits seen in E4FAD mice [33].

Other studies in E4FAD and E3FAD mice demonstrate that female E4FAD mice had greater cerebral cortex microbleeds and hemosiderin, an iron-storage compound that is often formed after bleeding, than male E4FAD mice. The authors looked for similar effects in human APOE4 patients but found no sex differences [34]. Although interesting, there may be limitations to the EFAD mouse model in its translatability to humans. One limitation of this model is the lack of development of tau pathology typically seen in AD. However, Zhou et al. demonstrated that E4FAD mice had greater site-specific tau phosphorylation, potentially due to calpain-CDK5 signaling, compared to E3FAD mice [35]. Although the tau phosphorylation is more restrained in this study then typically seen in AD, it is notable that APOE4 and/or FAD mutations lead to increased tau phosphorylation.

Next, Teter et al. demonstrated in a recent study that E4FAD mice, compared to E3FAD mice, had reduced miR146a, a microRNA in the brain and plasma that is increased in AD patients and helps regulate the inflammatory process by down regulating NFκB. Thus, it acts to decrease inflammation. The FAD mutations increase miR146a, however, the APOE4 allele appears to inhibit this process compared to the APOE3 allele, increasing the inflammatory process. Here, we see genotype differences in the inflammatory process independent of Aβ in an EFAD mouse model [36]. Female E4FAD mice were treated with epidermal growth factor (EGF), which prevented cognitive decline, decreased microbleeds, and limited cerebrovascular dysfunction. Interestingly, the female E4FAD mice had greater cognitive impairment, lower EGF serum

levels, and greater microbleeds than their male counterparts. It is unclear why E4FAD female mice have such an exacerbated response, but the authors attribute this to increased extracellular Aβ exhibited in female mice and/or an enhanced inflammatory response in the brain [37]. Finally, a recent study by Abdullah et. al. investigating the effect of the APOE genotype on blood phospholipids found that E4FAD mice had a greater plasma arachidonic acid/docosahexaenoic acid (DHA) ratio, a ratio associated with increased inflammation, compared to the E3FAD mice. This was further confirmed in human subjects, where this ratio preceded the diagnosis of AD. This is yet another marker of interest that the APOE4 allele may deleteriously impact AD risk [38].

Although the EFAD model is fairly new, a variety of studies have been published indicating that the combination of APOE4 and FAD mutations leads to AD through multiple mechanisms. However, mechanisms that originate from the gut impacting one's risk of developing AD has recently become of intense interest. The APOE allele has actually been implicated to impact the gut microbiome. In fact, the APOE4 allele actually appears to be protective against diarrhea, enteric infections, and malnutrition in children in the developing world such as in Brazil [39]. While these effects may not be as much of an issue in first world countries such as the United States, the APOE4 allele may save the lives of children in developing countries such as Brazil. However, they will still be at an increased risk of dementia as they age. Further, studies in AD mouse models have found alterations in amyloid pathology. Indeed, APP/PS1 transgenic mice

demonstrated an increase in amyloid pathology and immune reactivity in the intestines compared to wild-type mice [40]. In another study using this same APP/PS1 transgenic mouse model, Harach *et al.* found that germ-free (GF) mice had decreased amyloid pathology in the brain compared to mice that did have a gut microbiome [41]. Based off of this, certainly the APOE allele and FAD mutations play a role in the gut microbiome, although much has yet to be learned.

1.3   Gut Microbiome: Overview

The gut microbiome, or the trillions of bacteria that inhabit our gut, play a profound and ever-growing role on the host's health. The microbiome contains over 1,000 bacterial species, though it may actually be much higher than this, each exerting their own specific effects. However, there are just a few primary bacterial phyla: Firmicutes, Bacteroidetes, Actinobacteria, Verrucomicrobia, and Proteobacteria [42]. Interestingly, the ratio of Firmicutes to Bacteroidetes has become a well-known biomarker of certain diseases with an increased Firmicutes to Bacteroidetes ratio present in obesity. This may even lead to excessive low-grade inflammation [43]. Confusingly, in inflammatory bowel disease (IBD) patients, an increased and decreased Firmicutes to Bacteroidetes ratio has been observed [44, 45]. Importantly, this ratio is altered with age. Although not unanimous in the literature as diet and environment play a profound role, children typically have decreased amounts of Firmicutes, and thus a decreased Firmicutes to Bacteroidetes ratio, but this

increases dramatically as one enters into adulthood. However, after adulthood and into elderly status, a decreased Firmicutes to Bacteroidetes ratio is exhibited [46]. The mechanisms behind these changes are not currently well understood.

Certain bacterial species have been demonstrated to have important effects on the host, beneficial and deleterious. For example, *Akkermansia muciniphila* has been demonstrated to increase insulin sensitivity but decrease fat mass and inflammation [47]. In contrast, other bacterial species such as *Clostridium difficile*, or *C. diff*, an opportunistic bacterium that when in excess, produces two exotoxins, A and B, can cause diarrhea. Elderly hospital patients are particularly susceptible and deaths are not uncommon [48]. Considering there are over 1,000 bacterial species, the aforementioned two bacterial species are just the tip of the iceberg and thus, more research needs to be conducted to elucidate the effects of each.

The gut microbiota impacts host metabolism as demonstrated in germ-free (GF) mice studies. In one GF mice study, the GF mice have decreased body fat compared to control mice despite eating more calories [49]. This is indicative of the gut microbiota impacting energy harvest from food and subsequent fat storage. GF mice are even protected from insulin resistance [50] but when the feces of control mice were inserted into germ-free mice, an increase in body fat and insulin resistance ensued [51]. This may partly be due to the differences in the development of the gut epithelium with control mice having more small intestinal villi, promoting increased energy harvest. Further,

15

alterations in gene expression in the liver and adipose tissue are present between GF and control mice, altering lipid and mitochondrial metabolism [52, 53]. The alterations in fat storage may also be due to differential regulation of the intestinal expression of fasting-induced adipose factors (FIAF). FIAF inhibits lipoprotein lipase (LPL) in adipose tissue and activates the breakdown of triacylglycerol into fatty acids, used by muscle and adipose tissue. GF mice had elevated FIAF relative to control mice, leading to increased fat mass in control mice [51]. Similar studies have been performed in humans where fecal matter was transferred from lean donors to individuals with metabolic syndrome. One study found that the individuals with metabolic syndrome had increased microbial diversity and improved insulin sensitivity after the fecal donation [54]. Taken together, the gut microbiota regulates glucose and lipid metabolism while ultimately impacting fat mass and body weight.

Next, the gut microbiota synthesizes metabolites that affect host metabolism. This includes short chain fatty acids (SCFAs) and bile acids, among others. SCFAs are used extensively as an energy source for colonic cells as well as a ligand for G-protein coupled receptors (GPR), including GPR41 and GPR43, in many different tissues. Activation of these GPRs may help reduce body weight and improve insulin sensitivity in liver and muscle [51, 55]. One potential mechanism is increased secretion of anorexigenic hormones such as glucagon like peptide-1 (GLP-1) and peptide YY (PYY) via GPR signaling [56]. Indeed, these hormones are thought to beneficially impact

16

glucose metabolism [57, 58] and by working in the hypothalamus, decrease

appetite and thus, food intake [59].

The gut microbiota influences bile acid metabolism and thus impacts the

absorption of dietary lipids and fat-soluble vitamins. The primary bile acids

include cholate (CA) and chenodeoxycholate (CDCA), which are synthesized

in the liver. However, bile undergoes modifications before release into the

intestines via conjugation by glycine or taurine, boosting their function.

Although 95% of bile acid is reabsorbed by the ileum and returned to the liver,

the rest is converted into secondary bile acids by the gut microbiota [60]. The

secondary bile acids include deoxycholic acid (DCA) and lithocholic acid (LCA)

and have been demonstrated to decrease weight gain and serum cholesterol

[61]. In another study, taurine-conjugated DCA and CDCA were associated

with insulin resistance in nondiabetic individuals [62]. Although not particularly

well understood, bile acids may impact glucose metabolism through the

nuclear farnesoid X receptor (FXR) [63], explored next.

The production of bile acids is regulated by negative feedback inhibition

via the FXR [64], which the gut microbiota impacts. Indeed, the gut microbiota

has been demonstrated to cause diet-induced obesity via FXR signaling.

Further, Parseus et al. found the microbiota to increase adipose tissue

inflammation and hepatic expression of genes involved in lipid uptake [65]. It

has also been demonstrated that treatment with an FXR agonist increased

insulin sensitivity [66]. Interestingly, the activation of FXR by bile acids may

even impact the immune system via increased expression of inducible Nitric Oxide Synthase (iNOS) and IL-18 [67].

The gut microbiota has a profound effect on the immune system. One reason is due to SCFAs activation of GPRs, namely GPR43, impacting the immune system by regulation of colonic regulatory T-cells [68]. They have also been demonstrated to increase IL-10, an anti-inflammatory cytokine [69], suppress NF-κB and IL-2, regulate neutrophils [70], and suppress cytokine production by monocytes [71]. Quite interestingly, SCFAs even impact the brain by decreasing BBB permeability [72] and by regulating microglia maturity [73]. However, the SCFAs are not the only metabolites produced by the gut microbiota that impact the immune system. Indeed, aromatic amino acids such as tryptophan can be metabolized to, for example, indole 3-propionic acid (IPA). IPA is metabolized by the microbial species *Clostridium sporogenes* [74] and can act as a ligand for the pregnane X receptor (PXR). Through PXR, IPA can induce an increase in junctional protein mRNA expression while decreasing TNF-α [74], leading the host to better intestinal health and decreased inflammation.

Another way the gut microbiome interacts with the immune system is through lipopolysaccharide (LPS), an endotoxin from the outer cell membrane of Gram-negative bacteria, which can enter the circulation when a leaky gut is present in the host. Leaky gut is the increased permeability of the intestinal wall leading to low-grade inflammation and in extreme cases, sepsis [75]. Upon LPS entering the circulation, it can reach the liver or adipose tissue and

initiate an innate immune response. This response includes the activation of CD14 in the macrophage, activating toll-like receptor 4 (TLR4), which then activates NF-κB and activator protein 1 (AP-1)[76]. Furthermore, circulating endotoxin levels have also been linked to increased TNF-α and IL-6 in adipocytes [77]. Interestingly, this deleterious alteration in immune function may also lead to metabolic dysfunction. Indeed, Cani et al. demonstrated that continuous subcutaneous infusion of LPS in mice leads to hyperglycemia and insulinemia, weight gain, increased markers of inflammation, and liver insulin resistance [78]. Importantly, LPS has also been demonstrated to increase inflammation in the brain via activated microglia and increased expression of TNF-α, Monocyte Chemoattractant Protein (MCP-1), IL-1β, and NF-κB [79]. Clearly, the production of metabolites by the gut microbiome has a deep impact on the host immune system, even in the brain.

1.4   Gut-Brain Axis

The gut-brain axis (GBA) is the bi-directional communication between the gut and the brain. Although a fairly new development in research, a few methods of communication between the gut and brain have been identified. One such is through the SCFAs butyrate, acetate, and propionate, which are produced by certain bacterial species such as *Bacteroides* and *Roseburia inulinivorans* [80]. Specifically, butyrate has been demonstrated to prevent inflammatory responses via NFκB inhibition in murine N9 microglia, hippocampal slice cultures [81], and HT-29 cells [82]. Butyrate also affects BBB permeability [72] and along with

propionate, improves glucose sensitivity and body weight control via gut-brain neural circuits [83]. Further, excess acetate levels caused by an altered gut microbiota were demonstrated to lead to obesity via the microbiome-brain-β cell axis [84]. Another form of communication in the GBA is through tryptophan metabolites. One example is indole propionic acid (IPA), which has been demonstrated to inhibit Aβ fibril formation in neurons and neuroblastoma cells [85]. Another tryptophan metabolite is serotonin, a neurotransmitter in the brain and enteric nervous system (ENS). Interestingly, 95% of serotonin is produced by ENS neurons and gut mucosal enterochromaffin cells [86]. In the gut and periphery, serotonin impacts GI secretion and motility [87]. Additionally, the gut microbiota can communicate through neural pathways such as through the ENS and importantly, vagus nerve [88]. In fact, the vagus nerve appears, at least in part, to be responsible for central GABA receptor expression, anxiety and depression-like behavior, and corticosterone response [88]. In another study, the reduction of anxiety by the probiotic *Bifidobacterium longum* was absent in mice without a vagus nerve [89]. Next, numerous neurotransmitters that are produced by enteroendocrine cells (EECs) in the GI tract that are stimulated by gut microbial taxa or by-products thereof are also able to potentially impact the brain [90]. This includes peptide YY, neuropeptide Y (NPY), and cholecystokinin. Finally, another GBA communication pathway involves immune signaling [91]. Indeed, the gut microbiota is a very important immune organ that can impact the brain. Notably in this communication pathway, consumption of the probiotic *Bifidobacterium infantis* 35624 was found to enhance IL-10 in the periphery of

humans [92]. Meanwhile, when GF mice are given commensal bacteria,

increases in Treg and IL-10 occur [93]. Importantly, it is thought that certain

immune cells can generate neurotransmitters that can signal to the brain and

even influence behavior [91]. An example of this in one study in mice found that

Mycobacterium vaccae activated the peripheral immune system, which went on

to stimulate serotonergic neurons of the dorsal raphe nucleus of mice, increasing

serotonin metabolism [94]. The study further proposed this was an important part

of mood regulation. Collectively, the GBA and its various communication

pathways play a pivotal yet sparsely explored role in the health of an organism.

We believe this may be an exciting venue of research with the goal of preventing

neurological diseases such as AD.

1.5   Prebiotics: Overview

To beneficially modulate the gut microbiota, an individual could consume

prebiotics. Prebiotics are the non-digestible portion of food that stimulates the

growth of beneficial bacteria. Although the exact definition of prebiotics varies,

Bindels et al. proposed this definition: "a non-digestible compound that, through

its metabolization by microorganisms in the gut, modulates composition and/or

activity of the gut microbiota [95]." For clarity, these classifications must be met

for a compound to be considered a prebiotic: digested by gastric enzymes in the

upper gastrointestinal (GI) tract, stimulate the growth of certain beneficial

bacteria, and fermented in the colon to produce metabolites such as SCFAs.

Specific prebiotics include resistant starch, oligosaccharides, and inulin.

Prebiotics are, in general, non-digestible carbohydrates, or fiber, found in foods such as fruits, vegetables, whole grains, and legumes. Whole foods typically contain a mixture of insoluble and soluble fiber. Insoluble fiber does not dissolve in water, is minimally fermented, but promotes regular bowel movements and prevents constipation. On the other hand, soluble fiber forms a gel in water, can be fermented into beneficial metabolites such as SCFAs, decreases cholesterol, and regulates blood glucose. However, the benefits of soluble and insoluble often overlap [96]. Different kinds of prebiotics include oligosaccharides, resistant starch, inulin, etc. that are fermented by beneficial bacteria into SCFAs and other metabolites, producing many of their advantageous effects. Other benefits include improved gut barrier function, reduced colonies of pathogenic bacteria, decreased risk of CVD, promotion of weight loss, beneficial modulation of the immune system, enhanced mineral absorption, promotion of regular bowel movements and intestinal health, cancer prevention, and reduced cholesterol [97]. Although literature on prebiotics in regard to the GBA is scarce, prebiotics have been demonstrated to elevate central BDNF, levels of which decrease according to AD severity [98], and N-methyl-D-aspartate receptor (NMDA) [99], but reduce waking cortisol levels in human subjects [100]. Collectively, prebiotics have a vast array of benefits to the host and are easy to consume, making it an ideal nutritional intervention in the fight against neurological disorders such as AD.

1.5.1 Inulin

For our project, we will use the prebiotic inulin, a soluble dietary fiber and member of the fructans group, due to its well-documented ability to increase SCFA production and increase *Bifidobacterium* bacterial populations [101]. United States citizens ingest 1-4g of inulin-type fructans (ITFs) per day, considerably less than the 3-11g eaten by Europeans [102]. To be an ITF, a β-(2-1)-fructosyl-fructose glycosidic bond anywhere from 2 to 60 units long must be present, giving inulin its ability to resist gastric enzymes in the upper GI, only to be later fermented in the colon [101]. Notably, only gastrointestinal side effects have been reported with inulin consumption including diarrhea, abdominal rumbling, bloating, cramping, and excess flatulence. However, these effects are generally seen in intakes greater than 40g per day, although individual variation exists. A daily dose of 2.5-10g per day in humans is recommended to promote a healthy gut microbiota [103].

Inulin is derived from the chicory root but is also found in garlic, onions, artichoke, and in processed foods as a functional fiber. For food application, when adding inulin, health claims can be made on the product, potentially persuading consumers to eat the food for added health benefits. Inulin can also be used to replace fat or sugar as inulin can be processed to have a similar taste and/or texture [101].

ITFs include inulin, oligofructose, fructooligosacchardies (FOS), and bifidogenic oligo- or polysaccharide chains. The latter of which are more derived, smaller molecules. A way to classify these types is by their degree of

polymerization (DP) [101]. For example, inulin has not undergone extensive processing and is generally greater than 10 DP. However, oligofructose is less than 10 DP and has undergone partial hydrolysis with all long chain ITFs removed. Finally, FOS are very short chain inulin type fructans that are produced from sucrose. Unfortunately, the literature can vary on classifying the types of inulin by DP, so one should be careful when looking to specifically identify ITFs. Further, the DP of ITFs also determines the location they will exert their effects. If the product has a lower DP, it will exert effects towards the proximal colon, while less derived, higher DP ITFs will exert effects in the distal colon. In the colon, these ITFs are fully metabolized into carbon dioxide, hydrogen, SCFAs, lactate, and other metabolites. This fermentation also makes the colon more acidic, thought to be advantageous for the growth of beneficial bacteria, along with increasing fecal content size. Finally, ITFs do indeed affect the gut microbiota. Although not entirely conclusive due to differences in the type of inulin used in the literature and individual differences, ITFs stimulate *Bifidobacteria,* increasing its bacterial biomass. Indeed, *Bifidobacteria* can consume non-digestible carbohydrates as energy sources such as ITFs. This genus contains at least 51 different species that have numerous beneficial effects including production of B vitamins, maturation of immune system, protection of the gut barrier and pathogens, and production of SCFAs [104]. When examining the literature, one human study found that 20g of inulin was given for 8 days, and then ramped up to 40g a day for another 10 days. This dietary regimen produced significant increases in *Bifidobacteria,* whereas Enterococci and Enterobacteriaceae were

24

decreased. However, effects of ITFs on bacterial species other than

Bifidobacteria are inconclusive at this time. In a recent study by Vandeputte et al.

in human subjects, inulin was found to alter bacterial abundance at the genus-

level via increased *Bifidobacterium* and *Anareostipes* but decreased *Bilophila*

[105]. Notably, some evidence supports a dose-dependent response to

increasing levels of inulin intake although this may depend on the state of the

host and variation in their gut microbiota prior to treatment with inulin [101].

Inulin is well known in the literature in both human and animal models and,

despite some inconsistencies, has time and time again produced beneficial

effects, making it quite possibly the most studied and verified of all prebiotics.

Indeed, inulin has been suggested to help with constipation in elderly females by

increasing stool frequency and making them softer [106], while other studies

have not demonstrated notable effects [103]. Similarly, inulin has been

demonstrated, albeit inconsistently, to reduce total cholesterol, LDL-cholesterol,

VLDL-cholesterol, and triglycerides in dyslipidemic and obese subjects [107]. In a

recent meta-analysis examining the effect of ITFs on blood lipids and glucose

levels in humans that were healthy, dyslipidemic, obese, and T2D patients, ITFs

were demonstrated to decrease LDL across all groups. However, ITFs

decreased fasting insulin and increased HDL only in certain T2D subgroups. The

authors attribute the latter to the differences in the gut microbiota and

pathological state of the subjects, e.g. T2D patients have increased blood

glucose and lipids. Nevertheless, this meta-analysis does provide compelling

evidence that ITFs can indeed beneficially impact blood lipid profiles and glucose.

In animal models, ITFs have also been demonstrated to have anti-carcinogenic effects. Indeed, supplemented inulin has demonstrated anti-carcinogenic effects in one study using mice and rats that were induced with colon cancer using azoxymethane and dextran sulfate sodium (AOM/DSS). In mice, the group fed the inulin-like fructans had decreased intestinal polyps and decreased markers of inflammation such as TNF-α. Even more interesting, the inulin groups had increased bone densitometry in their femur and vertebra in a separate cohort of rats. However, serum calcium levels were not different [108]. Nevertheless, inulin has demonstrated anti-carcinogenic and anti-inflammatory effects in the colon. The inconsistencies in the literature may be due to amount of inulin given in each study.

Specific doses of inulin in animal models have varied but for the most part, show benefits. In one of the more extreme cases, Parnell et al. fed 8-week-old male lean and obese rats 0, 10%, or 20% of a 1:1 inulin and oligofructose mix for 10 weeks. The primary finding of this study was that the prebiotic fed groups had decreased serum cholesterol and a reduction in liver triacylglyceride (TAG) buildup compared to the obese control rats. A dose-response effect was not observed but the authors suggest the 10% dose may be more beneficial. Notably, these effects were not seen in the lean mice [109]. Another study also used the 10% dose with an inulin fiber product called Orafti Synergy to test the ability of rats to absorb iron and magnesium after being exposed to omeprazole,

which inhibits passive magnesium transport and absorption. The results revealed that inulin was able to restore calcium transport in the omeprazole treated rats, but not magnesium, compared to the control group. As a side note, levels of butyrate in the cecum and colon were also increased compared to the control group [110]. Similar findings have been found in humans, with one study in young healthy men demonstrating inulin to increase calcium absorption and balance. However, the absorption of magnesium, iron, and zinc were not altered [111].

In one study similar to the present dissertation project, Weitkunat et. al. looked at the effects of a 10% inulin and 10% cellulose diet in gnotobiotic C3H/HeOuJ mice colonized with a human microbiota, comprised of 8 represented bacteria, for 6 weeks. Firstly, the cellulose diet had significantly greater fecal bulk and energy than the inulin group and thus, the inulin group had 10% higher digestibility. However, the calculated energy assimilation was not different. This was apparent as the body weight and composition in the two groups was also not different. Nor was liver weight or epididymal white adipose tissue (eWAT). In regard to the gut microbiota, the inulin group had an increased total bacterial cell number due to the increase in 6 of the 8 members of their human gut microbiota. These included *Anaerostipes caccae*, *Bacteroides thetaiotaomicron*, *Bifidobacterium longum*, *Blautia producta*, *Clostridium butyricum*, and *Clostridium ramosum*. Importantly, the inulin group also had significantly increased amounts of the SCFAs acetate, propionate, and butyrate in the cecum and significantly increased acetate and propionate in the plasma of

the portal vein. Inulin also altered liver genes associated with lipogenesis and fatty acid elongation. Finally, the inulin group exhibited a decreased ratio of omega-6 to omega-3 in the plasma, liver, and eWAT. Together, the authors believe these results signify that inulin may alter and decrease hepatic lipid metabolism while the decreased omega-6 to omega-3 ratio may help decrease disease risk [112].

Collectively, inulin and ITFs have demonstrated a large array of benefits in the literature; however, more research needs be conducted in order to understand the aforementioned inconsistencies. Further, very little research exists regarding inulin and the brain, an exciting area of future discoveries.

1.6 Scope of Dissertation

The overall objective of our project is to use the prebiotic inulin to modulate the gut microbiota, reducing the risk of developing Alzheimer's disease (AD)-like symptoms. For all aims, we will use a mouse model of C57BL/6 background that overexpresses human Aβ via 5 familial-AD (5xFAD) mutations and expresses either the knocked-in human APOE3 (E3FAD) or APOE4 (E4FAD) gene. Notably, a prevention strategy can be utilized in these mice as this mouse model gives us a known timeline of when to treat the mice with the prebiotic inulin. Our *central hypothesis* is that the prebiotic inulin will restore metabolic function and reduce AD pathology, including Aβ and neuroinflammation, in asymptomatic E4FAD mice. Our rationale is that once we learn if manipulation of the gut microbiota with the prebiotic inulin can alter the

gut-brain axis and decrease AD risk factors, we can administer innovative treatments for its prevention. As such, we will test our central hypothesis by these three specific aims:

Specific Aim 1. To identify the effects of the prebiotic inulin on the gut microbiota and induced metabolism changes thereof between E3FAD and E4FAD mice. This chapter will discuss the differences in the gut microbiota between E3FAD and E4FAD mice along with the effect of the prebiotic inulin on thereof compared to the control diet. Further, it will test for potential metabolites, such as the short chain fatty acids (SCFAs), generated by the gut microbiota with and without prebiotic treatment in the cecum and in fecal culture.

Specific Aim 2. To identify the effects of the prebiotic inulin on metabolism in the periphery and central nervous system (CNS) between E3FAD and E4FAD mice. This chapter will discuss the effect of the prebiotic inulin on metabolism in blood plasma, *in vivo* brain, and brain tissue between E3FAD and E4FAD mice. Specifically, metabolites produced from the prebiotic inulin in the gut microbiota that may have an impact on the brain will be assessed.

Specific Aim 3. To identify the effects of the prebiotic inulin on AD risk factors and pathology between E3FAD and E4FAD mice. This chapter will discuss if the impact of the prebiotic inulin can reach the brain and decrease AD risk factors, including CBF, inflammation, anxiety, and cognition, and Aβ aggregation in E3FAD and E4FAD mice and any differences seen between E3FAD and E4FAD mice.

Chapter 2   Methods and Materials

2.1   Animals, Caging, and Diet Information

     For all aims, the EFAD transgenic mouse model (E3FAD and E4FAD) was used. This C57BL/6 background mouse model is a cross between transgenic mice that overexpress Aβ via 5 familial-AD (5xFAD) mutations with transgenic mice that have either the target replacement human APOE3 or APOE4 allele. We determined the sample size (N = 15/group, Male:Female = 50/50) via power analysis to ensure comparison at a 0.05 level of significance and a 90% chance of detecting a true difference of each measured variable between groups. Each mouse was given its own cage housed in a specific pathogen-free facility in order to avoid the potential for hostility when combining unfamiliar mice into one cage. Further, mice were house independently for gut microbiome analysis due to the potential for microbiome transfer, e.g. mice eating each other's feces giving them a very similar gut microbiome. Thus, the mice would be N = 1 for that particular cage. Individual housing will also help us avoid cage effects [113]. E3FAD and E4FAD mice were weighed biweekly, given *ad libitum* access to food and water, and fed either a prebiotic or vehicle control diet (detailed in Table 3.1) starting at 3 months of age. Both the prebiotic and vehicle control diet are modifications of TestDiet's AIN-93G Semi-Purified Diet 57W5. Experimental procedures, including magnetic resonance imaging and animal behavior tests, started when mice reached 7 months of age and after completion of these experiments, the mice were sacrificed with cecum weight measured and brain, blood, cecal contents, and intestinal tissue collected. All experimental procedures were

performed according to NIH guidelines and approved by the Institutional Animal Care and Use Committee (IACUC) at the University of Kentucky (UK).

2.2 Fecal Bacterial Culture

Fecal samples were collected from 7-month old E3FAD and E4FAD mice fed a standard chow diet and pooled together into their respective groups with 175 mg per sample weighed. The samples were placed in an anaerobic chamber and transferred to a clean tube containing 1.5 ml media. The samples were mashed into a semi-suspension, sealed, and taken out of the chamber. Samples are centrifuged at 500 rpm for 5 minutes. A 10-cc syringe is used to pull 8 mLs of the supernatant into an anaerobic tube. Samples are centrifuged again at 3000 rpm for 10 minutes. Next, the samples are aspirated and maintained in anaerobic conditions. The pellets are suspended in 9 mL media and separated into tubes. Next, either inulin (5g/L) or the control, glucose (5g/L) were added. The samples sit for either 24 or 48 hours with subsequent collection of 1 mL from each sample. The samples are centrifuged at 21,000 g for 2 minutes and supernatant collected. The samples can then be frozen until further analysis. All groups were run in triplicate.

2.3 Gut Microbiome Analysis

For fecal DNA amplification, fecal samples were collected from all mice per group (N = 15/group, M:F = 50/50). A DNeasy PowerSoil Kit (Qiagen, Hilden, Germany, Cat. No. 12888-100) was used for fecal DNA extraction, according to

the manufacturer's protocol. Genomic DNA was PCR amplified with primers CS1_515F and CS2_926R [114] targeting the V4-V5 regions of microbial 16S rRNA genes using a two-stage "targeted amplicon sequencing (TAS)" protocol [115, 116]. First stage amplifications were performed with the following thermocycling conditions: 95°C for 3 minutes, 28 cycles of 95°C for 45 seconds, 55°C for 45 seconds, 72°C for 90 seconds and final elongation at 72°C for 10 minutes. Barcoding was performed using a second-stage PCR amplification with Access Array Barcode Library for Illumina Sequencers (Fluidigm, South San Francisco, CA; Item# 100-4876). The pooled libraries, with a 15% phiX spike-in, were loaded on a MiSeq v3 flow cell, and sequenced using an Illumina MiSeq sequencer, with paired-end 300 base reads. Fluidigm sequencing primers, targeting the CS1 and CS2 linker regions, were used to initiate sequencing. De-multiplexing of reads was performed on instrument. Second stage PCR amplification and library pooling were performed at the DNA Services (DNAS) facility within the Research Resources Center (RRC) at the University of Illinois at Chicago (UIC). Sequencing was performed at the W.M. Keck Center for Comparative and Functional Genomics at the University of Illinois at Urbana-Champaign (UIUC).

For microbial analysis, forward and reverse reads were merged using PEAR [117]. Primer sequences were identified using Smith-Watermann alignment and trimmed from the sequence. Reads that lacked either primer sequence were discarded. Sequences were then trimmed based on quality scores using a modified Mott algorithm with a PHRED quality threshold of p =

0.01, and sequences shorter than 300 bases after trimming were discarded.

QIIME v1.8 was used to generate operational taxonomic unit (OUT) tables and

taxonomic summaries [118]. Briefly, the resulting sequence files were merged

with sample information. OTU clusters were generated in a *de novo* manner

using the UCLUST algorithm with a 97% similarity threshold [119]. Chimeric

sequences were identified using the USEARCH61 algorithm with the

GreenGenes 13_8 reference sequences [120]. Taxonomic annotations for each

OTU were using the UCLUST algorithm and GreenGenes 13_8 reference with a

minimum similarity threshold of 90% [119, 120]. Taxonomic and OTU abundance

data were merged into a single OTU table and summaries of absolute

abundances of taxa were generated for all phyla, classes, orders, families,

genera, and species present in the dataset. The taxonomic summary tables were

then rarefied to a depth of 10,000 counts per sample.

Shannon and Bray-Curtis dissimilarity indices were calculated with default

parameters in R using the vegan library [121, 122] and visualized as box plot and

NMDS plot, respectively. Shannon index is used to calculate α-diversity, or the

species richness within a single habitat, via $H = \sum_{i=l}^{S}(p_i * ln\ p_i)$ where H =

Shannon diversity index, p_i = fraction of the entire population made up of species

i, S = number of species, ln = natural logarithm, and Σ = sum of species. A higher

H value indicates a more diverse community within a particular sample. Bray-

Curtis dissimilarity is used to calculate β-diversity, the diversity of taxonomic

abundance between difference samples, via $BC_{ij} = 1 - \frac{2C_{ij}}{S_i+S_j}$ where i and j = the

two sites, S_i = total number of specimens on site i, S_j = total number of

specimens counted on site j, and C_{ij} = sum of only lesser counts for each species in both sites. The rarefied genus data, taxonomic level 6, were used to calculate both indices. Plots were generated in R using the ggplot2 library [123]. Significant differences among tested groups was determined using the Kruskal-Wallis one-way analysis of variance and analysis of variance using distance matrices (ADONIS). The group significance tests were performed on the rarefied genus data, taxonomic level 6 (genus), using the group_significance.py script within the QIIME v1.8 package.

2.4   Plasma Scyllo-Inositol

A subset of 10 mice per group (N = 10, M:F = 50/50) was used for testing with a total of 50 ul mouse plasma mixed with 200 ul acetone, for a final concentration of 80%, to precipitate protein at -80°C for 30 minutes. The precipitation was centrifuged out at 21000 g for 20 minutes at 4°C. The supernatants were lyophilized overnight and reconstituted in D2O (> 99.9%, Cambridge Isotope Laboratories, MA) containing 0.1 mM EDTA (Ethylenediaminetetraacetic acid, Sigma Aldrich, St. Louis, MO) and 0.5 mM d6-2,2-dimethyl-2-silapentane-5-sulfonate (DSS) (Cambridge Isotope Laboratories, Tewksbury, MA) as NMR internal standard. All NMR experiments including 1D ^{1}H and 2D ^{1}H HSQC were performed on an Agilent DD2 14.1 Tesla NMR spectrometer (Agilent Technologies, CA) equipped with a 3 mm inverse triple resonance HCN cryoprobe. All spectra were processed using MNova software (MestreLab, Spain). 1D ^{1}H spectra were acquired with standard PRESAT pulse

sequence at 15 °C with soft pulse pre-saturation on the HOD resonance frequency to suppress water signal. A total of 16,384 data points was acquired with 2 seconds acquisition time, 512 transients, 12 ppm spectral width, and 4 seconds recycle delay time during which water peak was irradiated by soft pulse for suppression. The spectra were then linear predicted and zero filled to 128 k points and apodized with a 1 Hz exponential line broadening function. For quantification, the peak intensities were extracted using the peak-fitting deconvolution method provided by MNova software. The peak intensity of scyllo-inositol resonant at 3.34 ppm were converted into nmoles by calibration against the peak intensity of internal standard DSS (with known quantify of 27.5 nmoles) at 0 ppm. 2D heteronuclear single quantum coherence (HSQC) were acquired to help confirm the peak assignments. The 2D HSQC spectra were recorded with ^{13}C adiabatic decoupling scheme for broad range decoupling during proton acquisition time of 0.25 seconds. 1,796 data points were collected each transient and a total of 16 transients were acquired with 12 ppm spectral width. A total of 256 increments were collected in the carbon F1 dimension with a spectral width of 200 ppm. The HSQC spectra were linear predicted once and zero filled to 4 k data points in the F2 proton dimension and 1 k points in the F1 carbon dimension. The scyllo-inositol peak resonance was at 3.34 ppm in proton dimension and 70.3 ppm in carbon dimension.

2.5   Metabolomics Profiling

For all aims, mouse blood, brain, and cecal contents were collected. The whole blood and brains were then sent to Metabolon (Durham, NC) for metabolomic profile (N = 8/group, M:F = 50/50). The cecal contents and whole blood were sent for SCFA analysis. For the metabolomic profiling, metabolon's standard solvent extraction method was used to prepare the samples, which were then equally split for analysis via liquid chromatography/mass spectrometry (LC/MS) or gas chromatography/mass spectrometry (GC/MS) using their standard protocol [124].

For SCFA analysis in the whole blood (N = 8/group in ng/mL) and cecal contents (N = 8/group in μg/g), 8 SCFAs were analyzed by LC-MS/MS. These were as follows: acetic acid (C2), propionic acid (C3), isobutyric acid (C4), 2-methylbutyric acid (C5), isovaleric acid (C5), valeric acid (C5), and caproic acid (C6). Both sets of samples are stable labelled with internal standards and homogenized in an organic solvent. The samples are then centrifuged followed by an aliquot of the supernatant used to derivatize to form SCFA hydrazides. This reaction mixture is subsequently diluted, and an aliquot is injected into an Agilent 1290/AB Sciex QTrap 5500 LCMS/MS system. This system is equipped with a C18 reversed phase UHPLC column operated in negative mode using electrospray ionization (ESI). The raw data was analyzed by AB SCIEX software (Analyst 1.6.2) with reduction of the data done in Microsoft Excel 2013. Analysis was done in a 96-well plate with two calibration curves and 6-8 quality control

samples per bath. Samples were labeled BLOQ if they fell below the quantitation limit and ALOQ if they fell above the quantitation limit.

For sample preparation of the rest of the samples, each sample was accessioned into a LIMS system, assigned a unique identifier, and stored at -70 ºC. To remove protein, dissociate small molecules bound to protein or trapped in the precipitated protein matrix, and to recover chemically diverse metabolites, proteins were precipitated with methanol, with vigorous shaking for 2 minutes (Glen Mills Genogrinder 2000) as described previously [124, 125]. The resulting extract was divided into four fractions: one for analysis by ultra-high-performance liquid chromatography-tandem mass spectrometry run in positive mode (UPLC-MS/MS+), one for analysis by UPLC-MS/MS run in negative mode (UPLC-MS/MS-), one for analysis by gas chromatography–mass spectrometry (GC-MS), and one aliquot was retained for backup analysis, if needed.

For mass spectrometry analysis, non-targeted UPLC-MS/MS and GC-MS analyses were performed at Metabolon, Inc. as described [124-126]. The UPLC/MS/MS portion of the platform incorporates a Waters Acquity UPLC system and a Thermo-Finnegan LTQ mass spectrometer, including an electrospray ionization (ESI) source and linear ion-trap (LIT) mass analyzer. Aliquots of the vacuum-dried sample were reconstituted, one each in acidic or basic LC-compatible solvents containing 8 or more injection standards at fixed concentrations (to both ensure injection and chromatographic consistency). Extracts were loaded onto columns (Waters UPLC BEH C18-2.1 x 100 mm, 1.7 µm) and gradient-eluted with water and 95% methanol containing

0.1% formic acid (acidic extracts) or 6.5 mM ammonium bicarbonate (basic extracts). The instrument was set to scan 99–1000 m/z and alternated between MS and MS/MS scans.

Samples destined for analysis by GC-MS were dried under vacuum desiccation for a minimum of 18 h prior to being derivatized using bis(trimethylsilyl)trifluoroacetamide (BSTFA) as described [127]. Derivatized samples were separated on a 5% phenyldimethyl silicone column with helium as carrier gas and a temperature ramp from 60° to 340°C within a 17-minute period. All samples were analyzed on a Thermo-Finnigan Trace DSQ fast-scanning single-quadrupole MS operated at unit mass resolving power with electron impact ionization and a 50–750 atomic mass unit scan range. The instrument is tuned and calibrated for mass resolution and mass accuracy daily.

For quality control, all columns and reagents were purchased in bulk from a single lot to complete all related experiments. For monitoring of data quality and process variation, multiple replicates of extracts from a pool of human plasma were prepared in parallel and injected throughout the run, interspersed among the experimental samples. Instrument variability was determined by calculating the median relative standard deviation (RSD) for the standards that were added to each sample prior to injection into the mass spectrometers (median RSD = 4%; n = 21 standards). Overall process variability was determined by calculating the median RSD for all endogenous metabolites (i.e., non-instrument standards) present in 100% of technical replicate samples created from a homogeneous pool containing a small amount of all study

samples (median RSD = 6%; n = 170 metabolites). In addition, process blanks and other quality control samples are spaced evenly among the injections for each day, and all experimental samples are randomly distributed throughout each day's run.

For compound identification, quantification, and data curation, metabolites were identified by automated comparison of the ion features in the experimental samples to a reference library of chemical standard entries that included retention time, molecular weight (m/z), preferred adducts, and in-source fragments as well as associated MS spectra and curated by visual inspection for quality control using software developed at Metabolon [128]. Identification of known chemical entities was based on comparison to metabolomic library entries of more than 2,800 commercially-available purified standards. Subsequent quality control (QC) and curation processes were utilized to ensure accurate, consistent identification and to minimize system artifacts, mis-assignments, and background noise. Library matches for each compound were verified for each sample. Peaks were quantified using area under the curve. Raw area counts for each metabolite in each sample were normalized to correct for variation resulting from instrument inter-day tuning differences by the median value for each run-day, therefore setting the medians to 1.0 for each run. This preserved variation between samples but allowed metabolites of widely different raw peak areas to be compared on a similar graphical scale. Missing values were imputed with the observed minimum after normalization. For bioinformatics, the LIMS system encompasses sample accessioning, preparation, instrument analysis and

reporting, and advanced data analysis. Additional informatics components include data extraction into a relational database and peak-identification software; proprietary data processing tools for QC and compound identification; and a collection of interpretation and visualization tools for use by data analysts. The hardware and software systems are built on a web-service platform utilizing Microsoft's .NET technologies which run on high-performance application servers and fiber-channel storage arrays in clusters to provide active failover and load-balancing.

For metabolite quantification and data normalization, peaks were quantified using area-under-the-curve and a data normalization step for multiple day studies was utilized to correct any variance in instrument inter-day tuning differences. For one day studies, no normalization is necessary except for when accounting for an additional factor to account for any differences in metabolite levels due to differences in amount present in each sample.

For statistical analysis, two types of statistical analyses were performed; significance tests and classification analysis. Statistical analysis is performed in ArrayStudio on log transformed data. For analyses not standard to ArrayStudio, either R or JMP are used. Multiple significance tests and classification methods are used. These include Welch's two-sample t-test, Matched Pairs t-test, one-way ANOVA, two-way ANOVA, and two-way repeated measures ANOVA. Also, correlation, and Hotelling's T2 test were used. For statistical significance testing, p-values and q-values using False Discovery Rate (FDR) were utilized. Finally,

Random Forest, hierarchical clustering, and Principal Components Analysis (PCA) were used.

2.6 Magnetic Resonance Imaging (MRI)

All MRI experiments were performed on a 7T MR scanner (Clinscan, Bruker BioSpin, Germany) at the Magnetic Resonance Imaging & Spectroscopy Center at the UK. A subset of mice were randomly chosen from each group to undergo testing (N = 8-10/group). Mice were anesthetized with 4.0% isoflurane for induction and then maintained in a 1.2% isoflurane and air mixture using a nose cone. Respiration rate (50-80 breaths/minute) and rectal temperature (37 ± 1 °C) were continuously monitored and maintained. T2-weighted structural images were acquired with field of view (FOV) =18 x18 mm^2, matrix = 256 x 256; slice thickness = 1 mm, 10 slices, repetition time (TR) = 1500 ms, and echo time (TE) = 35 ms. Quantitative CBF (with units of mL/g per minute) was measured using MRI-based pseudo-continuous arterial spin labeling (pCASL) techniques [129]. A whole-body volume coil was used for transmission and a mouse brain surface coil was placed on top of the head for receiving. Paired control and label images were acquired in an interleaved fashion with a train of Hanning window-shaped radiofrequency pulses of duration/spacing = 200/200 μs, flip angle = 25° and slice-selective gradient = 9 mT/m, and a labeling duration = 2100 ms [130]. The images were acquired by 2D multi-slice spin-echo echo planner imaging with FOV =18 x18 mm^2, matrix =128 x 128, slice thickness = 1 mm, 10 slices, TR = 4,000 ms, TE = 35 ms, and 120 repetitions. pCASL image analysis was

employed with in-house written codes in MATLAB (MathWorks, Natick, MA) to obtain quantitative CBF [131].

The next MRI technique used is magnetic resonance spectroscopy (MRS), or the measurement of metabolites in vivo [132]. MRS was being conducted in mouse brains, specifically in the hippocampus, with the following metabolites measured: alanine (Ala), total choline (TCho), glutamate-glutamine complex (Glx), myo-inositol (mI), lactate (Lac), NAA, phosphocreatine (PCr), total creatine (TCr), and taurine (Tau). These metabolites are plotted on a graph of signal intensity versus frequency. The following were used for a water-suppressed spectrum to test for these metabolites: TR = 1500 ms, TE = 135 ms, spectral width = 60 Hz, and average = 400. A voxel (2.0 mm x 5.0 mm x 1.3 mm) is placed over the bilateral hippocampus. Next, a non-water suppressed spectra is performed with 10 averages. Both of these spectra will be processed using the LCModel software to find the absolute concentration of the metabolites. To quantify the concentrations of the metabolites, the following equation was utilized: $[m] = (S_m/S_{water})[water]C_nC_{av}$ where $[m]$ is the metabolite concentration, S_m is the metabolite intensity acquired from MRS, S_{water} is the water intensity acquired from MRS, [water] is the concentration of water (55.14mM at 310K), C_n is the correction for the number of equivalent nuclei for each resonance, and C_{av} is the correction for the number of averages [133].

2.7 Amyloid-β Staining

Mouse brains were collected (N = 5/group, M:F = 50/50) upon sacrifice and immediately put into 10% neutral buffered formalin for 24-48 hours. After this time period, the brains were transferred into 90% ethanol. Next, the brains were sent to the COCVD Pathology Research Core at the University of Kentucky to be embedded and sectioned onto microscope slides for immunohistochemistry. The sectioned tissue undergoes rehydration followed by tissue pretreatment in 90% formic acid for 3 minutes. The tissue was then treated with 3% H_2O_2 and 10% methanol for 30 minutes. Next, a M.O.M. Kit (Vector Laboratories, Inc. Burlingame, CA) was used following the standard protocol. Aβ was identified using an anti-Aβ_{1-17} mouse monoclonal 6E10 antibody (1:3000; Signet Laboratories, Dedham, MA). Following this portion of the protocol, a DAB substrate kit (also Vector Laboratories, Burlingame, CA) was used for visualization. Next, a background stain utilizing NISSL was completed followed by dehydration. The slides were next imaged on the Aperio ScanScope XT Digital Slide Scanner System in the University of Kentucky Alzheimer's Disease Center Neuropathology Core Laboratory (20x magnificantion) and uploaded to the online database. Aperio ImageScope (version 12.3.2.8013) was used to analyze total anti-Aβ counted at 20x magnification (0.495px/um). 10 boxes (ROIs that are 600x600x600 microns) were randomly placed in each sample image and counted for percent positive Aβ (number of positive + number of strong positive/total number).

2.8   NanoString Array

For RNA isolation and quantification, dissected hippocampus was processed for RNA isolation following manufacturer's protocol (N = 5/group, all male) (Qiagen RNeasy Plus #74136). Quality and concentration of eluted RNA was measured by Nanodrop. 200ng of total RNA per sample was quantified using a NanoString array that consisted of 561 gene targets (Mouse Immunology v2 CodeSet). Following quality and housekeeping control normalization, there were a total of 318 genes that were above the background threshold.

2.9   Animal Behavior Tests

All behavior tests were conducted over a two-week period with each test starting at the same time each morning (N = 7-9/group, M:F = 50/50). For each mouse, Elevated Plus Maze (EPM) was done first immediately followed by the Open Field Test and the Novel Object Recognition (NOR) test the next day. Radial Arm Water Maze (RAWM) testing was then carried out starting the day after NOR. All tests were carried out in the Rodent Behavior Center at the University of Kentucky.

For elevated plus maze, all mice underwent three behavior tests. The first test is the EPM. We used the EPM to evaluate anxiety of the mice [129, 134]. The EPM consists of two open and two closed arms elevated 100 cm above the floor. Closed arms are perceived as safe zones, and thus mice with higher anxiety had tendency to stay in the closed arms. We determined the anxiety-related behavior by measuring the time spent in the closed arms over the 1-

minute test session by EthoVision XT 8.0 video tracking software (Noldus Information Technology).

For the open field test (OF), activity was recorded with EthoVision XT 8.0 video tracking software (Noldus Information Technology). Each chamber was divided into a central and peripheral zone with the peripheral zone being next to the walls of the chamber. Data was collected for 15 minutes with edge duration being the amount of time the mice spent in the peripheral zone. This test is designed to assess anxiety-like behavior in the mice in response to a new, novel environment [135].

For novel object recognition (NOR), the second behavioral test, used to test spatial recognition memory [136]. This task of recognition memory utilizes the fact that animals will spend more time exploring a novel object compared to an object that they are familiar with in order to satisfy their innate curiosity/exploratory instinct. Mice were given 10 minutes to explore two of the same objects in the "A/A" session. For the 10-minute "A/B" test session, one of the A objects was replaced by a novel object (B). There was a 2-hour delay between the A/A and A/B sessions. The total time mice spend investigating the objects was recorded and scored by the fully automated EthoVision XT 8.0 video tracking software (Noldus Information Technology). The D_2 discrimination index was calculated by: $D_2 = (T_B - T_A) \div (T_B + T_A)$, where T_B is the time spent with the novel object B, and T_A is the time spent with the familiar object A.

The final test is radial arm water maze (RAWM), used to measure both spatial working memory and spatial reference memory [129, 137, 138]. The

RAWM task was conducted as described previously [133], following a 2-day testing paradigm. A staggered training schedule was used, running the mice in cohorts of ten mice, while alternating the different cohorts through the trials over day 1 and day 2 of the test. This alternating protocol was used to avoid the learning limitations imposed by massed sequential trials and to avoid fatigue that may result from consecutive trials. Day 1 is the "learning" phase where mice went through three blocks (Blocks 1-3; 5 trials in each block) to test learning and short-term spatial memory. Day 2 is the "recall" phase where mice went through three additional blocks (Blocks 4-6) to test long-term memory after a 24-hour retention period to locate the platform. It is expected that after the two-day training, the mouse with intact memory can find the platform with minimal errors. Geometric extra-maze visual cues were fixed throughout the study on three sides of the curtains. Visual platform trials were included in the training and were used to determine if visual impairment could be a cofounding variable. Mouse performance was recorded by EthoVision XT 8.0 video tracking software (Noldus Information Technology) data analyzed by the EthoVision software for the number of incorrect arm entries, which are defined as errors. The video was reviewed for each mouse to ensure that the mice did not employ non-spatial strategies, such as chaining, to solve the task.

2.10 Statistical Analysis

All statistical analyses were completed using GraphPad Prism (GraphPad, San Diego, CA, USA). For all chapters, two-sample t-test and 2-way ANOVA was

performed for determination of differences between groups along with Tukey's multiple comparisons test. For Metabolon, log transformations were conducted followed by ANOVA for identification of biochemicals that were significantly different between groups. Between group differences were assessed using p-value and q-value, or false discovery rate. For the NanoString Array analysis, data are plotted as the mean ratio expression with their respective adjusted p-value (Benjamini-Hochberg corrected). Further, 2-way ANOVA was used along with Sidak posthoc multiple comparisons correction for the individual genes.

Chapter 3 Specific Aim 1: To identify the effects of the prebiotic inulin on the gut microbiota and induced metabolism changes thereof between E3FAD and E4FAD mice.

3.1 Summary

The gut microbiota plays a profound role on the host and recently, this has been found true in the brain and in neurological diseases such as AD. The differences between the gut microbiota and effects of consuming the prebiotic inulin on APOE3 and APOE4 carriers is unknown. PURPOSE: The purpose of this aim to identify the effects of the prebiotic inulin on the gut microbiota and induced metabolism changes thereof between E3FAD and E4FAD mice. RESULTS: Firstly, mice bodyweight and food intake were not changed due to the prebiotic diet, however, E3FAD and E4FAD mice fed the prebiotic inulin had a significantly larger cecum than control fed mice. In the cecal contents, both E3FAD and E4FAD fed the prebiotic inulin had significantly increased SCFAs but decreased isobutyrate. Next, our fecal culture experiment found an increase in scyllo-inositol in the inulin cultures compared to controls. In both the cecal contents and fecal culture, the E3FAD mice had a larger production of the aforementioned metabolites compared to the E4FAD mice. Further, the prebiotic inulin fed E3FAD mice altered the gut microbiota via decreased α-diversity, significantly different β-diversity, and increased beneficial and SCFA producing taxa, and decreased deleterious bacterial taxa. The E4FAD mice fed the prebiotic inulin saw more modest differences compared to the control fed mice with the gut microbiota showcasing a significantly different β-diversity, but not α-

diversity, and also increased levels of beneficial taxa at the genus level. However, there were no differences due to the FAD mutations. CONCLUSIONS: To conclude, the prebiotic inulin beneficially impacted the host through increased production of beneficial metabolites such as the SCFAs and scyllo-inositol along with increasing beneficial taxa and decreasing deleterious taxa However, the E3FAD mice and E4FAD mice fed the prebiotic inulin showcased variation in the aforementioned outcomes as E3FAD mice appeared to gain more benefit due to the prebiotic inulin than did the E4FAD mice. Due to this, we believe prebiotics can be a beneficial and translatable nutritional intervention to improve gut health but taking genetics into account is highly warranted.

3.2   Introduction

The gut microbiota, or the trillions of bacteria in our gut, play a profound role on our health [42]. Indeed, the gut microbiota has been demonstrated to beneficially impact the host a variety of ways including through the immune system [139]. Recently, the bi-directional communication between the gut and the brain, or gut-brain axis (GBA), has become a topic of intense investigation [140]. Indeed, it appears the gut microbiota plays a role in anxiety and depression [141], and in other neurological disorders such as AD [142]. Recent work has found that AD patients have a distinct gut microbiota compared to controls [143] with alterations also seen in an AD mouse model [144]. Further, Harach et al. found that in an AD mouse model, the germ-free mice had less amyloid pathology than those that actually had a gut microbiota [41]. It is worth

noting that studies by Oria et al. have found human APOE4 carriers to have protection from diarrhea in early childhood, providing a survival advantage [39]. Further, in favela children in Northeast Brazil, this group found that APOE4 was protective against cognitive deficits due to enteric infections and diarrhea [145]. Due to this, we believe that our E3FAD and E4FAD mice will show a vastly different response to the prebiotic inulin and metabolites produced but in both, beneficial modulation of the gut microbiota by the prebiotic inulin could help prevent AD-like symptoms.

Using prebiotics such as inulin may be used as a preventative measure in combating AD. Indeed, prebiotics are, as stated by one source, "a selectively fermented ingredient that allows specific changes, both in the composition and/or activity in the gastrointestinal microflora that confers benefits upon host well-being and health [146]." Prebiotics must resist upper gastrointestinal (GI) enzymes, be fermented in the lower GI, and selectively stimulate the growth of beneficial bacteria [147]. Further, during the fermentation of prebiotics, beneficial metabolites are produced such as the short chain fatty acids (SCFAs) butyrate, acetate, and propionate, demonstrated to beneficially impact the brain [148, 149]. The prebiotic chosen for this project is inulin, derived from chicory root, but also found in other vegetables, fruits, and grains. Inulin is quite possibly the most well studied prebiotic and is well known for its numerous beneficial properties including increased mineral absorption, decreased inflammatory bowel syndrome (IBS) scores, and reduced cholesterol [101, 103]. Further, the prebiotic inulin has been demonstrated to increase the size of the cecum, which is thought to

indicate increased fermentation of beneficial metabolites and microbial content [150, 151]. We believe that using the prebiotic inulin to beneficially modulate the gut microbiota in E3FAD and E4FAD mice will lead to a change in metabolism via an increase in the fermentation of beneficial metabolites that could potentially help prevent AD pathology.

The objective of this aim was to identify the effect of the prebiotic inulin and changes in the metabolism thereof between E3FAD and E4FAD mice. We hypothesized that the prebiotic inulin will beneficially modulate the gut microbiota and increase metabolite production in E3FAD and E4FAD mice. Specifically, we examined the body weight, food intake, and cecum weight of the mice along with an examination of the gut microbiota and its taxonomy in 16S rRNA sequencing and metabolites produced in the cecal contents and in fecal bacterial culture.

3.3 Results

3.3.1 Body Weight and Food Intake

Table 3.1 demonstrates the diet composition of the prebiotic and vehicle control diets with the prebiotic diet containing 8% fiber from inulin and the vehicle control diet containing 8% fiber from cellulose. E3FAD and E4FAD were fed either the prebiotic or control diet for 4-months beginning at 3-months of age. To ensure the prebiotic diet did not alter bodyweight and food intake in the mice, bodyweight and food intake were measured biweekly and compared between groups. E3FAD and E4FAD mice that were fed the prebiotic diet saw no

significant differences in body weight (Fig. 3.1a) or food intake (Fig. 3.1b) compared to control fed mice.

3.3.2 Cecum Weight and Cecal Metabolites

The cecum, with cecal contents intact, was weighed upon sacrifice when the mice were around 7-months of age. The cecal contents of the mice were then collected and sent to Metabolon (Durham, NC) for metabolomics profiling via LC-MS/MS. Due to the increased fermentation potential of the prebiotic inulin, we expected a change in cecum size between prebiotic and control fed mice. Indeed, mice that were fed the prebiotic inulin saw a drastically significant increase in cecum size compared to control fed mice in both E3FAD and E4FAD mice with an even greater increase seen in the E3FAD mice. Thus, we believed cecal metabolite production may vary between groups with mice fed the prebiotic inulin seeing more production. Indeed, both E3FAD and E4FAD mice fed the prebiotic inulin saw a significant increase in butyrate (Fig. 3.3b), acetate (Fig. 3.3c), and propionate (Fig. 3.3d) but a decrease in isobutyrate (Fig. 3.3e). Further, the E3FAD mice saw a significantly greater increase in cecal propionate compared to the E4FAD mice fed the prebiotic inulin. The full results of short chain fatty acids is in Table 3.2. Overall, these results indicate that the prebiotic inulin causes an increase in fermentation in the cecum leading to a larger cecum and more beneficial metabolite production with an even greater increase seen in E3FAD mice, perhaps due to bacterial composition of E3FAD mice better able to produce SCFAs.

3.3.3 Scyllo-Inositol in Fecal Bacterial Culture

To confirm that scyllo-inositol is indeed formed from gut microbiota bacteria, fecal samples from 7-month old E3FAD and E4FAD mice on a standard chow diet were collected and pooled into their respective groups and fecal cell suspensions were made under anaerobic conditions. The samples were given either inulin or a control, glucose, for 24 or 48 hours at which point the supernatant was collected and measured for scyllo-inositol via NMR. When inulin was added, scyllo-inositol formation was increased compared to the cultures that were only given glucose in both E3FAD and E4FAD mice, albeit only significantly in the E3FAD mice (Fig. 3.2a). However, the E3FAD fecal culture saw a much greater increase in scyllo-inositol compared to the E4FAD fecal culture (Fig. 3.2a). These results indicate that the prebiotic inulin does indeed increase scyllo-inositol formation in the gut microbiota in both E3FAD and E4FAD mice. Whether this change is due to inulin increasing proliferation of scyllo-inositol creating bacterial taxa or for other reasons remains to be determined. Further, E3FAD and E4FAD appear to have a different gut microbiota that impacts levels of scyllo-inositol production, a consideration that needs to be given to future studies and for carriers of these specific alleles.

3.3.4 Gut Microbiota Diversity and Taxonomy

To determine the differences in the gut microbiota between groups fed the prebiotic and control diet along with differences in E3FAD and E4FAD mice, fecal

samples were collected from each mouse upon reaching 7-months of age followed by DNA extraction and amplification. The DNA was then utilized for 16S rRNA sequencing and subsequent diversity and taxonomy analysis. For gut microbiota analysis in E3FAD mice, α-diversity, a measure of the diversity within a sample by measuring the richness and evenness of that sample, was measured via the Shannon Diversity Index, H value, for fecal microbial communities at the genus taxonomic level. A higher H value indicates a more diverse community within that particular sample. A significant decrease was seen in E3FAD mice fed the prebiotic inulin compared to the control group (Gausian link function results, $p < 0.0001$) (Fig. 3.4a). Next, β-diversity, a measure of the diversity of taxonomic abundance between different samples, was measured via the Bray-Curtis dissimilarity index at the genus taxonomic level. E3FAD mice fed the prebiotic inulin saw a significant difference in β-diversity compared to the controls (Fig. 3.4b) (ANOSIM R statistic = 0.877, p-value = 0.001). For E4FAD mice, no difference was seen in α-diversity (Gausian link function results, $p = 0.418$) (Fig. 3.4c) but a significant difference was observed in β-diversity (ANOSIM R statistic = 0.454, p-value = 0.001) (Fig. 3.4d). Significant changes in taxa were observed in numerous bacterial taxa due to the prebiotic inulin. In E3FAD mice fed the prebiotic inulin compared to the controls, a significant increase was seen in notable taxa at the genus level such as *Bifidobacterium*, *Lactobacillus*, *Escheridia*, *Allobaculum*, and *Prevotella* (Table 3.2). Moderate increases were seen in *Akkermansia* and *Mucispirillum*. In contrast, *Bacteroides*, *Turicbacter*, rc4-4, *Oscillospira*, and *Dehalobacterium* were decreased. At the

54

phylum level, Tenericutes were decreased in E3FAD mice fed the prebiotic inulin while Actinobacteria was increased. In E4FAD mice fed the prebiotic inulin at the genus level, notable taxa were increased such as *Prevotella*, *Lactobacillus*, and *Mucispirillum*. In contrast, *Akkermansia*, *Escheridia*, *Parabacteroides*, *Turibacter*, *SMB53*, *AF12*, and *Dehalobacterium* were decreased. No significant changes were present at the phylum level. There were also no notably significant differences due to the FAD mutations (Genotype). These results indicate that the prebiotic inulin alters the gut microbiota in E3FAD and E4FAD mice in, what we believe, a beneficial manner, despite a decrease in α-diversity in the E3FAD mice, but by increasing beneficial taxa. However, it appears the fermentation capabilities of E3FAD and E4FAD mice differ and this impacts the number of beneficial metabolites produced.

3.4   Discussion

Firstly, we see that the prebiotic inulin, 8% fiber from inulin, does not impact food intake and bodyweight in our mice compared to our control mice, 8% fiber from cellulose. Other studies have found similar results [152]. It is notable that inulin contains more kcal/g than cellulose, but the extra kcal/g may be consumed by the gut bacteria during fermentation. Nonetheless, this data helps us be rid of potential confounding factors that may be due to changes in body weight.

Our work found that feeding the prebiotic inulin increased cecum size in our mice, especially so in E3FAD mice. Previous studies using the prebiotic inulin

have also found increases in cecum size [152, 153]. This is likely due to the cecum being the primary site of inulin fermentation [150, 151]. Kuo et al. also postulated that this may also indicate increased microbial content [152]. We believe this increase in fermentation may lead to increased production of beneficial metabolites, which is precisely what we saw with the SCFAs acetate, butyrate, and propionate. Interestingly, propionate was even more significantly increased in the E3FAD group fed the prebiotic inulin compared to the E4FAD group fed the prebiotic inulin. However, isobutyrate was decreased in the E3FAD and E4FAD mice fed the prebiotic inulin compared to their respective controls for unknown reasons likely related to bacterial SCFA metabolism. Nonetheless, the dramatic increase in SCFAs due to the prebiotic inulin does indeed confirm other studies that inulin increases SCFA levels [112, 154]. Whether the increased levels of SCFAs reached the periphery will be explored in the next chapter.

Next, we demonstrate with our fecal culture experiment that the prebiotic inulin can increase scyllo-inositol production in the fecal microbiota. We can confirm that the production of scyllo-inositol does indeed come from the gut microbiota due to inulin feeding but we are unsure how exactly this occurs. To our knowledge, only one particular bacterial species has been identified to produce scyllo-inositol, *Bacillus subtilis* [155]. This taxon appears to produce scyllo-inositol from myo-inositol, the more common stereoisomer of scyllo-inositol found in foods such as fruits, beans, and nuts [156]. However, we do not understand why the taxon would generate the metabolite from myo-inositol or excrete the metabolite as opposed to using it as a carbon source. We also did

not see this bacterial species in our gut microbiota data. Nevertheless, we suspect that numerous other bacterial taxa increase scyllo-inositol production due to the prebiotic inulin as it is stimulating the growth of certain bacterial taxa that can produce this metabolite, increasing its production compared to the control. Interestingly, a study in inulin fed rats found that scyllo-inositol levels were dramatically increased in the myocardium and testes, although the reasons why were not understood [157]. It would appear that scyllo-inositol could be increased in numerous organs, not just the brain. Interestingly, our results demonstrate that the fecal microbiota of the E3FAD mice given inulin were able to produce much more scyllo-inositol at the 24- and 48-hour time points than the E4FAD mice given either inulin or the control. In fact, the E4FAD mice given inulin only saw an insignificant increase in scyllo-inositol at the 48-hour mark but at still considerably lower amounts than the E3FAD mice given the inulin at either timepoint. This indicates, similar to what we saw with the SCFAs of the cecal contents, that E3FAD mice are able to produce more beneficial metabolites than the E4FAD mice, probably due to better fermentation capacity. Thus, future work on identifying which bacterial taxa produce this and other metabolites and why the amounts may vary should be taken into consideration as these metabolites could potentially impact the brain and other organs in a therapeutic manner.

Although research on scyllo-inositol is fairly scarce, some studies have demonstrated that scyllo-inositol in the brain is the highest source in the body [158] as it can pass through the blood brain barrier [159]. In fact, it increases in the brain as we age [160], may beneficially impact GLUT4 translocation in

muscle [161], and that it could be disturbed in certain disease states such as in chronic alcoholism [162] and even AD [163]. Indeed, scyllo-inositol has been demonstrated to inhibit Aβ aggregation in in vivo and in vitro trials [159, 164-167]. It is still not particularly understood how exactly the metabolite inhibits the aggregation of Aβ, but it is thought it may cap off a plaque and inhibit further aggregation and growth. However, it does not appear to break the plaques up [168]. This would indicate that scyllo-inositol would work best as a preventative measure before plaques have already or just recently formed. When comparing scyllo-inositol to its much more common and ubiquitous stereoisomer form myo-inositol, scyllo-inositol proved to be more effective at inhibiting Aβ in an AD mouse model. In this study by McLaurin et al., they demonstrated that not only did their transgenic AD mice have a decrease in soluble and insoluble Aβ due to scyllo-inositol treatment, but they also had amelioration of memory deficits and a decrease in neuroinflammation, likely a consequence of Aβ inhibition [165]. Further in this study, they found that treatment in both younger, disease-free mice along with older mice with AD pathology, both saw significant benefits. In humans, clinical trials using scyllo-inositol as an orally administered fast track designation have been conducted. Unfortunately, in mild to moderate AD patients, the high dose scyllo-inositol (1000mg and 2000mg) groups saw increased kidney issues and thus, were discontinued. The lower dose group (250mg) did see a significant increase in brain ventricular volume and cerebral spinal fluid Aβ-42 but overall, the trial did not find significance in the primary clinical outcome [169].

In the gut microbiome, many significant differences were seen. Typically, an increased α-diversity is thought to be beneficial [170], however, in our study we found that the prebiotic fed mice had a decrease in α-diversity compared to controls. Previous work by our lab and others have also found a decrease in diversity with improvements in other outcomes [171-173]. This may indicate that the prebiotic inulin stimulates the growth of only certain beneficial taxa, decreasing diversity and deleterious taxa, but overall, still increasing the health of the gut microbiota. We believe this to be the case in the E3FAD mice as the prebiotic inulin did indeed decrease α-diversity compared to the control mice although the E4FAD mice did not see as significant a difference. Further, both E3FAD and E4FAD saw a significant difference in β-diversity, indicative of the powerful impact the prebiotic inulin has on the gut microbiota.

Next, we explored the differences in bacterial taxa that the prebiotic inulin made in both E3FAD and E4FAD mice. We found that E3FAD mice fed the prebiotic inulin demonstrated a significant increase in taxa at the genus level such as *Bifidobacterium*, *Lactobacillus*, *Escheridia*, *Allobaculum*, and *Prevotella* compared to controls. In contrast, *Bacteroides*, *Turicibacter*, *rc4-4*, *Oscillospira*, and *Dehalobacterium* were decreased. Interestingly, the prebiotic inulin increased both *Bifidobacterium* and *Lactobacillus*. Due to inulin being a prebiotic, it is expected that *Bifidobacterium* and perhaps even *Lactobacillus* would be increased, both of which are fairly well studied and benefit the host through immunomodulation and emotional behavior, among other things [88, 174]. Meanwhile, *Prevotella* seems to proliferate on complex carbohydrates such as

59

inulin and has even been associated with improved glucose metabolism in a study using barley kernels, a dietary fiber [175]. One notable bacterial genera that was decreased was *Bacteroides*, a taxa that appears to act as both commensal and virulent, perhaps depending on the amount present [176]. At the phylum level, Tenericutes were decreased in E3FAD mice fed the prebiotic inulin while Actinobacteria was increased. One study has also found a decrease in Tenericutes due to inulin although the impact of this phylum is not well understood [177]. Further, the Actinobacteria phylum was also found to be moderately increased in this same study but has been previously associated with obesity [178]. Notably, this phylum does house the genus *Bifidobacterium*. Oddly, the E4FAD mice found no such changes in phylum level. However, the E4FAD mice fed the prebiotic inulin did show many differences at the genus level. Notable taxa that were increased included *Prevotella*, *Lactobacillus*, and *Mucispirillum*, all also increased in the E3FAD mice as well. In contrast, *Akkermansia*, *Escheridia*, *Parabacteroides*, *Turibacter*, *SMB53*, *AF12*, and *Dehalobacterium* were decreased in the E4FAD mice. *Akkermansia* is a beneficial taxa with numerous known benefits [179], the decrease shown here would be seen as a negative consequence especially as the E3FAD mice actually saw a moderate increase in *Akkermansia*. *Bifidobacterium* was also not increased in the E4FAD mice, another negative consequence. Further, *SMB53* has been decreased by fermentation in one study using prebiotics [180] while little is known about the other decreased taxa. Collectively, although there were similarities in taxa that the prebiotic inulin was able to increase and decrease

60

between E3FAD and E4FAD mice, there were also many differences, particularly in *Akkermansia* and *Bifidobacterium*, leading us to believe that genetic factors may indeed impact the gut microbiota and how the host responds to the presence of a beneficial prebiotic such as inulin. However, it is also worth noting that many of the significantly different taxa in our project have little information associated to them, a limitation of all gut microbiota research as we have much to learn on this topic and their impact on the host. Surprisingly, we did not see any differences in the gut microbiota due to the FAD mutations despite literature suggesting there may be differences [41].

Altogether, the prebiotic inulin was able to increase cecum size and the fermentation of beneficial metabolites such as SCFAs and scyllo-inositol with the latter produced by the fecal microbiota, demonstrating that the fecal microbiota is indeed able to produce this metabolite. The prebiotic inulin also leads to beneficial modulation of the gut microbiota as evidenced by the increased number of beneficial taxa present. Interestingly, the E3FAD mice had a larger cecum, produced more beneficial metabolites, and appeared to gain more benefit in the gut microbiota compared to E4FAD mice. As far as we know, this is the first time that genetic differences have been shown to impact cecum size, metabolite production, and the response to the prebiotic inulin. Whether these beneficial outcomes by the prebiotic inulin are able to reach and benefit the periphery and brain will be explored in subsequent chapters.

Table 3-1 Diet composition

Diet	Prebiotic Diet	Vehicle Control Diet
Protein %	18.2	18.2
Carbohydrate %	67.8	60.2
Fat %	7.1	7.1
Fiber %	8.0 (Inulin)	8.0 (Cellulose)
Energy (kcal/g)	4.08	3.78

Table 3-1 Diet composition

      The diet composition of the prebiotic and vehicle control diet. The prebiotic diet contains 8% fiber from inulin while the vehicle control diet contains 8% fiber from cellulose.

Figure 3-1 Food intake and body weight
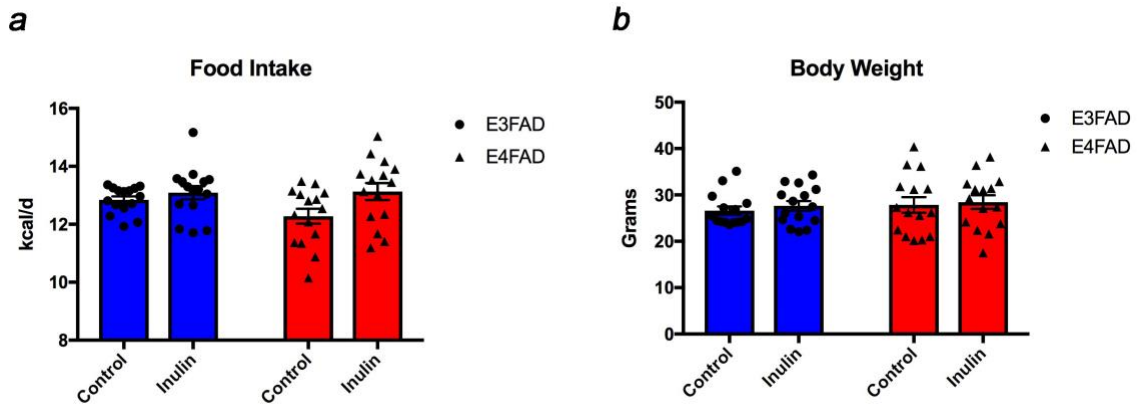
Figure 3-1 Food intake and body weight.

Food intake and body weight of E3FAD and E4FAD mice fed either the prebiotic or control diet for 4-months beginning at 3-months of age. **a** Inulin fed mice had no differences in food intake. **b** Inulin fed mice had no differences in body weight. Statistics were completed using 2-way ANOVA (N = 15/group, M:F = 50/50). Error bars show mean ± SEM.

Figure 3-2 Cecum weight and cecal metabolites
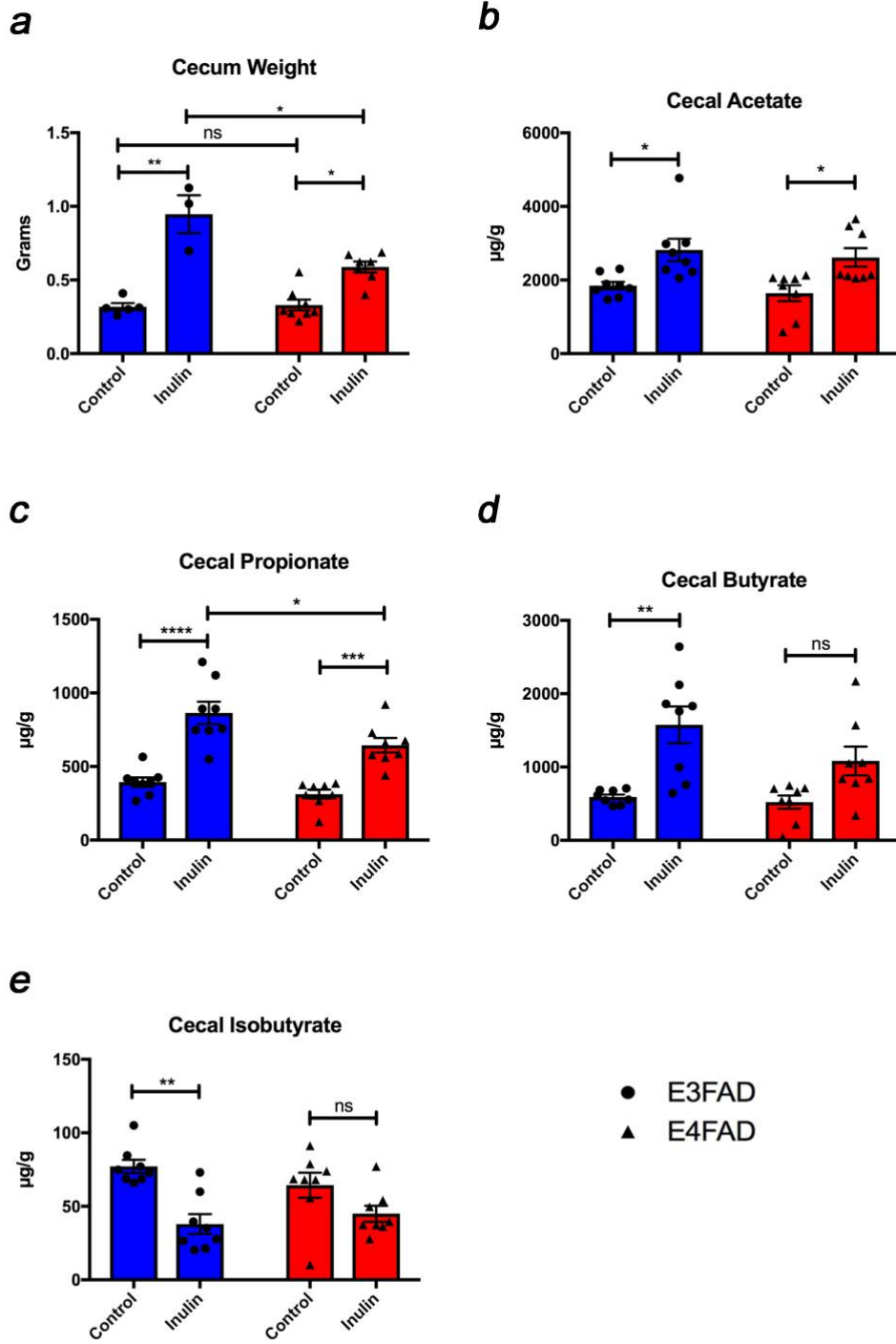
Figure 3-2 Cecum weight and cecal metabolites

Cecum weight and cecal metabolites. The cecum, with cecal contents intact, was weighed upon sacrifice when the mice were around 7-months of age. The cecal contents of the mice were then collected and sent to Metabolon (Durham, NC) for metabolomics profiling via LC-MS/MS. For more details, see Chapter 2, section 2.5. **a** Both E3FAD and E4FAD mice fed inulin saw a significant increase in cecum weight. Similarly, the cecal contents of both E3FAD and E4FAD inulin fed mice saw a significant increase in **b** acetate, **c** propionate, and **d** butyrate but a decrease in **e** cecal isobutyrate. Statistics were completed using 2-way ANOVA (N = 6-8/group, M:F = 50/50). Error bars show mean ± SEM, ns = not significant; *$p < 0.05$; **$p < 0.01$, ***$p < 0.001$; ****$p < 0.0001$.

Table 3-2 Cecal metabolites – short chain fatty acids

Short Chain Fatty Acids	E3FAD Control	E3FAD Inulin	E4FAD Control	E4FAD Inulin
Cecal Contents	Concentration Mean (µg/g)	Concentration Mean (µg/g)	Concentration Mean (µg/g)	Concentration Mean (µg/g)
Acetic Acid	1848 ± 106.1	2817.5 ± 305.4*	1642 ± 213	2614 ± 251.9*
Propionic Acid	394.1 ± 31.6	864 ± 76.2*	312.3 ± 30.7	644.3 ± 50.4*[a]
Isobutyric Acid	77.2 ± 4.5	37.95 ± 6.8*	64.3 ± 8.5	44.9 ± 5.4
Butyric Acid	590.9 ± 33.3	1575.9 ± 249.4*	521.4 ± 91.1	1083 ± 197.1*
2-Methylbutyric Acid	47.9 ± 3.8	37.96 ± 7.8	36.7 ± 4.8	39.3 ± 5.5
Isovaleric Acid	47.8 ± 6.5	24.73 ± 8.1*	43.5 ± 7.4	26.3 ± 2.7*
Valeric Acid	78 ± 11.8	70.58 ± 14.4	73.5 ± 12	65.7 ± 3.3
Hexanoic Acid	2.3 ± 0.3	2.81 ± 1.4	1.9 ± 0.4	1.8 ± 0.2

Table 3-2 Cecal metabolites – short chain fatty acids.

      The prebiotic inulin altered short chain fatty acid production in the cecal contents. Acetic acid, propionic acid, and butyric acid were significantly increased in the E3FAD and E4FAD mice fed the prebiotic inulin compared to their respective controls. In contrast, isobutyric acid and isovaleric acid were significantly decreased. Further, propionic levels in the E4FAD mice fed the prebiotic inulin were significantly decreased compared to E3FAD mice fed the prebiotic control. Statistics were completed using 2-way ANOVA (N = 8/group) with data presented as mean $\pm$ SEM. *$p < 0.05$ comparing E3FAD and E4FAD mice fed the prebiotic inulin to their control fed counterparts; [a]$p < 0.05$ comparing E4FAD mice fed the prebiotic inulin to E3FAD mice fed the prebiotic inulin.

Figure 3-3 Scyllo-inositol fecal culture experiment
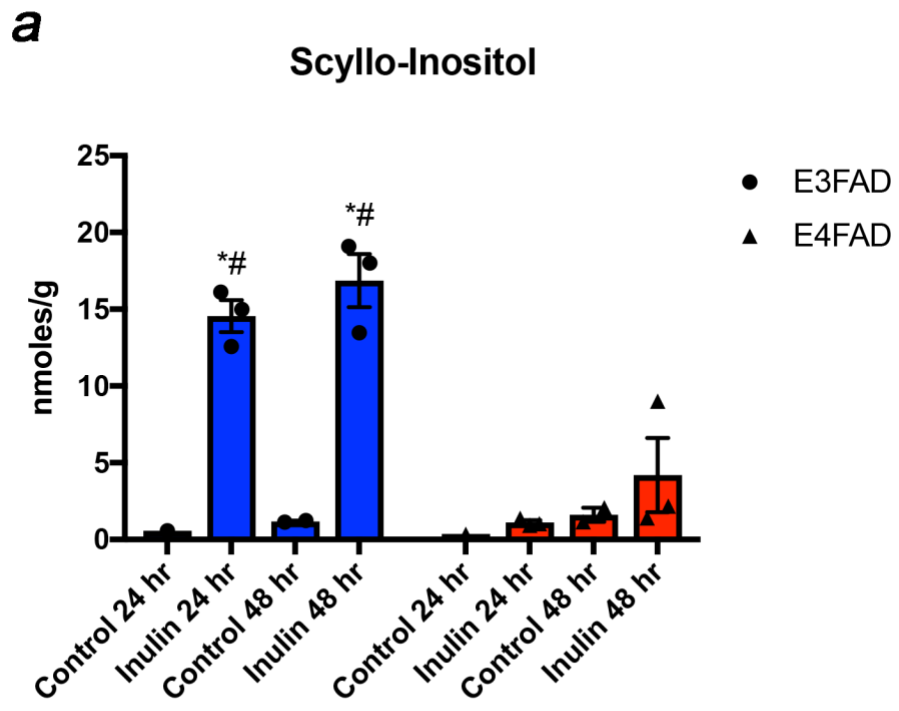
Figure 3-3 Scyllo-inositol fecal culture experiment

Scyllo-inositol levels in fecal culture. Fecal samples of 7-month old E3FAD and E4FAD mice (M:F = 50/50) on a standard chow diet were collected and pooled into their respective groups and fecal cell suspensions were made under anaerobic conditions. The samples were given either inulin or a control, glucose, for 24 or 48 hours at which point the supernatant was collected and measured for scyllo-inositol via NMR. For more details, see Chapter 2, section 2.2. **a** In fecal culture, bacteria from the E3FAD mice that were given inulin saw significant increases in scyllo-inositol compared to those that received the control while bacteria from E4FAD mice saw an insignificant increase. The E3FAD inulin culture samples saw a significantly greater increase in scyllo-inositol when compared to the E4FAD inulin culture samples. Statistics were completed using 2-way ANOVA (groups were run in triplicate). Error bars show mean ± SEM, * $p <$ 0.001 between conditions, # $p < 0.05$ between groups.

Figure 3-4 Gut microbiota diversity

a - E3FAD α-diversity, p < 0.0001

b - E3FAD β-diversity, p = 0.001

c - E4FAD α-diversity, p = 0.418

d - E4FAD β-diversity, p = 0.001
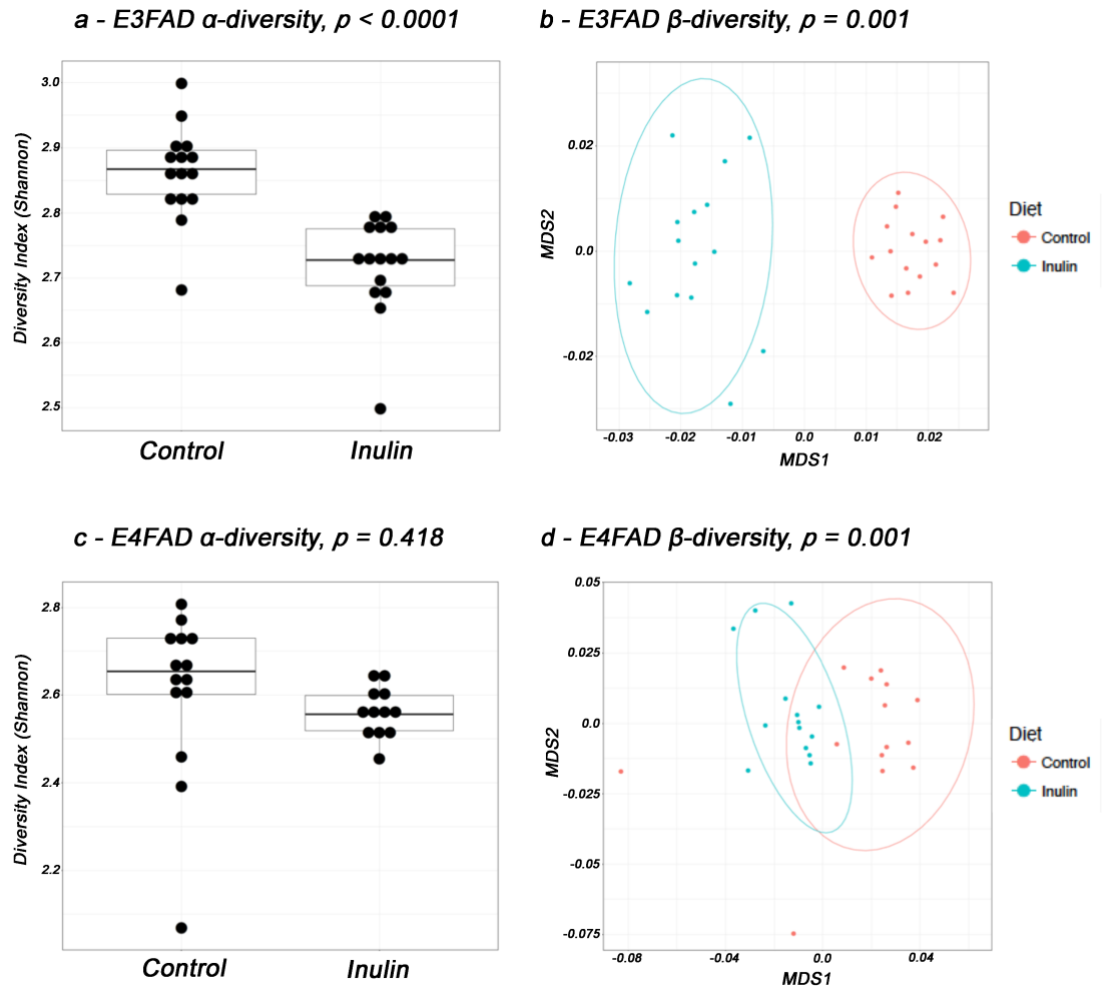
Figure 3-4 Gut microbiota diversity

E3FAD and E4FAD α- and β-diversity. Fecal samples were collected from each mouse upon reaching 7-months of age followed by DNA extraction and amplification. The DNA was then shipped to UIC for 16S rRNA sequencing and subsequent diversity and taxonomy data analysis. For more details, see Chapter 2, section 2.3. E3FAD mice fed the prebiotic inulin saw a significant difference in **a** α- (Gausian link function results, p = 0.00000943) and **b** β-diversity (ANOSIM R statistic = 0.877, p-value = 0.001). E4FAD saw no difference in **c** α- (Gausian link function results, p = 0.418) but a significant difference in **d** β-diversity (ANOSIM R statistic = 0.454, p-value = 0.001) (N = 15/group, M:F = 50/50).

Table 3-3 Gut microbiota taxonomy

Observation - Genus Level	Diet: PValue	Diet: QValue	Genotype: PValue	Genotype: QValue	Inulin(+)/Control(+): logFC	Inulin(+)/Control(+): logCPM	Inulin(+)/Control(+): PValue	Inulin(+)/Control(+): QValue	Inulin(-)/Control(-): logFC	Inulin(-)/Control(-): logCPM	Inulin(-)/Control(-): PValue	Inulin(-)/Control(-): QValue
E3FAD												
k__Bacteria;p__Actinobacteria;c__Actinobacteria;o__Bifidobacteriales;f__Bifidobacteriaceae;g__Bifidobacterium	5.37E-08	2.20E-06	0.91	0.96	2.10	13.07	1.65E-08	2.26E-07	1.85	12.85	3.41E-06	3.49E-05
k__Bacteria;p__Firmicutes;c__Bacilli;o__Turicibacterales;f__Turicibacteraceae;g__Turicibacter	1.73E-07	2.96E-06	0.12	0.61	-2.11	14.91	4.90E-10	2.01E-08	-1.51	15.38	2.27E-04	1.23E-03
k__Bacteria;p__Firmicutes;c__Clostridia;o__Clostridiales;f__Peptococcaceae;g__rc4-4	2.48E-07	2.96E-06	0.80	0.94	-2.79	12.17	1.76E-06	1.44E-05	-2.33	12.16	2.66E-07	7.03E-06
k__Bacteria;p__Tenericutes;c__Mollicutes;o__RF39;Other;Other	2.88E-07	2.96E-06	0.68	0.94	-1.27	13.42	4.69E-07	4.81E-06	-1.13	13.20	3.02E-06	3.49E-05
k__Bacteria;p__Bacteroidetes;c__Bacteroidia;o__Bacteroidales;f__Bacteroidaceae;Other	2.96E-06	2.43E-05	0.18	0.68	1.09	12.94	1.36E-04	6.99E-04	0.78	13.02	2.40E-04	1.23E-03
k__Bacteria;p__Firmicutes;c__Clostridia;o__Clostridiales;f__Dehalobacteriaceae;g__Dehalobacterium	3.64E-06	2.49E-05	0.13	0.61	-1.91	10.85	9.49E-09	1.95E-07	-1.14	11.39	0.01	0.03
k__Bacteria;p__Proteobacteria;c__Gammaproteobacteria;o__Enterobacteriales;f__Enterobacteriaceae;g__Escherichia	6.50E-05	3.81E-04	0.07	0.57	2.52	11.57	9.32E-05	5.46E-04	1.98	12.25	1.65E-03	5.20E-03
k__Bacteria;p__Firmicutes;c__Bacilli;o__Lactobacillales;f__Lactobacillaceae;g__Lactobacillus	1.89E-04	9.69E-04	0.39	0.94	1.21	16.22	8.33E-04	3.80E-03	1.20	16.49	7.62E-04	3.22E-03
k__Bacteria;p__Bacteroidetes;c__Bacteroidia;o__Bacteroidales;f__[Paraprevotellaceae];g__[Prevotella]	2.43E-04	1.11E-03	0.60	0.94	1.48	12.54	3.53E-06	2.41E-05	1.82	13.02	1.36E-03	4.65E-03
k__Bacteria;p__Bacteroidetes;c__Bacteroidia;o__Bacteroidales;f__Rikenellaceae;Other	1.90E-03	7.77E-03	0.27	0.84	-0.65	15.97	5.99E-03	0.02	-0.85	15.94	5.68E-06	4.66E-05
k__Bacteria;p__Firmicutes;c__Clostridia;o__Clostridiales;Other;Other	3.89E-03	0.01	0.58	0.94	0.58	16.90	0.03	0.07	0.28	16.79	0.23	0.36
k__Bacteria;p__Firmicutes;c__Clostridia;o__Clostridiales;f__Ruminococcaceae;g__Oscillospira	3.90E-03	0.01	7.49E-03	0.31	-0.79	15.41	8.19E-03	0.03	-6.38E-03	14.95	0.98	0.98
k__Bacteria;p__Firmicutes;c__Erysipelotrichi;o__Erysipelotrichales;f__Erysipelotrichaceae;g__Allobaculum	6.38E-03	0.02	0.35	0.94	0.56	14.36	0.03	0.08	0.74	14.63	7.86E-04	3.22E-03
k__Bacteria;p__Bacteroidetes;c__Bacteroidia;o__Bacteroidales;f__Bacteroidaceae;g__Bacteroides	7.23E-03	0.02	0.83	0.94	-0.62	15.31	0.01	0.04	-0.52	15.28	8.03E-03	0.02
k__Bacteria;p__Bacteroidetes;c__Bacteroidia;o__Bacteroidales;f__Prevotellaceae;Other	8.49E-03	0.02	0.78	0.94	0.56	10.71	0.03	0.07	0.26	10.56	0.33	0.44
k__Bacteria;p__Bacteroidetes;c__Bacteroidia;o__Bacteroidales;f__S24-7;Other	8.86E-03	0.02	0.44	0.94	0.38	18.05	0.08	0.14	0.29	18.05	0.13	0.22
k__Bacteria;p__Proteobacteria;c__Deltaproteobacteria;o__Desulfovibrionales;f__Desulfovibrionaceae;g__Desulfovibrio	8.89E-03	0.02	0.51	0.94	1.35	11.42	0.03	0.07	2.53	11.96	3.43E-07	7.03E-06
k__Bacteria;p__Actinobacteria;c__Coriobacteriia;o__Coriobacteriales;f__Coriobacteriaceae;Other	9.28E-03	0.02	0.66	0.94	0.76	10.95	0.04	0.08	1.18	11.35	4.98E-05	3.40E-04
k__Bacteria;p__Firmicutes;c__Clostridia;o__Clostridiales;f__Ruminococcaceae;Other	0.01	0.03	0.48	0.94	-0.52	14.10	0.02	0.06	-0.27	13.94	0.20	0.32
k__Bacteria;p__Bacteroidetes;c__Bacteroidia;o__Bacteroidales;f__[Odoribacteraceae];Other	0.02	0.05	0.91	0.96	-0.94	10.90	0.02	0.06	-1.07	10.67	7.46E-03	0.02
k__Bacteria;p__Deferribacteres;c__Deferribacteres;o__Deferribacterales;f__Deferribacteraceae;g__Mucispirillum	0.04	0.07	0.40	0.94	0.45	14.71	0.07	0.12	0.28	14.76	0.28	0.40
k__Bacteria;p__Firmicutes;c__Clostridia;o__Clostridiales;f__Clostridiaceae;Other	0.04	0.07	0.90	0.96	-0.82	13.02	0.04	0.09	-1.07	12.89	1.79E-03	5.25E-03
k__Bacteria;p__Verrucomicrobia;c__Verrucomicrobiae;o__Verrucomicrobiales;f__Verrucomicrobiaceae;g__Akkermansia	0.04	0.08	0.64	0.94	0.36	14.63	0.09	0.14	0.39	14.68	0.13	0.22
E4FAD												
k__Bacteria;p__Proteobacteria;c__Alphaproteobacteria;o__RF32;Other;Other	3.54E-09	1.45E-07	0.84	0.88	5.25	11.02	1.17E-07	4.79E-06	1.61	8.40	0.01	0.10
k__Bacteria;p__Verrucomicrobia;c__Verrucomicrobiae;o__Verrucomicrobiales;f__Verrucomicrobiaceae;g__Akkermansia	8.90E-06	1.82E-04	0.37	0.73	-0.97	14.53	1.45E-05	2.75E-04	-0.92	14.38	0.04	0.14
k__Bacteria;p__Proteobacteria;c__Gammaproteobacteria;o__Enterobacteriales;f__Enterobacteriaceae;g__Escherichia	6.41E-05	8.76E-04	0.57	0.75	-3.28	12.00	2.01E-05	2.75E-04	-3.70	12.44	2.93E-04	6.01E-03
k__Bacteria;p__Bacteroidetes;c__Bacteroidia;o__Bacteroidales;f__[Paraprevotellaceae];g__[Prevotella]	2.12E-04	2.17E-03	0.03	0.16	1.78	12.33	8.48E-05	5.80E-04	0.04	12.28	0.95	0.97
k__Bacteria;p__Bacteroidetes;c__Bacteroidia;o__Bacteroidales;f__Bacteroidaceae;Other	1.00E-03	8.22E-03	4.22E-07	1.73E-05	1.61	11.02	8.44E-04	5.80E-04	-0.76	12.10	0.18	0.41
k__Bacteria;p__Bacteroidetes;c__Bacteroidia;o__Bacteroidales;f__Porphyromonadaceae;g__Parabacteroides	1.40E-03	9.57E-03	0.02	0.15	-1.09	14.79	1.15E-03	6.72E-03	-0.27	14.16	0.61	0.81
k__Bacteria;p__Bacteroidetes;c__Bacteroidia;o__Bacteroidales;Other;Other	3.83E-03	0.02	0.32	0.69	-0.77	12.41	0.02	0.04	-0.98	12.66	0.03	0.12
k__Bacteria;p__Firmicutes;c__Bacilli;o__Lactobacillales;f__Lactobacillaceae;g__Lactobacillus	3.45E-03	0.02	0.03	0.16	1.48	16.39	4.97E-05	5.10E-04	0.86	16.78	0.11	0.26
k__Bacteria;p__Actinobacteria;c__Coriobacteriia;o__Coriobacteriales;f__Coriobacteriaceae;Other	4.95E-03	0.02	0.03	0.16	2.55	11.85	5.73E-03	0.02	-1.40	11.05	0.10	0.25
k__Bacteria;p__Firmicutes;c__Bacilli;o__Turicibacterales;f__Turicibacteraceae;g__Turicibacter	8.20E-03	0.03	0.44	0.75	-0.47	13.99	0.06	0.11	-0.33	13.92	0.45	0.63
k__Bacteria;p__Firmicutes;c__Clostridia;o__Clostridiales;f__Clostridiaceae;g__SMB53	0.01	0.05	0.73	0.79	-1.07	10.86	0.01	0.04	-1.10	10.59	0.04	0.14
k__Bacteria;p__Bacteroidetes;c__Bacteroidia;o__Bacteroidales;f__Rikenellaceae;Other	0.02	0.05	0.63	0.75	0.99	16.58	9.21E-03	0.03	1.08	16.49	0.02	0.11
k__Bacteria;p__Bacteroidetes;c__Bacteroidia;o__Bacteroidales;f__Rikenellaceae;g__AF12	0.02	0.05	0.01	0.14	-1.39	8.93	0.05	0.11	0.11	7.93	0.95	0.97
k__Bacteria;p__Deferribacteres;c__Deferribacteres;o__Deferribacterales;f__Deferribacteraceae;g__Mucispirillum	0.02	0.05	0.45	0.75	1.24	14.32	1.65E-03	8.44E-03	0.17	14.17	0.78	0.88
k__Bacteria;p__Firmicutes;c__Clostridia;o__Clostridiales;f__Dehalobacteriaceae;g__Dehalobacterium	0.02	0.05	0.40	0.75	-1.27	8.73	6.63E-03	0.02	-0.76	9.17	0.32	0.52

Table 3-2 Gut microbiota taxonomy

Taxonomic differences at the genus level between E3FAD and E4FAD prebiotic and control fed mice. Diet and genotype p- and q-values were calculated for each taxon along with each group. LogFC (log (fold change)) and LogCPM (base intensity of taxon (log (average counts per million))) were calculated for each taxon of each group. Diet refers to differences between mice fed either the prebiotic inulin or control diet. Genotype refers to differences in FAD mutations with (+) referring to the mice being positive for FAD mutations and (–) referring to the mice being negative for FAD mutations. The data is written as a heat map with the darker the respective color indicative of more significance (N = 15/group, M:F = 50/50).

Chapter 4   Specific Aim 2: To identify the effects of the prebiotic inulin on metabolism in the periphery and central nervous system (CNS) between E3FAD and E4FAD mice.

4.1   Summary

The gut microbiota of APOE4 carriers appears to protect against foodborne illness and diarrhea in childhood, showcasing the differences that may be found in the gut microbiota due to genetics. This may also play a role in the absorption of beneficial metabolites from the gut microbiota into the periphery and brain between E3FAD and E4FAD mice. We found that the prebiotic inulin is fermented into beneficial metabolites such as SCFAs and scyllo-inositol in Chapter 3, which may be able to reach the periphery and potentially generate effects on the host and reverse metabolic deficits seen in APOE4 carriers. PURPOSE: The objective of this aim was to identify the effects of the prebiotic inulin on metabolism in the periphery and central nervous system (CNS) between E3FAD and E4FAD mice. RESULTS: In the blood, scyllo-inositol was significantly increased due to the feeding of the prebiotic inulin compared to control fed animals in E3FAD mice but not in E4FAD mice. Meanwhile, SCFA levels followed suit to a moderate degree. Metabolites in the blood were also dramatically different between E3FAD and E4FAD mice fed the prebiotic inulin compared to controls and between E3FAD and E4FAD mice. This included tryptophan, tyrosine, pentose pathway, and TCA Cycle metabolites. Next, scyllo-inositol was dramatically increased in the hippocampus while numerous other metabolites were also altered in the brain due to the prebiotic inulin. Differences

were also seen between E3FAD and E4FAD mice in the recently aforementioned metabolites. CONCLUSIONS: This aim has demonstrated that the beneficial metabolites that the prebiotic inulin are fermented into in the gut microbiota are indeed able to reach the bloodstream and brain. However, the levels of these metabolites that are absorbed into the blood and brain between E3FAD and E4FAD mice are different, having implications for prevention and treatment of AD and other pathologies in human APOE3 and APOE4 carriers.

4.2 Introduction

Guerrant et al. have demonstrated that the APOE4 allele may have a protective effect against foodborne illness and diarrhea in underdeveloped countries such as in Northeast Brazil, providing a survival advantage [39, 145]. Thus, the gut microbiota of our E3FAD and E4FAD mice may be vastly different not only in the metabolites they produce from the fermentation of prebiotics, such as SCFAs and scyllo-inositol as demonstrated in chapter 3, but also in how these metabolites are absorbed and utilized in the periphery. Based on the literature, SCFAs can indeed be increased in the circulation [181] and have an impact on peripheral tissue through direct and indirect modulation of the immune system [182, 183]. Indeed, the SCFAs have even been found to beneficially impact the brain through modulation of neuroinflammation [184] and to decrease blood brain barrier permeability by increasing tight junction proteins [72]. It has been postulated that butyrate may be able to reach the brain and improve glucose metabolism and mitochondrial function [148]. Not only this but children consuming a high fiber diet were found to have better memory and learning

[185]. However, other gut-brain axis metabolites have also been identified including tryptophan-derived indole compounds [186]. One such is indole-3-propionic acid (IPA), which has been demonstrated to protect neurons via a reduction in DNA damage and lipid peroxidation [187].

From Chapter 3, we see that the metabolite scyllo-inositol is increased in the fecal gut microbiota due to the feeding of the prebiotic inulin. This metabolite has been given as an orally administered therapeutic in AD patients [169] as it is able to be absorbed into the blood stream, pass through the blood brain barrier [159], and reach the brain. Indeed, scyllo-inositol has been demonstrated to decrease Aβ aggregation [159, 164-167] and, for unclear reasons, become altered in AD patients as evidenced in one neuroimaging study [163]. Altogether, the gut-brain axis involves a variety of metabolites, many of which may be unknown, that can benefit the brain and metabolism thereof. However, the production, absorption, and usage of these beneficial metabolites may vary between APOE3 and APOE4 carriers. This may be of vast importance as carriers of the APOE4 allele display an altered brain metabolism and exhibit metabolic dysfunction via impaired glucose, ketone, and mitochondrial metabolism decades before the onset of the disease [188]. Further, hypometabolism of the brain has been exhibited in APOE4 carriers in studies that utilize FDG PET imaging to measure cerebral metabolic rates of glucose [189] while mitochondrial dysfunction has also been linked to the disease [190]. Collectively, these impairments due to the APOE4 allele, dependent and independent of Aβ, lead to an increased risk to develop AD [191] and we believe that the beneficial

metabolites from the fermentation of prebiotics may help alleviate these symptoms.

The objective of this aim was to identify the effects of the prebiotic inulin on metabolism in the periphery and central nervous system (CNS) between E3FAD and E4FAD mice. We hypothesized that the prebiotic inulin will beneficially alter metabolism in the periphery and CNS via increased beneficial metabolites in E3FAD and E4FAD mice. Specifically, we examined plasma and hippocampal scyllo-inositol, increased due to feeding of the prebiotic inulin in the gut microbiota, and metabolites associated with the gut microbiota in the plasma and brain.

4.3 Results

4.3.1 Plasma Scyllo-Inositol and SCFAs

After demonstrating that scyllo-inositol was indeed formed by gut microbiota bacteria, we set out to see if scyllo-inositol was absorbed and reached the bloodstream in our mice. By using NMR, we found that in the plasma of E3FAD mice that were fed the prebiotic inulin, there was significantly higher scyllo-inositol levels compared to mice given the control diet, however, this was not the case in the E4FAD mice. Moreover, the control fed E4FAD mice had a significant decrease in scyllo-inositol compared to the E3FAD control fed mice (Fig. 4.1a). SCFA levels in the blood were measured by Metabolon via LC-MS/MS, and were also found to be changed, albeit not as significantly as in the cecal contents, in the mice fed the prebiotic diet. This includes acetate (Fig.

79

4.1b), propionate (Fig. 4.1c), and butyrate (Fig. 4.1d). The full panel of SCFAs are in Table 4.1. Collectively, these results indicate that the prebiotic inulin's effect of increasing scyllo-inositol and SCFAs in the gut microbiota can indeed reach the periphery.

4.3.2   Blood Metabolites

With Metabolon, we found a variety of metabolites in the blood that were increased due to the prebiotic inulin and differences in blood metabolites between E3FAD and E4FAD mice (Table 4.2 and Table 4.3). Tryptophan metabolites were significantly increased due to the prebiotic inulin compared to controls. These included indoleacrylate, indolepropionate (IPA), serotonin, indoleacetylglycine, and N-acetyltryptophan in the E3FAD mice fed the prebiotic inulin and indoleacrylate and IPA in the E4FAD mice fed the prebiotic inulin. In contrast, tyrosine metabolites were decreased including phenol sulfate and phenol glucuronide in E3FAD mice fed the prebiotic inulin compared to controls. In both E3FAD and E4FAD mice fed the prebiotic inulin compared to controls, p-cresol glucuronide was decreased. Next, N-acetylglutamine was increased in mice fed the prebiotic inulin compared to their control diet counterparts. This metabolite was also increased in E4FAD mice compared to E3FAD mice. Next, N-acetylhistidine saw a similar result except for no difference in E3FAD fed the prebiotic inulin compared to their control diet counterpart. N6-methyllysine and N-acetylarginine were also both decreased in E4FAD mice compared to E3FAD mice.

Numerous pentose metabolism markers were altered in E4FAD mice fed the prebiotic inulin compared to controls. This included ribose, increased in both E3FAD and E4FAD mice fed the prebiotic inulin compared to their respective controls, while ribitol, ribonate, ribulose, xylose, arabitol, arabonate, and sedoheptulose were all significantly increased in E4FAD mice fed the prebiotic inulin compared to controls. The advanced glycation end-product N6-carboxymethyllysine was significantly increased due to the prebiotic inulin in E3FAD and E4FAD mice compared to their control diet counterparts.

In TCA Cycle metabolites, aconitate was increased in E3FAD mice fed the prebiotic inulin compared to controls while isocitric lactone, alpha-ketoglutarate, succinate, fumarate, and malate were increased in the E4FAD mice fed the prebiotic inulin compared to the E4FAD mice fed the control. In contrast, succinylcarnitine was decreased in both groups due to the prebiotic inulin. Next, myo-inositol was increased due to the prebiotic inulin in both groups while 2'-deoxyuridine was increased in E4FAD mice compared to E3FAD mice. P-cresol sulfate was also decreased in both groups due to the prebiotic inulin.

4.3.3 Hippocampal Scyllo-Inositol

After reaching the bloodstream, we wanted to confirm that scyllo-inositol is indeed able to cross the blood brain barrier, as has been reported [159], and become increased in the brain. Subsets of mice per group (N = 8/group, M:F = 50/50) were randomly chosen for MRS upon reaching 7-months of age. All mice were anesthetized during the experiment. In both E3FAD and E4FAD mice fed

the prebiotic inulin compared to controls, scyllo-inositol was drastically increased in the hippocampus of the brain, a region susceptible to AD pathology (Fig. 4.2a). An increase in scyllo-inositol was also seen in the E4FAD prebiotic fed mice compared to the E3FAD prebiotic fed mice. A representative MRS spectra for each are showcased with the arrow pointing to scyllo-inositol (Fig. 4.2b, Fig. 4.2c, Fig. 4.2d, Fig. 4.2e). These results indicate that the prebiotic inulin's effect of increasing scyllo-inositol in the gut microbiota and plasma can reach the hippocampus of the brain and provide dramatic increases in both E3FAD and E4FAD mice. However, the E4FAD mice fed the prebiotic diet saw an even greater increase in scyllo-inositol compared to E3FAD mice fed the prebiotic diet, indicative that the E4FAD mice may have less scyllo-inositol absorbed from the gut but greater absorption into the brain. Whether this effect is a protective mechanism in E4FAD mice, as scyllo-inositol has not only been determined to inhibit Aβ aggregation but also provide an anti-inflammatory effect, albeit likely from the inhibition of Aβ [165], remains to be seen.

4.3.4 Brain Metabolites

The prebiotic inulin altered numerous brain metabolites (Table 4.4), measured by Metabolon, in both E3FAD and E4FAD mice. There were also differences between E3FAD and E4FAD mice themselves. Firstly, N-acetylglutamine, N-acetylhistidine, homocarnosine, N-acetylphenylalanine, N-acetyltyrosine, N-acetylglucosaminylasparagine, palmitoleoyl ethanolamine, glycerophosphoinositol, 1-(1-enyl-palmitoyl)-2-palmitoleoyl-GPC, 2'deoxyuridine,

ascorbate, and pyridoxamine were significantly increased in E4FAD mice compared to E3FAD mice. In contrast, N6-methyllysine, 2-aminoadipate, N-acetylarginine, mannonate were decreased in E4FAD mice compared to E3FAD mice. The prebiotic inulin caused an increase in imidazole propionate, N6-carboxymethyllysine, acetylcarnitine, and scyllo-inositol in both groups. In contrast, the prebiotic inulin caused a decrease in myo-inositol and p-cresol sulfate.

4.4   Discussion

In Chapter 3, we saw that scyllo-inositol was drastically increased during our fecal culture experiment, especially so in E3FAD mice. The next step was seeing if these changes could reach the blood stream. We see that in the plasma of E3FAD mice fed the prebiotic inulin, scyllo-inositol is indeed significantly increased compared to controls. However, there was no difference seen in the E4FAD mice. In fact, even when comparing E3FAD and E4FAD mice fed the control diet, scyllo-inositol was significantly greater in the E3FAD mice. It is possible that the level of scyllo-inositol in the plasma may be somewhat dependent on when the mice eat and when that food is fermented and absorbed into the bloodstream and this may have impacted the results seen in the E4FAD mice. However, it is more likely that less scyllo-inositol is absorbed from the gut by E4FAD mice compared to E3FAD mice for reasons that are currently unclear but has important implications for APOE4 carriers. This could even be due to receptor or transporter differences in the gut or perhaps scyllo-inositol is binding to metabolites or other metabolic products that are produced more so in E4FAD

mice with subsequent clearance via the fecal matter. Our next step was to see if scyllo-inositol was able to be increased in the brain, specifically in the hippocampus, a region susceptible to AD pathology and important for learning and memory [192]. In fact, we saw a dramatic increase in hippocampal scyllo-inositol in both E3FAD and E4FAD mice that were fed the prebiotic inulin with the E4FAD mice having an even greater increase. In Chapter 3, we saw that the E4FAD mice had an increase in scyllo-inositol in the fecal culture experiment but to a lesser extent than the E3FAD mice fed the prebiotic inulin. Further, previous results in this chapter indicated that less scyllo-inositol is being produced by the gut microbiota and absorbed into the blood in E4FAD mice fed the prebiotic inulin compared to E3FAD mice fed the prebiotic inulin. Despite this, it appears that scyllo-inositol is taken into the brain at a higher rate in E4FAD mice compared to E3FAD mice. When comparing E3FAD and E4FAD mice fed the control, there was no significant difference in scyllo-inositol although there was a slight increase in E4FAD mice compared to the E3FAD mice. Notably, scyllo-inositol has been demonstrated before to be increased in AD patients [163]. We suspect this may be due to a compensatory mechanism in an attempt to decrease inflammation and halt Aβ aggregation in the brain in APOE4 carriers. Due to the fact that scyllo-inositol has been demonstrated to inhibit Aβ aggregation and through this, decrease inflammation, these outcomes will be further explored in Chapter 5. Nevertheless, these results are quite intriguing and deserve further attention as to why APOE4 carriers may have differences in production and absorption of certain metabolites into the periphery and brain.

In Chapter 3, we also saw that the SCFAs were dramatically increased in the cecal contents and we wanted to see if these metabolites were absorbed into the bloodstream. Here, we do see that the prebiotic inulin increased SCFAs in the bloodstream but to a much lesser degree than that of the cecal contents. There are a number of reasons for this. Firstly, SCFAs can be taken up by colonocytes and especially in the case of butyrate, used as an important energy source [154]. Next, the liver takes up and clears SCFAs in the portal circulation as too high of levels may become toxic. Here in the liver, the SCFAs can act as precursors to other processes. The SCFAs can also activate G protein-coupled receptors, such as Ffar2 and Ffar3, that help regulate glucose and lipid metabolism and can be found on immune cells [154]. Receptors expressed by other organs are likely present, but little is known about them at this time. Finally, SCFAs can also simply be excreted through the fecal contents [154]. Whether this increase in the bloodstream leads to a decrease in AD pathology is a question that will be addressed in the next chapter.

We next looked a variety of other metabolites that were altered in the whole blood of our mice and saw vast differences. Firstly, dramatic changes were seen in tryptophan and tyrosine metabolism, especially in our E3FAD mice fed the prebiotic inulin. Indeed, indoleacrylate, IPA, serotonin, indoleacetylglycine, and N-acetyltryptophan were all increased in E3FAD mice while only indoleacrylate and IPA were increased in E4FAD mice. In fact, even more dramatic increases were seen in the E4FAD mice in these two metabolites. Tryptophan metabolism in the gut includes metabolization of tryptophan to either

kynurenine, serotonin, and/or indole pathways, the latter two shown here. The serotonin pathway is important as 90% of serotonin is produced in the gut, although peripheral serotonin does not often cross the BBB but may communicate with the CNS nonetheless [193] and activate receptors in the gut that increase satiety and absorption of nutrients [194]. Although much is not understood about this process, SCFAs have been implicated in initiating serotonin biogenesis. Due to the increase in SCFAs we saw in the cecal contents, this increase in serotonin would make sense here although there was only a significant increase in serotonin in E3FAD mice fed the prebiotic inulin. Further, IPA, a part of the indole pathway through tryptophan metabolism, has been shown to inhibit Aβ aggregation [85] and here we see that the prebiotic inulin can indeed increase this metabolite in both groups. Next, metabolites that play a role in tyrosine metabolism were decreased due to the prebiotic inulin including phenol sulfate, phenol glucuronide, and p-cresol glucuronide in E3FAD mice. E4FAD mice fed the prebiotic inulin only saw a decrease in p-cresol glucuronide. One study using resistant maltodextrin in mice found a decrease in both phenol sulfate and p-cresol sulfate, linking them both to inflammation [195]. *Bacteroides*, which we saw decreased in E3FAD mice fed the prebiotic inulin, has been linked to their production, however, *Bifidobacterium* has been linked as well [196]. Overall, there is surprisingly little known on tyrosine metabolites and we hope our results shed some light on this matter. Collectively, it appears that the prebiotic inulin increases tryptophan metabolism in the gut microbiota while decreasing tyrosine metabolism.

Next in the blood, we found that N-acetylglutamine and N-acetylhistidine were both increased in the E4FAD mice compared to the E3FAD mice with the prebiotic inulin increasing N-acetylglutamine in both E3FAD and E4FAD mice. N6-methyllysine and N-acetylarginine were decreased in the E3FAD mice compared to E4FAD mice. Next, N6-carboxymethyllysine was increased in both E3FAD and E4FAD mice fed the prebiotic inulin compared to controls. Due to the prebiotic inulin, myo-inositol was increased in both groups while in the E4FAD mice compared to E3FAD mice, it was also increased. 2'-deoxyuridine saw a decrease in E3FAD mice fed the prebiotic inulin but an increase in E4FAD mice compared to E3FAD mice. Finally, p-cresol sulfate saw significant decreases in both E3FAD and E4FAD mice fed the prebiotic inulin. Little is known on these metabolites aside from the aforementioned myo-inositol and p-cresol sulfate.

A variety of metabolites involved in Pentose Phosphate Pathway (PPP) metabolism, responsible for NADPH production, were dramatically increased in the E4FAD mice fed the prebiotic inulin compared to E4FAD control mice. This includes ribose, ribitol, ribonate, ribulose, xylose, arabitol, arabonate, and sedoheptulose. Ribonate, xylose, and sedoheptulose were increased in the E4FAD mice compared to E3FAD mice. It is not currently known why E4FAD mice fed the prebiotic inulin would have such increases in these metabolites while the E3FAD mice fed the prebiotic inulin do not. However, one study did find an increase in the PPP linking it as a way for neurons to get energy as an alternative to glucose [27] as APOE4 carriers do indeed have hypometabolism and alterations in glucose metabolism. This paper further postulated that

changes in the PPP may be a novel target that connects APOE4 to changes in glucose metabolism and oxidative stress. Further confirming this idea, we also found changes in the TCA cycle especially in E4FAD mice fed the prebiotic inulin with significant increases in isocitric lactone, alpha-ketoglutarate, succinate, fumarate, and malate compared to E4FAD mice fed the control. In contrast, a significant decrease was seen in succinylcarnitine. The E3FAD mice fed the prebiotic inulin only saw significant increases in aconitate and alpha-ketoglutarate but also an insignificant decrease in succinylcarnitine. Similar to the changes found in E4FAD mice fed the prebiotic inulin in the PPP, we see large changes in the TCA cycle, indicative of altered glucose metabolism. Again, it is unusual that there were so few differences between the E3FAD and E4FAD mice themselves especially given that it is known that APOE4 carriers have alterations in glucose metabolism. It is quite unclear why the prebiotic inulin would be causing such dramatic effects in only E4FAD mice fed the prebiotic inulin, but we hope this is indicating that the prebiotic inulin is decreasing the hypometabolism and metabolic alterations that occur in APOE4 carriers as they age.

Our results indicate that numerous markers were altered in the brain due to the prebiotic inulin and differences between E3FAD and E4FAD mice were also present. Firstly, N-acetylglutamine, N-acetylhistidine, homocarnosine, N-acetylphenylalanine, N-acetyltyrosine, N-acetylglucosaminylasparagine, palmitoleoyl ethanolamine, glycerophosphoinositol, 1-(1-enyl-palmitoyl)-2-palmitoleoyl-GPC, 2'deoxyuridine, ascorbate, and pyridoxamine were significantly increased in E4FAD mice compared to E3FAD mice. N-acetyl amino

acids have been found to be altered in the gut microbiota when compared to germ-free mice [197]. In contrast, N6-methyllysine, 2-aminoadipate, N-acetylarginine, mannonate were decreased in E4FAD mice compared to E3FAD mice. The prebiotic inulin caused an increase in imidazole propionate, N6-carboxymethyllysine, acetylcarnitine, and scyllo-inositol in both groups. In contrast, the prebiotic inulin caused a decrease in myo-inositol and p-cresol sulfate. Many of these differences were also present in the blood of the mice. Myo-inositol was increased in the blood due to the prebiotic inulin in both groups but decreased in the brain while scyllo-inositol, confirming the MRS findings in this chapter, was increased in both groups as well. Myo-inositol is thought to be increased in the asymptomatic stages of AD [198] but scyllo-inositol treatment has been shown to decrease its levels and improve neuropsychiatric symptoms [199]. In one study, Yamashita et al. believed it was possible that myo-inositol could be converted to scyllo-inositol in blood and skeletal muscle [161] but the evidence was fairly weak. Further, due to the increases in scyllo-inositol seen in the gut and blood of our mice fed the prebiotic inulin, this seems unlikely to be a major cause of the scyllo-inositol increase seen here in the brain. P-cresol sulfate was decreased in both groups due to the prebiotic inulin in both the blood and brain and has been linked to inflammation [195]. In contrast, N6-carboxymethyllysine, an advanced glycation-end product, was increased in both groups in the blood and brain due to the prebiotic inulin. While this could be considered a new gut-brain axis component, advanced glycation-end products have been implicated in diabetes [200]. This metabolites role in the brain is

unknown. N-acetylglutamine was increased due to the prebiotic inulin in both groups in the blood but not in the brain. Meanwhile, E4FAD mice also saw an increase in this metabolite in both the blood and brain compared to E3FAD mice. Finally, N-acetylhistidine, N-acetylarginine, and N6-methyllysine were decreased in both the blood and brain in E4FAD mice compared to E3FAD mice. However, little is known about these metabolites.

Collectively, the prebiotic inulin caused a vast array of metabolic changes in the blood and brain of both E3FAD and E4FAD mice fed the prebiotic inulin compared to controls while changes between E3FAD and E4FAD mice were also evident. It is also notable that the prebiotic inulin was able to enhance the metabolism of multiple GBA components: SCFAs, IPA, and the newly discovered scyllo-inositol. Whether these changes will make an impact in the brain and decrease AD pathology will be the subject of Chapter 5.

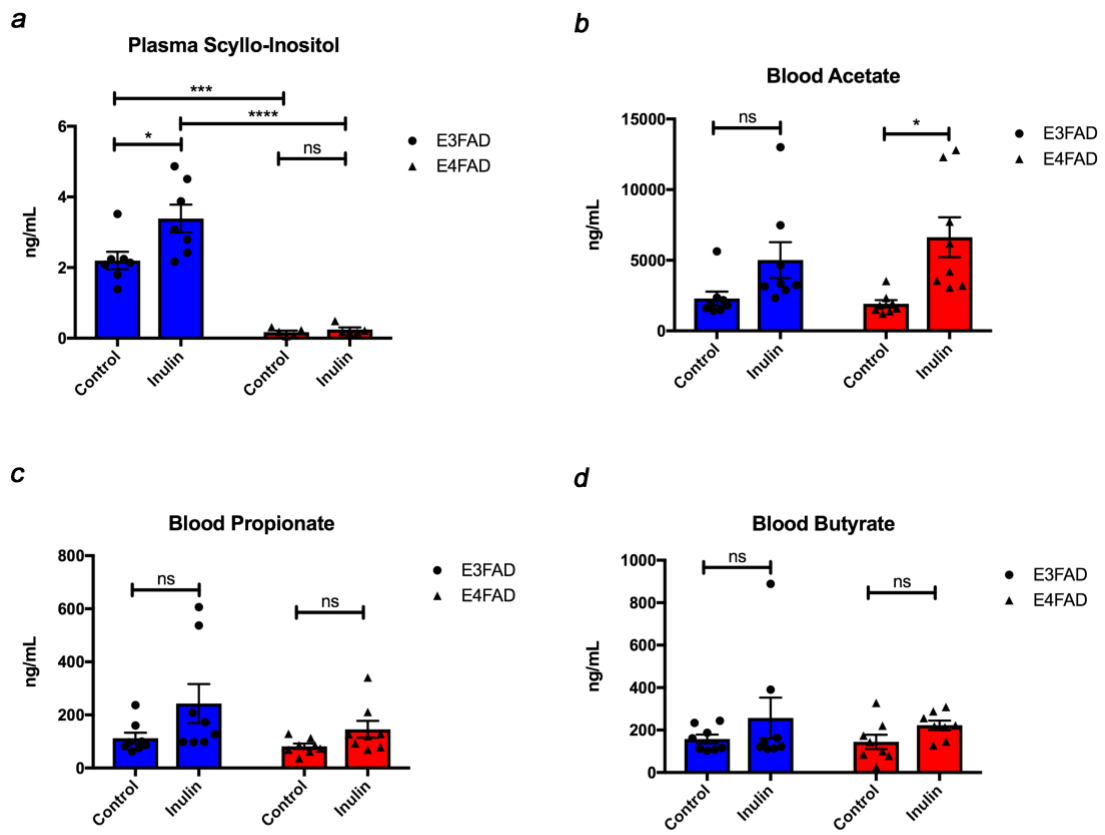**Figure 4-1** Plasma scyllo-inositol and SCFAs

Figure 4-1 Plasma scyllo-inositol and SCFAs

Plasma scyllo-inositol and SCFAs. E3FAD and E4FAD mice were sacrificed at around 7-months of age with plasma and whole blood collected. Plasma scyllo inositol was measured via NMR. More details can be found in Chapter 2, section 2.4. For blood SCFA measurement, Metabolon utilizes LC-MS/MS. More details can be found in Chapter 2, section 2.5. **a** Scyllo-inositol in the plasma of E3FAD and E4FAD mice found a significant increase between E3FAD mice fed the prebiotic inulin and their respective control group. Plasma scyllo-inositol levels were also significantly increased in E3FAD mice compared to E4FAD mice. **b** Other metabolites increased due to the prebiotic diet include the SCFAs butyrate, propionate, and acetate but the only significant increase was acetate in the E3FAD mice fed the prebiotic inulin compared to their respective control group. Statistics were completed using 2-way ANOVA (For plasma scyllo-inositol measurement, N = 10/group (M:F = 50/50) and for SCFA measurement, N = 8/group (M:F = 50/50). Error bars show mean ± SEM, ns = not significant; $*p < 0.05$; $**p < 0.01$; $***p < 0.001$; $****p < 0.0001$.

Table 4-1 Blood metabolites – short chain fatty acids

Short Chain Fatty Acids	E3FAD Control	E3FAD Inulin	E4FAD Control	E4FAD Inulin
Blood	Concentration Mean (ng/mL)	Concentration Mean (ng/mL)	Concentration Mean (ng/mL)	Concentration Mean (ng/mL)
Acetic Acid	2290 ± 490.9	5012.5 ± 1274.9	1918 ± 261.1	6632 ± 1410.3*
Propionic Acid	112.6 ± 20.6	242.9 ± 73.3	82 ± 10.3	145.9 ± 31.9
Isobutyric Acid	35.3 ± 4.7	35.6 ± 4.8	25.4 ± 3	29.9 ± 5.2
Butyric Acid	157.9 ± 20.5	257.1 ± 96	144.4 ± 33.9	222.6 ± 22.7
2-Methylbutyric Acid	24.6 ± 3.5	27.7 ± 3.6	20.8 ± 2.9	31.8 ± 7.3
Isovaleric Acid	8.8 ± 1.9	7.1 ± 1	8.6 ± 1.5	6.7 ± 1.9
Valeric Acid	10 ± 3.3	10.8 ± 3.5	5.4 ± 1.9	12.6 ± 5.7
Hexanoic Acid	51.9 ± 5.7	42.3 ± 6.7	60.9 ± 17	70.4 ± 11.6

Table 4.1 Blood metabolites – short chain fatty acids

A table showcasing the levels of short chain fatty acids in the blood. E4FAD mice fed the prebiotic inulin saw a significant increase in propionic acid compared to E4FAD mice fed the control diet. Statistics were conducted using 2-way ANOVA (N = 8/group, M:F = 50/50) with data presented as mean $\pm$ SEM. *p < 0.05.

Table 4-2 Blood metabolites – tryptophan and tyrosine metabolism

Table				Fold Change Welch's Two-Sample t-Test			
				Inulin / Ctrl		E4FAD / E3FAD	
Super Pathway	Sub Pathway	Biochemical Name	Platform	E3FAD	E4FAD	Ctrl	Inulin
Amino Acid	Tryptophan Metabolism	indoleacrylate	LC/MS neg	2.91	5.68	2.04	4.00
Amino Acid	Tryptophan Metabolism	indolepropionate	LC/MS pos early	6.42	9.68	1.34	2.02
Amino Acid	Tryptophan Metabolism	serotonin	LC/MS pos early	1.37	1.29	1.11	1.05
Amino Acid	Tryptophan Metabolism	indoleacetylglycine	LC/MS neg	1.55	0.65	1.86	0.78
Amino Acid	Tryptophan Metabolism	N-acetyltryptophan	LC/MS neg	1.30	0.81	0.98	0.61
Amino Acid	Tyrosine Metabolism	phenol sulfate	LC/MS neg	0.23	0.87	1.24	4.71
Amino Acid	Tyrosine Metabolism	phenol glucuronide	LC/MS neg	0.21	2.11	0.71	7.08
Amino Acid	Tyrosine Metabolism	p-cresol glucuronide*	LC/MS neg	0.08	0.14	0.60	1.02
Amino Acid	Glutamate Metabolism	N-acetylglutamine	LC/MS neg	1.61	1.95	1.38	1.67
Amino Acid	Histidine Metabolim	N-acetylhistidine	LC/MS pos early	1.20	1.53	1.53	1.96
Amino Acid	Lysine Metabolism	N6-methyllysine	LC/MS pos early	0.82	0.87	0.32	0.34
Amino Acid	Urea Cycle, Arginine, and Proline Metabolism	N-acetylarginine	LC/MS pos early	1.11	1.04	0.62	0.58

Table 4-2 Blood metabolites – tryptophan and tyrosine metabolism

A table showcasing the changes in tryptophan and tyrosine metabolites, and other select metabolites, due to the prebiotic inulin and differences between E3FAD and E4FAD mice in the blood. The whole blood of the mice was sent to Metabolon (Durham, NC) for metabolomic profiling. For more details, see Chapter 2, section 2.5. Heat map of statistically significant biochemicals profiled when comparing groups are labeled as follows: A dark red box indicates that $p < 0.05$ and the group means fold of change > 1.00. A dark green box indicates that $p < 0.05$ and the group means fold of change < 1.00. A light red box indicates that $0.05 < p < 0.10$ and group means fold of change > 1.00. A light green box indicates that $0.05 < p <$ and group means fold of change < 1.00 (N = 8/group, M:F = 50/50).

Table				Fold Change			
				Welch's Two-Sample t-Test			
				Inulin / Ctrl		E4FAD / E3FAD	
Super Pathway	Sub Pathway	Biochemical Name	Platform	E3FAD	E4FAD	Ctrl	Inulin
Carbohydrate	Pentose Metabolism	ribose	LC/MS polar	1.67	1.41	0.97	0.82
Carbohydrate	Pentose Metabolism	ribitol	LC/MS polar	0.99	2.01	0.78	1.58
Carbohydrate	Pentose Metabolism	ribonate	LC/MS polar	1.46	2.08	1.03	1.46
Carbohydrate	Pentose Metabolism	ribulose/xylulose	LC/MS polar	1.00	1.37	0.95	1.30
Carbohydrate	Pentose Metabolism	xylose	LC/MS polar	0.63	1.53	0.62	1.49
Carbohydrate	Pentose Metabolism	arabitol/xylitol	LC/MS polar	0.87	2.67	0.56	1.73
Carbohydrate	Pentose Metabolism	arabonate/xylonate	LC/MS polar	1.22	1.36	1.02	1.14
Carbohydrate	Pentose Metabolism	sedoheptulose	LC/MS polar	0.82	1.68	0.78	1.60
Carbohydrate	Advanced Glycation End-Product	N6-carboxymethyllysine	LC/MS pos early	1.55	1.74	0.88	0.99
Energy	TCA Cycle	citrate	LC/MS neg	1.16	0.89	1.37	1.06
Energy	TCA Cycle	aconitate [cis or trans]	LC/MS neg	1.24	1.13	1.21	1.11
Energy	TCA Cycle	isocitric lactone	LC/MS polar	1.28	1.73	1.35	1.82
Energy	TCA Cycle	alpha-ketoglutarate	LC/MS polar	1.73	2.53	1.39	2.03
Energy	TCA Cycle	succinylcarnitine (C4-DC)	LC/MS pos early	0.82	0.79	0.95	0.92
Energy	TCA Cycle	succinate	LC/MS polar	1.03	2.00	0.57	1.11
Energy	TCA Cycle	fumarate	LC/MS polar	1.23	1.60	0.81	1.05
Energy	TCA Cycle	malate	LC/MS neg	1.24	1.44	0.85	1.00
Lipid	Inositol Metabolism	myo-inositol	LC/MS polar	1.69	1.32	1.19	0.93
Nucleotide	Pyrimidine Metabolism	2'-deoxyuridine	LC/MS neg	0.76	0.72	2.94	2.78
Xenobiotics	Benzoate Metabolism	p-cresol sulfate	LC/MS neg	0.12	0.16	0.59	0.81

Table 4-3 Blood metabolites – pentose metabolism and TCA cycle

Table 4.3 Blood metabolites – pentose metabolism and TCA cycle

A table showcasing the changes in pentose and TCA cycle metabolites, and other select metabolites, due to the prebiotic inulin and differences between E3FAD and E4FAD mice in the blood. The whole blood of the mice was sent to Metabolon (Durham, NC) for metabolomic profiling. For more details, see Chapter 2, section 2.5. Heat map of statistically significant biochemicals profiled when comparing groups are labeled as follows: A dark red box indicates that $p < 0.05$ and the group means fold of change > 1.00. A dark green box indicates that $p < 0.05$ and the group means fold of change < 1.00. A light red box indicates that $0.05 < p < 0.10$ and group means fold of change > 1.00. A light green box indicates that $0.05 < p <$ and group means fold of change < 1.00 (N = 8/group, M:F = 50/50).

Figure 4-2 Hippocampal scyllo-inositol

a

Scyllo-Inositol

● E3FAD
▲ E4FAD

b - E3FAD Control

Scyllo

c - E3FAD Inulin

Scyllo

d - E4FAD Control

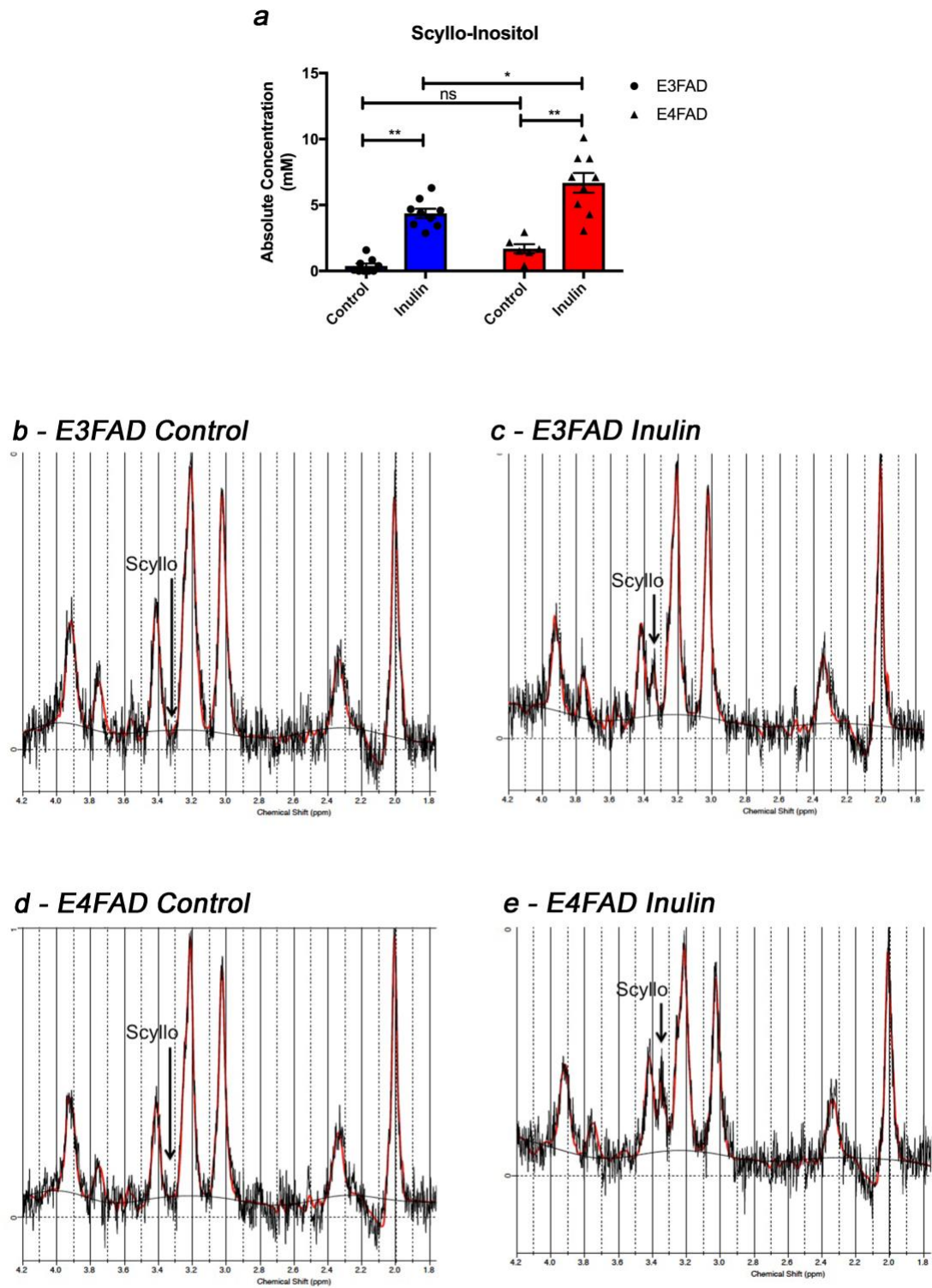Scyllo

e - E4FAD Inulin

Scyllo

99

Figure 4-2 Hippocampal scyllo-inositol

Hippocampal scyllo-inositol. Scyllo-inositol in the hippocampus was measured via MRI when the mice reached 7-months of age. Specifically, MRS was utilized while the mice were anaesthetized. For more details, see Chapter 2, section 2.6. **a** Scyllo-inositol was dramatically increased in the hippocampus of inulin-fed E3FAD and E4FAD mice compared to controls. Both groups of E4FAD mice saw a significant increase in scyllo-inositol when compared to their diet counterparts. Representative spectra are shown for (**b**) E3FAD Control, (**c**) E3FAD inulin, (**d**) E4FAD Control, and (**e**) E4FAD inulin groups with the arrow pointing to scyllo-inositol. Statistics were completed using 2-way ANOVA (N = 8/group, M:F = 50/50). Error bars show mean ± SEM, ns = not significant; *$p <$ 0.05; **$p <$ 0.01.

Table 4-4 Brain metabolites

Super Pathway	Sub Pathway	Biochemical Name	Platform	Fold Change Welch's Two-Sample t-Test			
		Table		Inulin / Ctrl		E4FAD / E3FAD	
				E3FAD	E4FAD	Ctrl	Inulin
Amino Acid	Glutamate Metabolism	N-acetylglutamine	LC/MS neg	1.04	0.77	1.89	1.39
Amino Acid	Histidine Metabolism	N-acetylhistidine	LC/MS pos early	1.09	0.77	2.13	1.52
Amino Acid	Histidine Metabolism	imidazole propionate	LC/MS pos early	1.65	1.88	1.21	1.37
Amino Acid	Histidine Metabolism	homocarnosine	LC/MS pos early	1.01	1.05	1.32	1.37
Amino Acid	Lysine Metabolism	N6-methyllysine	LC/MS pos early	0.92	1.06	0.16	0.19
Amino Acid	Lysine Metabolism	2-aminoadipate	LC/MS polar	0.97	1.17	0.67	0.80
Amino Acid	Phenylalanine Metabolism	N-acetylphenylalanine	LC/MS neg	0.89	0.66	2.34	1.73
Amino Acid	Tyrosine Metabolism	N-acetyltyrosine	LC/MS neg	1.19	0.74	3.19	1.99
Amino Acid	Tryptophan Metabolism	5-hydroxyindoleacetate	LC/MS pos early	1.09	0.67	1.23	0.76
Amino Acid	Urea Cycle, Arginine, and Proline Metabolism	N-acetylarginine	LC/MS pos early	1.03	0.94	0.64	0.58
Carbohydrate	Aminosugar Metabolism	N-acetylglucosaminylasparagine	LC/MS pos early	1.10	0.99	1.43	1.29
Carbohydrate	Advanced Glycation End-Product	N6-carboxymethyllysine	LC/MS pos early	1.42	1.38	1.03	1.01
Lipid	Fatty Acid Metabolism	acetylcarnitine (C2)	LC/MS pos early	1.18	1.19	1.12	1.12
Lipid	Endocannabonoid	palmitoleoyl ethanolamide*	LC/MS pos late	0.87	0.91	1.21	1.28
Lipid	Inositol Metabolism	myo-inositol	LC/MS polar	0.85	0.81	1.02	0.97
Lipid	Inositol Metabolism	scyllo-inositol	LC/MS polar	1.40	2.00	1.00	1.43
Lipid	Phospholipid Metabolism	glycerophosphoinositol*	LC/MS pos early	1.02	1.00	1.23	1.20
Lipid	Plasmologen	1-(1-enyl-palmitoyl)-2-palmitoleoyl-GPC (P-16:0/16:1)*	LC/MS pos late	0.92	0.85	1.75	1.61
Nucleotide	Pyrimidine Metabolism	2'-deoxyuridine	LC/MS neg	0.90	0.89	1.62	1.61
Cofactors and Vitamins	Ascorbate Metabolism	ascorbate (Vitamin C)	LC/MS neg	0.97	1.04	1.67	1.79
Cofactors and Vitamins	Vitamin B6 Metabolism	pyridoxamine	LC/MS pos early	1.01	0.98	1.13	1.10
Xenobiotics	Benzoate Metabolism	p-cresol sulfate	LC/MS neg	0.26	0.50	0.52	1.00
Xenobiotics	Food Component/Plant	mannonate*	LC/MS polar	1.08	1.15	0.51	0.55

Table 4-4 Brain metabolites

Mice fed the prebiotic diet had altered metabolites in the brain. Differences between E3FAD and E4FAD mice were also present. Upon sacrifice around 7-months of age, the brains of the E3FAD and E4FAD mice were collected followed by being shipped to Metabolon (Durham, NC) for metabolomics. Heat map of statistically significant biochemicals profiled when comparing groups are labeled as follows: A dark red box indicates that $p < 0.05$ and the group means fold of change > 1.00. A dark green box indicates that $p < 0.05$ and the group means fold of change < 1.00. A light red box indicates that $0.05 < p < 0.10$ and group means fold of change > 1.00. A light green box indicates that $0.05 < p <$ and group means fold of change < 1.00 (N = 8/group, M:F = 50/50).

Chapter 5   Specific Aim 3: To identify the effects of the prebiotic inulin on AD risk factors and pathology between E3FAD and E4FAD mice.

5.1   Summary

AD is a progressive neurodegenerative disorder with Aβ aggregation and increased inflammation being two major hallmarks of the disease. APOE4 carriers are particular susceptible to these hallmarks and have an increased risk of AD development compared to APOE3 carriers. However, the gut microbiota is able to ferment prebiotics such as inulin into metabolites, as seen in previous chapters, that can provide benefits to the brain, potentially decreasing AD risk factors and pathology in APOE4 carriers. PURPOSE: To identify the effects of the prebiotic inulin and the associated generated metabolites on AD risk factors and pathology between E3FAD and E4FAD mice compared to their respective control diet counterparts. Further, to compare E3FAD and E4FAD mice. RESULTS: The prebiotic inulin did not change CBF, amyloid-β aggregation, or anxiety and spatial recognition, working, and reference memory. However, markers of inflammation revealed significant differences due to the prebiotic inulin. CONCLUSIONS: The prebiotic inulin was able to decrease AD risk factors in E4FAD mice by decreasing certain markers of inflammation. Thus, utilizing the prebiotic inulin, displaying effects likely via beneficial metabolites produced from its fermentation in the gut, as a preventative measure may be one way to diminish inflammation and help decrease AD risk factors.

5.2 Introduction

AD is a progressive neurodegenerative disorder with a variety of symptoms that include memory loss and the inability to learn new things [201], decreased cerebral blood flow [202], and increased inflammation and Aβ aggregation [203]. This is especially true in APOE4 carriers who exhibit decreased CBF and increased BBB permeability via the activation of the inflammatory cyclophilin A-nuclear factor-κB-matrix-metalloproteinase-9 pathway [20]. Further, APOE4 carriers do indeed have increased amyloid deposition as evidenced in humans [204] and in APOE4 transgenic mice [205]. APOE4 carriers also appear to have increased inflammation. In one study displaying this in APOE4 transgenic mice, the APOE4 mice were demonstrated to have increased inflammation, via increased microglial and NF-κB gene expression, compared to APOE3 mice [206]. It is also thought that the increase in Aβ aggregation may also increase inflammation [207]. However, the gut microbiota and associated metabolites have literature that support the potential reversal of these symptoms, discussed next.

The prebiotic inulin is fermented into a variety of metabolites that can benefit the brain by potentially decreasing AD pathology. Firstly, scyllo-inositol, increased due to feeding of the prebiotic inulin in Chapter 3, has been demonstrated to inhibit Aβ aggregation in in vivo and in vitro trials [159, 164-167]. It is thought that through this inhibition, scyllo-inositol also decreases inflammation [165]. Next, SCFAs produced from the fermentation of the prebiotic inulin, also seen in Chapter 3, decrease BBB permeability through the increase

of BBB tight junction proteins [72]. The SCFAs can also modulate the immune system through a variety of ways. One study found that SCFAs were able to suppress Th17 cell production, promote Treg cells from CD4$^+$ naive T cells, and activate the lipin2-JIP2 pathway, all subduing inflammation [208]. They also help regulate T cell size and function in the colon [209]. Further, SCFAs can act as histone deacetylase (HDAC) inhibitors, further promoting an anti-inflammatory effect [210]. Specifically, sodium butyrate has been used in an AD mouse model to restore histone acetylation activity with effects reaching the brain as genes associated with learning and memory were upregulated [211].

The objective of this aim was to identify the effects of the prebiotic inulin on AD risk factors, including CBF, inflammation, anxiety, and cognition, and Aβ aggregation between E3FAD and E4FAD mice. We hypothesized that the prebiotic inulin will decrease AD risk factors and Aβ aggregation in E3FAD and E4FAD mice. Specifically, we examined the differences between E3FAD and E4FAD mice and the effect of the prebiotic inulin on CBF, inflammation, metabolism, anxiety and cognition, and Aβ aggregation. This is the pay-off chapter from all our previous work!

5.3   Results

5.3.1   Cerebral Blood Flow

Subsets of mice per group (N = 8-10/group, M:F = 50/50) were randomly chosen to undergo MRI. Specifically, PCASL was utilized to measure CBF while the mice were anesthetized. Due to CBF being decreased with age [212] and in

105

AD [213], we anticipated the prebiotic inulin may be able to impact CBF. However, this was not the case as the prebiotic inulin found no effect on cerebral blood flow in the hippocampus of the brain compared to controls. There were also no differences between E3FAD and E4FAD mice.

5.3.2 Amyloid-β Aggregation

In multiple in vivo and in vitro studies, scyllo-inositol has been demonstrated to inhibit Aβ aggregation [159, 164-167]. We took a subset of brains from each group of E4FAD mice when the mice were sacrificed at around 7-months of age for Aβ staining (N = 5/group, M:F = 50/50). These were sent to the COCVD Pathology Research Core at the University of Kentucky to be embedded and sectioned onto microscope slides. Immunohistochemistry was then performed for identification of Aβ followed by a background stain utilizing NISSL. After the slides were imaged via the Aperio ScanScope XT Digital Slide Scanner System in the University of Kentucky Alzheimer's Disease Center and uploaded to the online database, Aperio ImageScope was used to analyze total anti-Aβ counts. We found that the prebiotic inulin had no effect on amyloid deposits in E4FAD mice (Fig. 5.1a with 5.1b and 5.1c as representative images of each group). These results indicate that the increase in scyllo-inositol due to the prebiotic inulin was unable to inhibit Aβ aggregation. Perhaps if the prebiotic inulin was given for a longer period of time, effects may have been evident.

5.3.3 NanoString Array

E4FAD mice were sacrificed around 7-months of age with the brains collected and hippocampus dissected. Next, RNA was isolated and then quantified via the NanoString array. Specifically, we first wanted to see if the FAD mutations and/or the prebiotic inulin are able to alter markers of inflammation in the brain. This was completed by looking at 561 gene targets, with 318 genes being above the background threshold. When comparing the differential expression between APOE4 mice with and without the FAD mutations, 52 genes were significantly enriched by greater than one Log2 fold change (Fig. 5.3a). Among these 52 genes in E4FAD mice, we next wanted to examine the effect of the prebiotic inulin on these 52 genes via the mean Log2 difference between E4FAD mice fed either the prebiotic inulin or control diet. Among the 52 genes, 4 genes had around a 2-fold decrease in expression due the prebiotic inulin (Fig. 5.3b). Two of these genes were significantly decreased while 2 of the genes were insignificantly decreased due to the prebiotic inulin. The two significantly decreased genes were chemokine (C-C motif) ligand 4 (CCL4) (Fig. 5.3c) and Fc receptor IgG low affinity 4 (Fcgr4) (Fig. 5.3f) while the insignificantly decreased genes were C-X-C motif chemokine 10 (CXCL10) (Fig. 5.3d) and integrin alpha X (Itgax) (Fig. 5.3e).

5.3.4 Animal Behavior Tests

We wanted to measure the impact of the prebiotic inulin on multiple animal behavior tests. At 7-months of age, E3FAD and E4FAD mice underwent behavior

testing over a two-week period starting at the same time each morning. The behavior tests included elevated plus maze, evaluating the anxiety of mice, open field test, evaluating the anxiety of the mice in a new environment, novel object recognition, testing spatial recognition memory, and radial arm water maze, testing both spatial working and reference memory. When looking at radial arm water maze (Fig. 5.4a), no difference was seen between mice fed the prebiotic inulin and control diet. This also held true for the open field test (Fig. 5.4b), elevated plus maze (Fig. 5.4c), and novel object recognition test (Fig. 5.4d). Differences were also not apparent between E3FAD and E4FAD mice.

5.4   Discussion

As one ages, a decline in CBF occurs [212] and in APOE4 carriers, a decline is even seen before other AD-like symptoms occur [19]. Bell et. al. demonstrated that the breakdown of the BBB due to the APOE4 allele may be responsible for this decline in CBF [20]. Interestingly, SCFAs have been demonstrated to impact the BBB [72] and with the increase of SCFAs in the periphery due to the prebiotic inulin, we anticipated an increase in CBF. Although it is difficult to draw definitive conclusions, we did not see a difference in CBF due to the prebiotic inulin. However, there were also no differences between E3FAD and E4FAD mice as we expected to see a decrease in E4FAD mice compared to E3FAD mice. This may indicate that the deficits in CBF that APOE4 is thought to invoke may not have occurred yet, perhaps due to the mice not being advanced enough in age.

We next looked at the effect of the prebiotic inulin on amyloid aggregation.

In E4FAD mice that were fed either the prebiotic or control diet, there were no differences between groups. Due to the increases in GBA components because of the prebiotic inulin, we suspected that the prebiotic fed mice may see a significant decrease in Aβ aggregation. However, this was not the case as no differences were seen between groups in E4FAD mice. If the mice had begun being fed before they reached 3-months of age or if we allowed the study to go for a longer period of time, perhaps the effects of the prebiotic inulin would have been more pronounced.

However, we do see that the prebiotic inulin was able to change markers of inflammation. Firstly, the effect of the FAD mutations in APOE4 mice was analyzed. Mice with FAD mutations have been demonstrated in the literature to have increases in inflammatory markers [214] and this was further confirmed here. Among the 52 genes that were shown to be altered due to the FAD mutations, there was a noticeable downward trend in the E4FAD mice fed the prebiotic inulin compared to the control group. Specifically, significant decreases were seen in CCL4 and Fcgr4 while insignificant decreases were seen in CXCL10 and Itgax. CCL4 is a chemokine that has been found to be increased in mice with the APP/PS1 mutations and has been associated with the progression of Aβ in the brain [215] while also being altered in human APOE4 carriers [216]. Fcgr4, along with other Fcgr's, have been found to potentially stimulate vascular damage and neurodegeneration while also being upregulated due to increased systemic inflammation, neuroinflammation, and aging [217, 218]. Next, CXCL10 is a chemokine found in high concentrations in certain AD mouse models and

even in AD patients [219, 220]. In fact, cerebrospinal fluid CXCL10

concentrations have been positively correlated with cognitive impairment [221].

Notably, the receptor of CXCL10 is CXCR3 and in one study using CXCR3-

deficient APP/PS1 mice, Aβ and plaque burden were greatly reduced along with

a decrease in behavioral impairment, showcasing the importance of this pathway

in AD disease progression [219]. Finally, Itgax is an integrin protein that appears

to be induced in microglia in AD [222] but is actually downregulated in APOE

knock-out APP/PS1 mice [223]. Since inflammation is notably increased in AD

and is an important aspect of AD pathology [224], the decrease in inflammatory

genes seen here, especially those that appear to play a role in AD pathology and

progression, due to the prebiotic inulin may be a convenient, translatable way for

a nutritional intervention to decrease AD pathology over time.

Finally, we wanted to see if the prebiotic inulin was able to impact animal

behavior tests. Increased anxiety is thought to be a symptom preceding AD [225]

and diminished mental capabilities and cognition are AD symptoms [1]. Firstly,

we did not see any differences in the elevated plus maze or open field test, two

tests measuring the anxiety of the mice. Further, we saw no differences in radial

arm water maze and novel object recognition test, tests that measure spatial

working and reference memory, and spatial recognition memory, respectively.

Oddly, we also saw no differences between E3FAD and E4FAD mice. In fact, Liu

et. al. found behavior deficits via the Morris Water Maze, assesses spatial

working and reference memory, and Y-maze, assesses spatial recognition

memory, when comparing 6-month old E4FAD mice to E3FAD mice although the

effects were quite modest [33]. Nevertheless, perhaps if our mice were older we would have seen more deficits in cognition between E3FAD and E4FAD mice and more of an impact from the prebiotic inulin.

Collectively, the prebiotic inulin was able to decrease markers of inflammation but was unable to effect CBF, Aβ aggregation, or any animal behavior tests. Notably, there were also no differences between E3FAD and E4FAD mice in CBF or any of the behavior tests. This may indicate the mice were not old enough to develop deficits in CBF, anxiety, and/or spatial working, reference, or recognition memory. Effects may also have been more apparent if the sample size was larger in certain experiments. Nevertheless, the prebiotic inulin was able to decrease markers of inflammation, which we believe over time may help decrease AD risk factors and pathology.
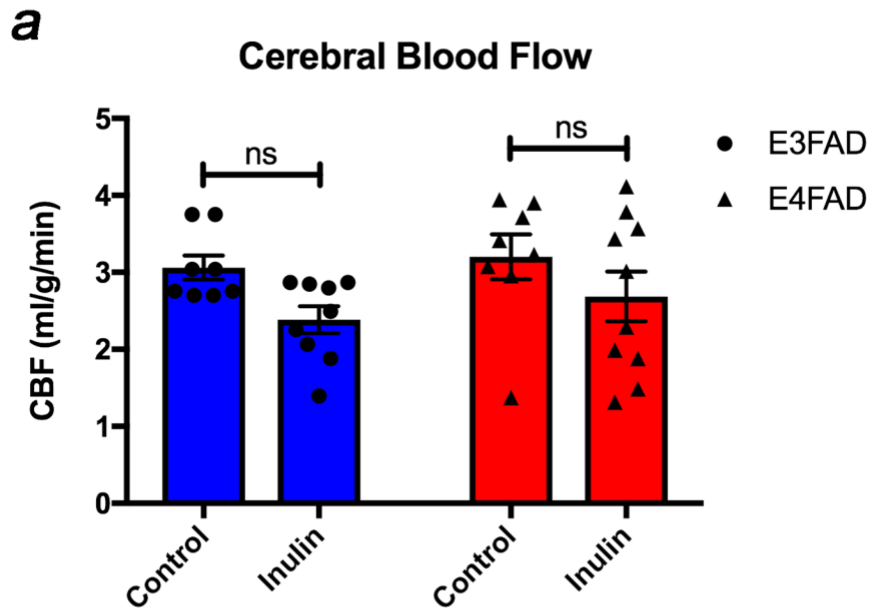
Figure 5-1 Hippocampal cerebral blood flow

**Figure 5-1** Hippocampal cerebral blood flow

The prebiotic inulin did not impact CBF in the hippocampus. Subsets of mice per group were randomly chosen upon reaching 7-months of age to undergo MRI. Specifically, PCASL was utilized to measure CBF while the mice were anesthetized. For more details, see Chapter 2, section 2.6. **a** E3FAD and E4FAD mice fed the prebiotic inulin did not see differences when compared to their control fed counterparts. Further, there were no differences between E3FAD and E4FAD mice. Statistics were conducted using 2-way ANOVA (N = 8-10/group, M:F = 50/50). Error bars show mean ± SEM. ns = not significant.

Figure 5-2 Amyloid-β staining

a
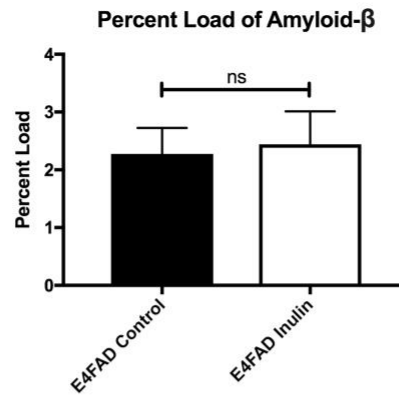
b - Representative Image of Control Fed E4FAD Mice
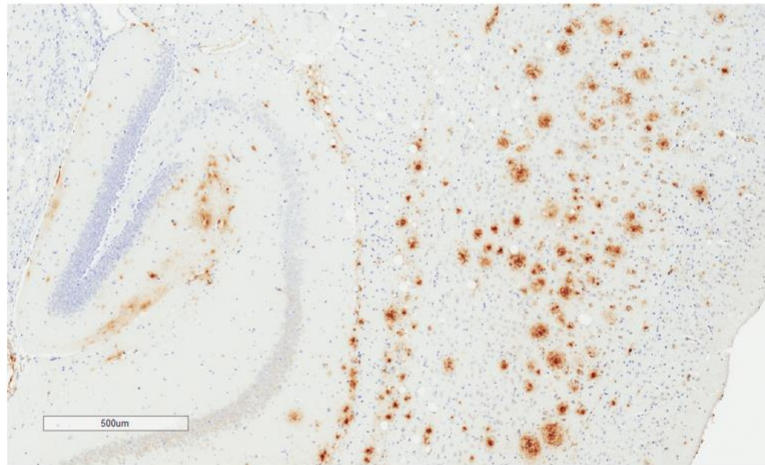
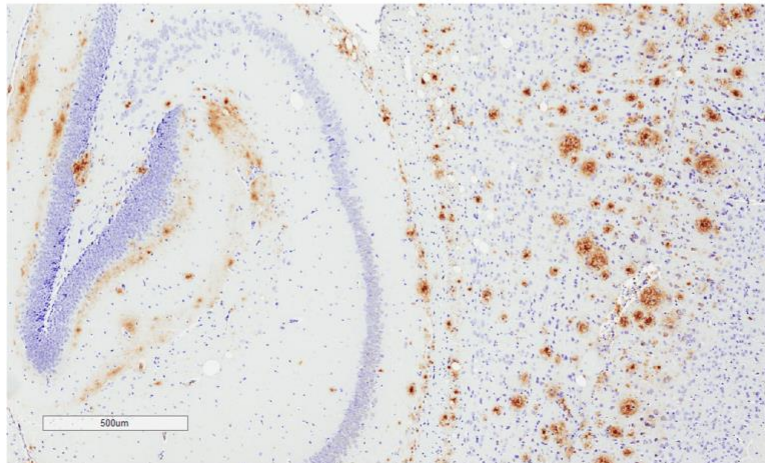

c - Representative Image of Inulin Fed E4FAD Mice

Figure 5-2 Amyloid-β staining

Aβ staining in the brains of E4FAD mice. The mouse brains were collected upon sacrifice around 7-months of age and sent to the COCVD Pathology Research Core at the University of Kentucky to be embedded and sectioned onto microscope slides. Immunohistochemistry was then performed for identification of Aβ followed by a background stain utilizing NISSL. After the slides were imaged via the Aperio ScanScope XT Digital Slide Scanner System in the University of Kentucky Alzheimer's Disease Center and uploaded to the online database, Aperio ImageScope was used to analyze total anti-Aβ counts. For more details, see Chapter 2, section 2.7. **a** E4FAD mice fed the prebiotic diet did not see differences in Aβ aggregation (percent load) in the brain. **b** Representative image of E4FAD mice fed the control diet. **c** Representative image of E4FAD mice fed the prebiotic diet. Statistics were conducted using 2-way ANOVA (N = 5/group, M:F = 50/50). Error bars show mean ± SEM. ns = not significant.

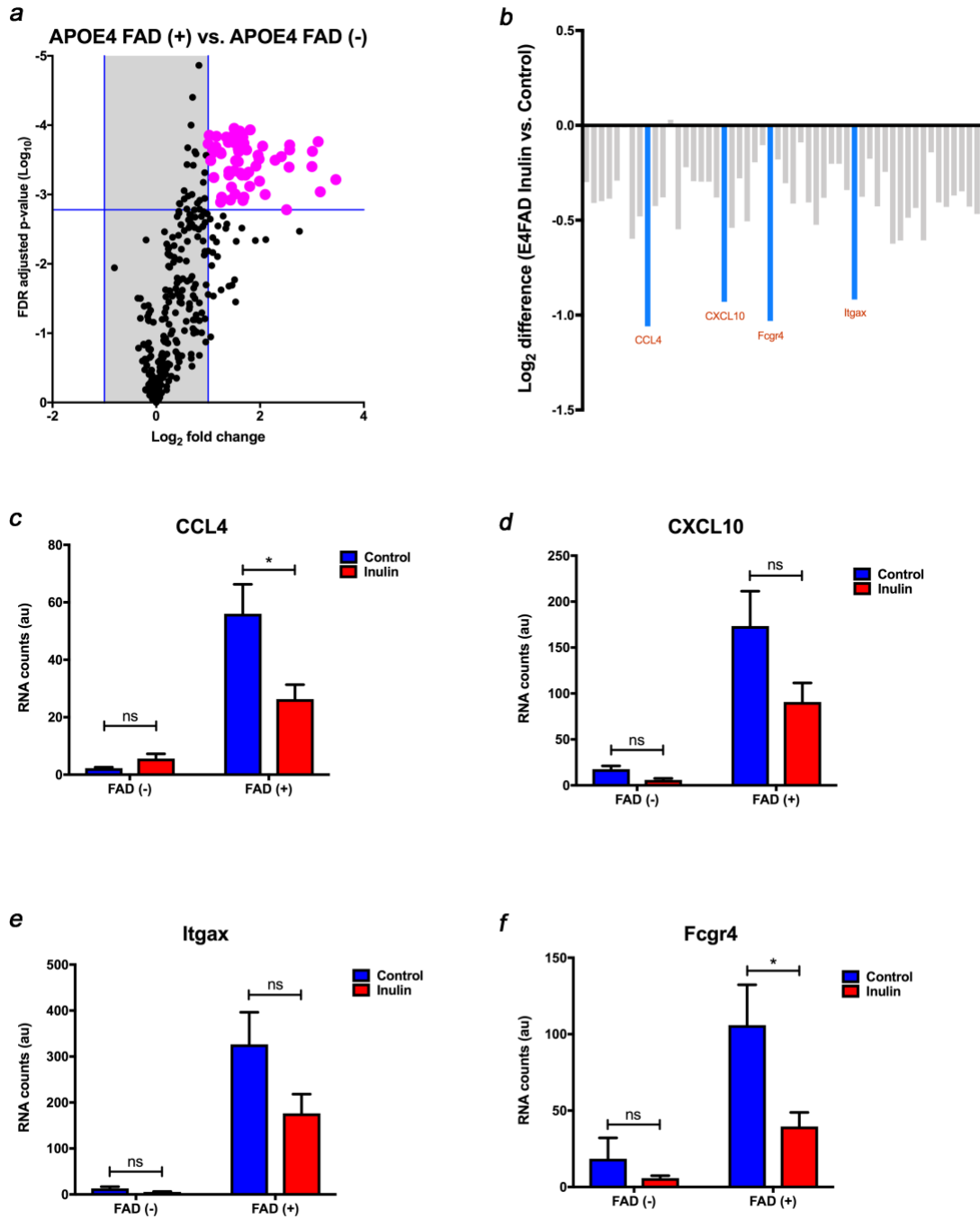**Figure 5-3** NanoString array analysis

Figure 5-3 NanoString array analysis

The impact of the FAD mutations and prebiotic inulin on markers of inflammation. E4FAD mice were sacrificed around 7-months of age with the brains collected and hippocampus dissected. Next, RNA was isolated and then quantified via the NanoString array. For more details, see Chapter 2, section 2.8. **a** In APOE4 mice with and without the FAD mutations, data are plotted as the mean ratio expression with their respective adjusted p-value. This revealed 52 genes that were significantly differentially enriched (magenta) with greater than one Log2 fold change due to the FAD mutations. **b** The 52 genes that were enriched due to the FAD mutations were further examined under the context of diet manipulation. Overall, there was a trend for most of the 52 genes to be downregulated due to the prebiotic inulin in E4FAD mice. Further, a 2-fold decrease in expression was seen in 4 genes (aquamarine). Among these, **c** CCL4, and **f** Fcg4 were significantly decreased and **d** CXCL10 and **e** Itgax were insignificantly decreased due to the prebiotic inulin. Statistics were completed using 2-way ANOVA (Sidak posthoc multiple comparisons correction) (N = 5/group, all male). For more details, see section 2.8. Error bars show mean ± SEM, ns = not significant; *$p < 0.05$.

Figure 5-4 Behavior tests

a Radial Arm Water Maze

b Open Field Test

c Elevated Plus Maze
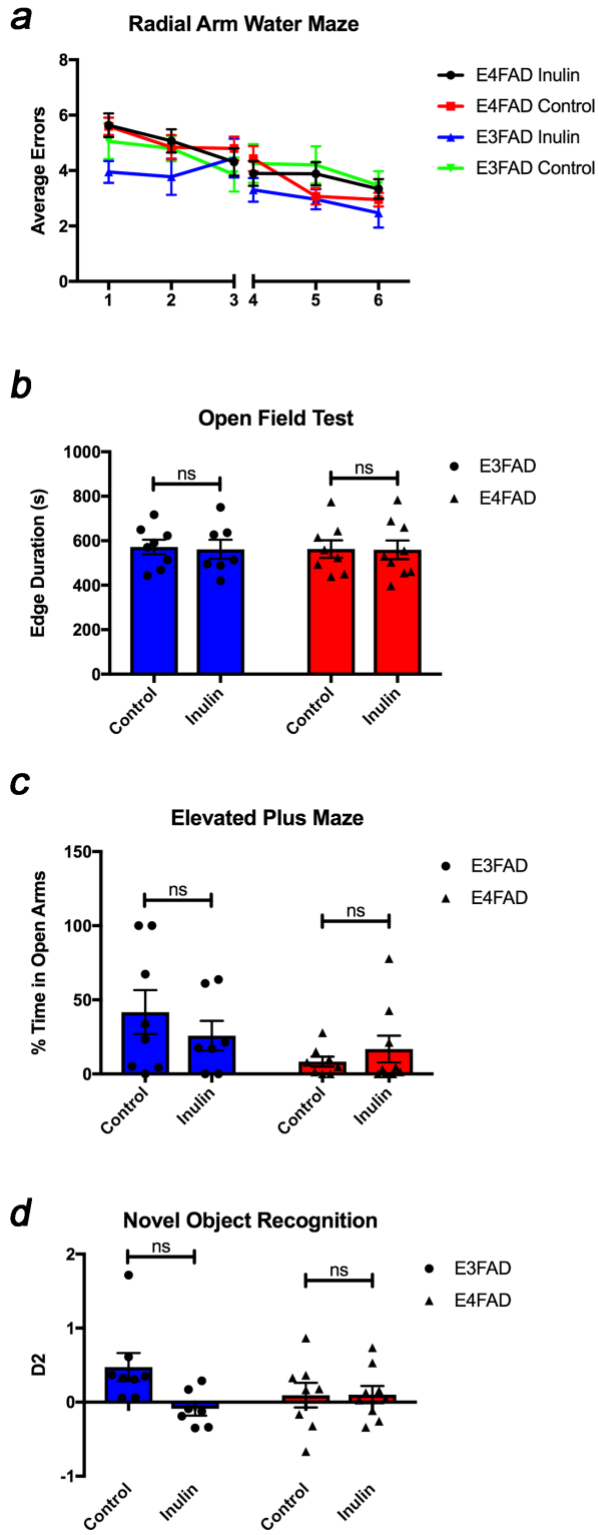
d Novel Object Recognition

Figure 5-4 Behavior tests

The impact of the prebiotic inulin on animal behavior tests. At 7-months of age, E3FAD and E4FAD mice underwent behavior testing over a two-week period starting at the same time each morning. The behavior tests included elevated plus maze, evaluating the anxiety of mice, open field test, evaluating the anxiety of the mice in a new environment, novel object recognition, testing spatial recognition memory, and radial arm water maze, testing both spatial working and reference memory. For more details, see section 2.9. In E3FAD and E4FAD mice fed the prebiotic inulin compared to their control fed counterparts and when comparing E3FAD and E4FAD mice, no differences were seen in **a** radial arm water maze, **b** open field test, **c** elevated plus maze, or **d** novel object recognition. All behavior tests were conducted in the Rodent Behavior Center at the University of Kentucky when the mice reached 7-months of age. Statistics were conducted using 2-way ANOVA (N = 7-9/group, M:F = 50/50). Error bars show mean ± SEM. ns = not significant.

Chapter 6   General Discussion

6.1   Discussion

This project uncovered many remarkable findings that will prove to be impactful in the field. Firstly, we see that the prebiotic inulin is able to significantly alter the gut microbiota in both E3FAD and E4FAD mice. Not only this but the response of the mice to the prebiotic inulin was different to where E3FAD mice appear to gain more benefit than do E4FAD mice. This includes greater increases in beneficial taxa such as *Bifidobacteria*, *Lactobacillus*, and *Akkermansia* in the E3FAD mice. Interestingly, we found that due to the prebiotic inulin, scyllo-inositol was increased by the fecal microbiota population and that the SCFAs levels were also considerably higher in the cecal contents. Amazingly, the E4FAD mice fed the prebiotic inulin had less of an increase in scyllo-inositol, propionate, and butyrate than did the E3FAD mice fed the prebiotic inulin, indicative that the gut microbiota of E4FAD mice are unable to produce as much beneficial metabolites. Due to work by Dr. Richard Guerrant where children who were APOE4 carriers were more resistant to enteric infection and thus had improved cognition [226], our lab thought E4FAD mice in our study may have a more beneficial gut microbiota. We did not come to such a conclusion based on our data but the benefits of the APOE4 allele during development have been well noted in the literature [227]. Nevertheless, it is possible that the gut microbiota of APOE4 carriers is resistant to enteric infection but for reasons we have yet to understand. Further, the gut of APOE4 carriers may need a higher dosage of prebiotics to receive similar benefits compared to

APOE3 carriers and this should be considered when looking improve the gut health of APOE4 carriers. Also in the gut microbiota, we found no notable differences due to the FAD mutations in either E3FAD or E4FAD despite other studies indicating that these mutations increased amyloid-like proteins in the gut [40] and impacted amyloid deposition in the brain [41]. Notably, a slightly different AD mouse model was used in these studies that involved just the APP and PS1 mutations and at different ages than our study. While it is still certainly possible that the APOE4 allele provides protection against enteric infection and certain FAD mutations alter the gut microbiota, we cannot confirm such effects.

One important aspect of the gut microbiota is how much of the benefits actually make it to the periphery and play a role on the host. In our project, we see that scyllo-inositol, SCFAs, and even IPA are increased due to the prebiotic inulin in the blood. However, E4FAD mice saw little scyllo-inositol in the blood in either the prebiotic or control group. Nevertheless, this is a landmark finding as inulin is seen here to increase multiple GBA components and we are able to declare scyllo-inositol a GBA component for the first time. Not only this but there were many other metabolic differences that were altered due to the prebiotic inulin in both E3FAD and E4FAD mice. There was an increase in tryptophan metabolism and a decrease in tyrosine metabolism. While we cannot assuredly say this will benefit the host, although the increase in the tryptophan metabolite IPA may be beneficial due to its inhibitory effects on $A\beta$ aggregation [85], this is a major finding in the prebiotic field. It would be of interest if these findings could be repeated with other prebiotics. Also, in the blood, we also found differences in the

PPP and TCA Cycle. While it is known that APOE4 carriers develop hypometabolism and have altered glucose metabolism [228], the PPP has been recently implicated [27] and may be a research avenue that needs more exploring.

The next step in the project was to see if the effect of the prebiotic inulin in the gut microbiota could not only reach the periphery but also the brain. Here we do indeed see that scyllo-inositol was increased in the hippocampus of both E3FAD and E4FAD mice fed the prebiotic inulin. Contrary to what you may think due to the findings in Chapters 3 and 4 where greater increases in scyllo-inositol in the gut and absorption thereof into the periphery were found in E3FAD mice compared to E4FAD mice fed the prebiotic inulin, the E4FAD mice actually saw a greater increase in hippocampal scyllo-inositol compared to E3FAD mice. This indicates that E4FAD mice may have a compensatory effect, perhaps due to increased inflammation in the brain, that enables more scyllo-inositol, which can decrease inflammation via inhibition of Aβ aggregation [165], to be brought into the brain compared to E3FAD mice. Reasons how this occurs are not available as scyllo-inositol is a little studied metabolite. It is also plausible that myo-inositol could be converted to scyllo-inositol, or vice-versa in the blood and/or brain but the only evidence of this is in the blood [161]. In this study, scyllo-inositol was administered in the blood of mice with a subsequent increase seen in myo-inositol levels. This evidence is not particularly strong, but the possibility still remains.

The next and final step was to see if the changes due to the prebiotic inulin were able to not only reach the periphery and brain but to also decrease AD risk factors and pathology. We did indeed see alterations in inflammation in mice fed the prebiotic inulin, but many AD risk factors and pathology were not altered. This included no differences seen in CBF, anxiety and cognition, and Aβ aggregation. Due to the increase in gut-brain axis components that have literature supporting their ability to inhibit Aβ aggregation, we suspected the prebiotic inulin may indeed be able to decrease Aβ. However, this was not the case. It is possible if we began the prebiotic diet on the mice at an earlier age or fed them for a longer period of time, then differences would become more evident. Nevertheless, we did see a notable downward trend in inflammatory genes due to the prebiotic inulin via a decrease in 52 genes that were increased by the FAD mutations. Among these, CCL4 and Fcgr4 were significantly decreased while CXCL10 and Itgax were insignificantly decreased. It is quite notable that these aforementioned inflammatory markers have been associated with AD pathology and disease progression. Due to this, we do indeed believe the consumption of the prebiotic inulin may be a convenient, translatable way to decrease AD risk factors and pathology over time.

Collectively, we see that the prebiotic inulin is able to increase numerous components of the gut-brain axis that were able to reach the brain. In fact, a new gut-brain axis component has been revealed in scyllo-inositol. Aβ aggregation and numerous AD risk factors were unable to be impacted by the prebiotic inulin, however, markers of inflammation in the brain were decreased due to the

prebiotic inulin. Overall, this research enables a paradigm shift as taking

preventative measures to decrease AD risk factors in APOE4 carriers may be

effective in helping to prevent the disease.

6.2   Limitations

A limitation of our project was the use of our animal model. Although we

believe that the EFAD mouse model is the most state-of-the-art and translatable

AD mouse model available, as it allows us to see AD pathology within just a few

months of age in the mice, AD mouse models have historically translated poorly

to clinical outcomes [229]. It also cannot be discounted that mice and humans

are different species that will vary in results.

A major limitation of Aim 1 involves the gut microbiota; however, this is the

same limitation present with gut microbiota research in general. Although the

method to extract DNA from the fecal sample appears to have minimal impact,

the varying techniques used to target the bacterial 16S rRNA gene of the mice

can impact the results and reproducibility in a major way [230]. Further, the

husbandry of the mice also varies and can impact results, among other

challenges [231]. In our study, the groups were split into two batches and thus, a

batch effect was present to where a direct comparison of E3FAD and E4FAD

mice became impossible. However, this will be considered in all our future

endeavors.

Another limitation related to the gut microbiota involves scyllo-inositol.

Bacillus subtilis is the only known bacterial taxa to increase this metabolite [155]

and we did not find this taxon in our 16S rRNA sequenced data. We do know that

scyllo-inositol was increased due to our fecal bacterial culture experiment. Thus, we believe that other bacterial species are also able to produce this metabolite and identifying these taxa could be a future direction of our lab's research.

In Aim 3, we found that the prebiotic inulin was unable to impact CBF and animal behavior tests or decrease Aβ aggregation. This may be due to stopping the study before they reached an advanced enough age to develop deficits in CBF and in animal behavior tests. Due to the E4FAD mice not having deficits in CBF and in the animal behavior tests compared to E3FAD mice, we do indeed suspect the mice at 7-months of age were not old enough to develop such deficits. This may also be true in regard to the lack of decrease in Aβ aggregation in E4FAD mice fed the prebiotic inulin, however, we do not necessarily believe that the amyloid cascade hypothesis, the hypothesis that Aβ plaques are the primary culprit for the disease, is solely responsible for AD [232]. Indeed, studies have shown that normal cognitive people have amyloid plaques and that decreasing these plaques in AD patients has no effect on their symptoms [232]. The amyloid cascade hypothesis has also consistently failed clinically to meet primary endpoints although this may also be due to beginning treatment too late in AD pathology [232, 233]. Nevertheless, we believe with the prebiotic inulin able to decrease inflammation and alter the metabolism of E4FAD mice, utilizing this nutritional intervention may be a paradigm shift in preventing AD.

And finally, the last notable limitation is that we did not look for neurofibrillary tangles, one of the primary hallmarks of the disease and potential causative agent of AD [234].

6.3   Significance and Implications

This project has major significance and implications towards the future of GBA and AD research. The findings from Aim 1 demonstrate that E3FAD and E4FAD mice are both able to ferment the prebiotic inulin into beneficial metabolites but in dissimilar amounts. Indeed, the E3FAD mice appear to get more benefit from the prebiotic inulin than the E4FAD mice. This indicates that the genetic makeup of an organism can impact the gut microbiota, their response to prebiotics, and ability to ferment prebiotics into metabolites. This signifies that personalizing treatments based on one's genetics may be more effective in preventing and treating AD compared to a standard approach.

Aim 2 is significant because we see that the metabolites produced from the fermentation of the prebiotic inulin are indeed able to reach the bloodstream and brain to potentially exert effects. Although prebiotics may be fermented by the gut microbiota, their impact is exerted beyond into other organs. This may pave the way for other interventions that benefit the gut microbiota to come into the limelight, be moved into clinical trials, and eventually, used as a part of a personalized AD prevention plan, especially for those that are genetically predisposed to the disease. In this aim, we also see scyllo-inositol as a new, novel component of the GBA. As more and more GBA components are revealed, more treatment and prevention plan that look to benefit the GBA could be utilized. We also saw the increase in SCFAs and IPA, known GBA components, that provides compelling evidence that the prebiotic inulin can impact numerous

GBA components. Interestingly, we also saw metabolic differences between E3FAD and E4FAD mice in the blood and brain, indicating that the absorption of metabolites from the gut and impact thereof in the periphery is also different depending on one's genetics.

Aim 3 is significant because we see that a nutritional intervention is able to decrease AD risk factors via diminished inflammation. Due to pharmacological interventions primarily failing [5], it has been suggested that preventative measures may be more effective in preventing and treating AD [6]. Our results confirm that a nutritional intervention such as prebiotics can be effective in helping to decrease AD risk factors, signifying a paradigm shift in how we approach AD care in human patients. Indeed, benefiting the gut microbiota and GBA may be the first preventative measure that one should undertake to prevent AD.

6.4   Future Directions

The future directions for this research are vast! Firstly, a better understanding of what bacterial taxa produce certain metabolites would greatly help us understand the gut microbiota and the benefits it can produce on the host, including that of the taxa that produce scyllo-inositol. Next, using different prebiotics, such as inulin, resistant starch and galacto-oligosaccharides, and comparing the effects of these prebiotics to each other on the gut microbiota and brain would greatly influence the literature and translatability to humans. It is plausible that all prebiotics are able to increase the production of beneficial

metabolites. However, it is also possible that only the prebiotic inulin is able to increase scyllo-inositol while other prebiotics cannot produce scyllo-inositol but can increase other, unique metabolites. Combining multiple prebiotics would be very beneficial as well as the human diet would more likely contain a mixture of different foods and prebiotics as opposed to specializing in the consumption of just one. Subsequently, using different dosages of prebiotics and seeing if there is a dose-dependent effect of benefits and metabolite production would also be highly valuable. This could greatly impact how this research can be translated to humans and what exactly humans should be consuming, and in what amounts, for optimal gut microbiota and GBA health. Next, further understanding the differences between APOE3 and APOE4 carriers would help in translating findings to humans as a personalized approach may be more effective depending on one's genes in preventing and treating AD compared to a standard treatment that doesn't take this into account. However, to fully understand the significance and implications of this project, studies in clinical trials looking at the impact of the prebiotic inulin on the GBA and AD, in APOE3 and APOE4 carriers alike, need to be completed.

The final notable future direction is to feed the mice for a longer period of time and until the mice reach an older age. Considering there were no deficits in CBF and animal behavior tests between E3FAD and E4FAD mice at 7-months of age, it may be worth measuring these outcomes again when the mice reach 10 or 12-months of age and then seeing the impact of the prebiotic inulin on AD pathology.

Chapter 7 [Supplement] Age Drives Distortion of Brain Metabolic, Vascular, and Cognitive Functions, and the Gut Microbiota

Authors: Jared D. Hoffman, Ishita Parikh, Stefan J. Green, George Chlipala, Roberty Mohney, Mignon Keaton, Bjoern Bauer, Anika M.S. Hartz, and Ai-Ling Lin

7.1 Summary

Advancing age is the top risk factor for the development of neurodegenerative disorders, including Alzheimer's disease (AD). However, the contribution of aging processes to AD etiology remains unclear. Emerging evidence shows that reduced brain metabolic and vascular functions occur decades before the onset of cognitive impairments, and these reductions are highly associated with low-grade, chronic inflammation developed in the brain over time. Interestingly, recent findings suggest that the gut microbiota may also play a critical role in modulating immune responses in the brain via the brain-gut axis. In this study, our goal was to identify associations between deleterious changes in brain metabolism, cerebral blood flow, gut microbiome, and cognition in aging, and potential implications for AD development. We conducted our study with a group of young mice (5-6 months of age) and compared those to old mice (18-20 months of age) by utilizing metabolic profiling, neuroimaging, gut microbiome analysis, behavioral assessments, and biochemical assays. We found that compared to young mice, old mice had significantly increased levels of numerous amino acids and fatty acids that are highly associated with

inflammation and AD biomarkers. In the gut microbiome analyses, we found that old mice had increased *Firmicutes*/*Bacteroidetes* ratio and alpha diversity. We also found impaired blood-brain barrier function and reduced cerebral blood flow as well as compromised learning and memory and increased anxiety, clinical symptoms often seen in AD patients, in old mice. Our study suggests that the aging process involves deleterious changes in brain metabolic, vascular and cognitive functions, and gut microbiome structure and diversity, all which may lead to inflammation and thus increase the risk for AD. Future studies conducting comprehensive and integrative characterization of brain aging, including crosstalk with peripheral systems and factors, will be necessary to define the mechanisms underlying the shift from normal aging to pathological processes in the etiology of AD.

7.2   Introduction

Advancing age increases the risk factor for developing dementia, with imaging and biomarker data suggesting that the pathophysiological processes of Alzheimer's disease (AD) begin more than a decade prior to the diagnosis of dementia [23, 235-237]. However, how aging processes contribute to AD etiology still remains unclear. Bioenergetic imbalance over time has been considered as one of the primary causes for these chronic disorders [238]. In the central nervous system, brain energy supply declines with age [239]. Failure to maintain brain metabolism causes dysfunctional cellular energy status and nucleotide biosynthesis [240], leading to cognitive impairment and brain volume atrophy

[241]. In addition, this energetic imbalance leads to neuroinflammation accompanied by reduced neuronal activity and increased glial activation [242-245]. Glial over-activation can cause release of inducible nitric oxide synthase (iNOS), which can result in inflammation and sepsis [246]. Chronic neuroinflammation can further lead to retention of amyloid beta (Aβ) plaques and tau tangles as seen in AD, and ultimately, memory loss, and dementia [224].

Emerging evidence shows the metabolic imbalance and inflammatory responses may not only originate in the brain per se, but also from gut microbiota [247]. The gut microbiota is the community of microorganisms in the intestines that contains over 1,000 different bacterial species, categorized into four primary phyla: *Firmicutes*, *Bacteroidetes*, *Actinobacteria*, and *Proteobacteria* [248]. A number of studies have demonstrated that the gut microbiota changes with age [249-251]. In particular, an increased *Firmicutes/Bacteroidetes* (F/B) ratio is associated with increased inflammation and excess energy harvest from food in obese patients [252]. Increased F/B ratio is associated with the weakening of the epithelial tight junctions, allowing proinflammatory cytokines produced by pathogenic bacteria transfer to the brain from the blood stream or vagus nerve [72, 253]. Inflammation due to leaky gut syndrome has also been shown to increase the risk for anxiety and depression [254], which can exacerbate learning and memory performance [255, 256].

Leaky gut syndrome also leads to neurovascular defects, evident by increased blood-brain barrier (BBB) permeability [72]. The reduction of BBB transporters may lead to impaired clearance of Aβ [20, 237], enhancing the risk

of dementia like symptoms [257]. Impaired BBB function is also linked with reduced cerebral blood flow (CBF) [20]. Indeed, reductions in CBF with age have been known for years [212]. These neurovascular risks are highly associated with accelerated decline in language ability, verbal memory, attention and visuospatial abilities, and increased anxiety and depression in aging [236, 237, 258-260].

Collectively, the cognitive aging and risk for AD may be driven by deleterious changes of brain physiology originated from the central nervous system as well as the peripheral systems. Nonetheless, the associations between brain metabolism, perfusion, cognition, and gut microbiome remain largely unknown. In this study, our objective was to examine the effects of aging on the brain and the gut in young and old mice and how these effects collectively alter neurological function. To achieve this, we used metabolomics for brain metabolite assessment, 16s ribosomal RNA (rRNA) gene amplicon sequencing to analyze the gut microbiome, neuroimaging to examine brain vascular functions, and behavioral testing to determine memory and anxiety. We hypothesized that age-related deleterious changes would be exhibited in the brain and gut, effecting brain metabolic, vascular and cognitive functions, which may increase the risk for developing AD.

7.3 Methods

7.3.1 Animals

Young (5-6 mo) and old (18-20 mo) male C57BL/6N mice were acquired from the National Institute of Aging Colony. We determined the sample size via power analysis to ensure comparison at a 0.05 level of significance and 90% chance of detecting a true difference of each measured variable between the two groups. Each mouse was caged individually and housed in a specific pathogen-free facility. In order to avoid the potential for aggression when combining multiple male mice into one cage, mice were housed individually. Further, mice should be housed individually for gut microbiome analysis due to cage effects from microbiome transfer, e.g. mice eating each other's feces giving them a very similar gut microbiome and thus, the mice would be N = 1 for that particular cage [113]. The mice were weighed weekly and given *ad libitum* access to food and water. All experimental procedures were performed according to NIH guidelines and approved by the Institutional Animal Care and Use Committee (IACUC) at the University of Kentucky (UK).

7.3.2 Gut Microbiome Analysis

For fecal DNA amplification, fecal samples were collected from young (N =39) and old (N= 28) mice and frozen at -80˚C until further use. A PowerSoil DNA Isolation Kit (MO BIO Laboratories, Inc.) was used for fecal DNA extraction, according to the manufacturer's protocol. Genomic DNA was PCR amplified with primers CS1_515F and CS2_926R [114] targeting the V4-V5 regions of microbial

16S rRNA genes using a two-stage "targeted amplicon sequencing (TAS)" protocol [115, 116]. First stage amplifications were performed with the following thermocycling conditions: 95°C for 3mins, 28 cycles of 95°C for 45sec, 55°C for 45sec, 72°C for 90sec and final elongation at 72°C for 10 minutes. Barcoding was performed using a second-stage PCR amplification with Access Array Barcode Library for Illumina Sequencers (Fluidigm, South San Francisco, CA; Item# 100-4876). The pooled libraries, with a 15% phiX spike-in, were loaded on a MiSeq v3 flow cell, and sequenced using an Illumina MiSeq sequencer, with paired-end 300 base reads. Fluidigm sequencing primers, targeting the CS1 and CS2 linker regions, were used to initiate sequencing. De-multiplexing of reads was performed on instrument. Second stage PCR amplification and library pooling was performed at the DNA Services (DNAS) facility, Research Resources Center (RRC), University of Illinois at Chicago (UIC). Sequencing was performed at the W.M. Keck Center for Comparative and Functional Genomics at the University of Illinois at Urbana-Champaign (UIUC).

For microbial analysis, forward and reverse reads were merged using PEAR [117]. Primer sequences were identified using Smith-Watermann alignment and trimmed from the sequence. Reads that lacked either primer sequence were discarded. Sequences were then trimmed based on quality scores using a modified Mott algorithm with PHRED quality threshold of $p = 0.01$, and sequences shorter than 300 bases after trimming were discarded. QIIME v1.8 was used to generate OTU tables and taxonomic summaries [118]. Briefly, the resulting sequence files were merged with sample information. Operational

134

taxonomic unit (OTU) clusters were generated in a *de novo* manner using the UCLUST algorithm with a 97% similarity threshold [119]. Chimeric sequences were identified using the USEARCH61 algorithm with the GreenGenes 13_8 reference sequences [120]. Taxonomic annotations for each OTU were using the UCLUST algorithm and GreenGenes 13_8 reference with a minimum similarity threshold of 90% [119, 120]. Taxonomic and OTU abundance data were merged into a single OTU table and summaries of absolute abundances of taxa were generated for all phyla, classes, orders, families, genera, and species present in the dataset. The taxonomic summary tables were then rarefied to a depth of 10,000 counts per sample.

Shannon and Bray-Curtis indices were calculated with default parameters in R using the vegan library [121, 122]. The rarefied species data, taxonomic level 7, were used to calculated both indices. Plots were generated in R using the ggplot2 library [123]. Significant difference among tested groups was determined using the Kruskal-Wallis one-way analysis of variance. The group significance tests were performed on the rarefied species data, taxonomic level 6 (genus), using the group_significance.py script within the QIIME v1.8 package.

The gene amplicon sequence data generated as part of this study have been submitted to the NCBI BioProject database under accession number (PRJNA400638).

7.3.3 Behavior Testing

All behavior tests were conducted over a two-week period with each test starting at the same time each morning. For each mouse, Elevated Plus Maze (EPM) was done first followed by Novel Object Recognition (NOR) the next day. Radial Arm Water Maze (RAWM) testing was then carried out starting the day after NOR. A subset of young (N = 22) and old (N =18) mice underwent three behavior tests. For more details on the three behavior tests, please see Chapter 2, section 2.9.

7.3.4 Cerebral Blood Flow Measurement

A subset of young and old mice (N = 12 per group) were used to measure *in vivo* CBF using magnetic resonance imaging (MRI). For more details on this, please see Chapter 2, section 2.6.

7.3.5 Blood-Brain Barrier Function Determination and Western Blotting

BBB function was determined by measuring P-glycoprotein (P-gp) transport activity in isolated brain capillaries. P-gp is an ATP-driven transporter highly expressed at the BBB that facilitates transport of Aβ from brain to blood. This technique was previously established via a confocal imaging-based assay to assess P-gp transport activity in freshly isolated brain capillaries from mice [261, 262]. This assay measures within capillary lumens accumulation of [N-ε(4-nitro-benzofurazan-7-yl)-D-Lys(8)]-cyclosporin A (NBD-CSA), a fluorescent P-glycoprotein substrate.

For capillary isolation, after euthanasia, mouse brain capillaries (N= 7 per group) were isolated according to a previously described protocol [261, 263]. Briefly, mice were euthanized by CO_2 inhalation and decapitated; brains were immediately harvested and collected in ice-cold DPBS buffer supplemented with 5 mM D-glucose and 1 mM Na-pyruvate, pH 7.4. Brains were dissected by removing meninges, choroid plexus and white matter, and homogenized in DPBS. The brain homogenate was mixed with Ficoll® and centrifuged at 5,800g for 20 minutes at 4°C. The capillary pellet was resuspended in 1% BSA buffer and first passed through a 300 μm nylon mesh and then through a 27 μm nylon mesh. Capillaries retained by the 27 μm nylon mesh were collected and washed with DPBS buffer and used for experiments.

For p-glycoprotein transport activity, isolated capillaries were incubated for 1 h at room temperature with 2 μM NBD-CSA (custom-synthesized by R. Wenger (Basel, Switzerland)) in DPBS buffer. Ten capillary images were acquired by confocal microscopy (Leica TSP SP5 Confocal Microscope with Environmental Chamber, 63 × D-Water UV objective, numerical aperture 1.2, Zoom: 4, 488-nm line of an argon laser, Leica Microsystems). Confocal images were analyzed by quantitating luminal NBD-CSA fluorescence with Image J software (v.1.45s; Wayne Rasband, NIH). Specific, luminal NBD-CSA fluorescence was taken as the difference between total luminal fluorescence and fluorescence in the presence of the P-glycoprotein-specific inhibitor PSC833 (5 μM, Novartis, Basel, Switzerland) [264].

For western blotting and quantification to determine protein expression, isolated brain capillaries were homogenized in tissue lysis buffer containing a cocktail of protease inhibitors. Homogenized brain capillary samples were centrifuged at 10,000 g for 15 minutes at 4°C, followed by a centrifugation of the denucleated supernatants at 100,000 g for 90 minutes at 4°C. Pellets (crude brain capillary plasma membranes) were resuspended and protein concentrations were determined using the Bradford protein assay. Normalized brain capillary membrane samples were separated on a NuPAGE™ 4-12% Bis-Tris Protein Gels (1.0 mm, 15-wells; Thermo Fisher Scientific, Waltham, MA, USA) and transferred onto an Invitrolon™ PVDF membrane (0.45 µm pore size; Thermo Fisher Scientific, Waltham, MA, USA) membrane using the NuPAGE® electrophoresis and blotting system (Invitrogen, Carlsbad, CA, USA). After protein transfer, the blotting membranes were incubated overnight with antibody to P-gp (C219; MA1-26528, ThermoFisher, 1µg/ml) and β-actin (ab8226 from Abcam, 1:1000, 1 µg/ml). Proteins were detected using SuperSignal® West Pico Chemoluminescent substrate (Pierce, Rockford, IL, USA) and protein bands were visualized with a BioRad Gel Doc™ XRS imaging system. P-gp was visualized first, membranes were then stripped with Restore™ Western Blot Stripping Buffer (Thermo Fisher Scientific, Waltham, MA, USA) and incubated with the antibody against β-actin. Image Lab 5.0 software from Bio-Rad Laboratories was used for densitometric analyses of band intensities and digital molecular weight analyses; the molecular weight marker was RPN800E (GE

Healthcare, Chalfont St. Giles, Buckinghamshire, UK). Linear adjustments of contrast and brightness were applied to entire Western blot images.

7.3.6 Inducible Nitric-Oxide Synthase Measurement

Total RNA from frontal cortex and hypothalamus homogenate (N =7-8 per group) was isolated using TRI Reagent solution (Ambion), and cDNA was synthesized from 1ug total RNA from each individual sample using SuperScript III (Invitrogen). qRT-PCR was performed using TaqMan real time PCR (ViiA™ 7, Applied Biosystems). All reactions were performed with non-template negative control, and all data are mean ± SEM of two independent biological replicates. The gene probes and master mix were also purchased from Applied Biosystems. The probe sets were as follows: Mm00440502-m1 (inducible nitric-oxide synthase (Nos2)), Mm00446968-m1 (hypoxanthine guanine phosphoribosyl transferase (Hprt)). The relative expression levels were measured using the relative quantitation ΔCt (delta counts) method and normalized to Hprt.

7.3.7 Metabolomic Profiling

Please see Chapter 2, section 2.5 for more detail.

7.3.8 Statistical Analysis

All statistical analyses were completed using GraphPad Prism (GraphPad, San Diego, CA, USA). One-tailed Student's *t*-test was performed for determination of differences between groups. Levels of statistical significance

were reached when $p < 0.05$. For Metabolon, missing values in the data are assumed to be below the level of detection of the used instruments. Log transformations and imputation of missing values with the minimum observed values for each metabolite was conducted. This was followed by ANOVA to identify biochemicals that were significantly different between groups. Given the multiple comparisons inherent in analysis of metabolites, between-group relative differences are assessed using both p-value and false discovery rate analysis (q-value).

7.4   Results

7.4.1   Altered Gut Microbiome and Increased Body Weight with Age

Alpha diversity (*e.g.*, Shannon index, H value) was measured for fecal microbial communities of all samples, at the taxonomic level of genus (Figure 1A). Older mice had a significantly higher alpha diversity than young mice (Kruskal-Wallis p-value = 0.022). Although no significant differences in beta diversity were observed (Analysis of similarity, ANOSIM R statistic=0.006, p-value=0.307, 999 permutations), and no specific taxa were significantly different between the groups of young and old mice (Kruskal-Wallis, false discovery rate, FDR-corrected p-value <0.05), the ratio of Firmicutes/Bacteroidetes was significantly different between age groups. Old mice had significantly higher *Firmicutes/Bacteroidetes* (F/B) ratio (Fig. 1B, 46% increase, $p < 0.05$). Further, we found that the body weight of the old mice was significantly higher compared with that of the young mice (Fig. 1C, 24% increase, $p < 0.05$).

7.4.2 Enhanced Proinflammatory Metabolism with Age

The quantification of the brain metabolites is shown in Table 7.1. We observed several significant age-dependent changes in basal brain metabolites (after 6 hours of final feeding). Notably, the old group had a 31-83% change in markers of the methionine cycle with significantly greater methionine, cysteine, cysteine-glutathione disulfide, and cystathionine. Firstly, methionine is an amino acid that may be accountable for increased mitochondrial reactive oxygen species (ROS)[265]. Due to this, we believe the old mice exhibit increased oxidative stress in the brain. We also found lipids related to inflammatory responses significantly elevated in the old mice, including a 82% increase in prostaglandin D2, and a 80% increase in prostaglandin E2. Further, markers associated with Alzheimer's disease (AD) were significantly greater in the old mice compared to the young, including a 21% increase in 24(S)-hydroxycholesterol, 28% increase in mead acid (20:3n9), 37% increase in phenylalanine, 58% increase in spermidine, 22% increase in docosapentaenoate (n6 DPA; 22:5n6), 11% increase in creatine, and 12% increase in phosphocholine [266-272]. In contrast, CDP-choline, a metabolite that has shown to alleviate AD symptoms [273], saw a 6% decrease in the old group. In addition, old mice also demonstrated a 114% increase in citrate. Collectively, the metabolic profiling indicates that the old mice had enhanced proinflammatory metabolism. These data are consistent with our observation of significantly increased iNOS levels in the brain of old mice compared to that of young mice (Fig. 2A, 17% increase, p = 0.02).

We found that two of the brain metabolites related to gut microbiota were also significantly different between young and old cohorts. Compared to the young mice, old mice had significantly higher 3-indoxyl sulfate (Fig. 2B, 380% increase, $p < 0.05$) and phenol sulfate (Fig. 2C, 144% increase, $p < 0.05$) in their brain within 2 hours after their final feeding, however, the levels of the two metabolites returned to the baseline after 6 hours of feeding. 3-indoxyl sulfate is generated in the liver as a result of gut microbiome metabolism of tryptophan; phenol sulfate is a metabolite derived from bacterial metabolism of phenylalanine. The results suggest that the gut microbiome may play an important role in modulating brain metabolism. Because 3-indoxyl sulfate and phenol sulfate both are related to neurological toxicity and inflammation [274, 275], it implies that old mice had higher neuroinflammation, which may of resulted from age-dependent changes in the gut microbiota.

7.4.3 Impaired Neurovascular Functions with Age

We found impaired BBB function in the old mice. Figure 3A shows representative confocal images of capillaries; the intensity of fluorescence in the capillary lumen reflects the amount of P-glycoprotein (P-gp), an efflux transporter of Aβ. The corresponding quantitative results are shown in Figure 3B; the old mice had significantly reduced P-gp transport activity ($p = 0.0031$) compared to the young mice. We also measured P-gp protein expression levels (Fig. 3C). Similar to the results of P-gp activity, we found that the old mice had significant reduction in P-gp protein levels compared to the young mice (decrease to 63.7 ±

5.4 % over 100% young; $p < 0.001$; Fig. 3C). We also observed reduced CBF in the old mice. Figure 3D shows the representative CBF images of the young and old mice. The CBF level is colorized in a linear scale, indicating that the young mice have overall higher CBF compared to the old mice, which was confirmed by the quantitative global CBF values (Fig. 3E, 87% increase, $p < 0.001$). We did further CBF analyses in brain regions associated with cognitive functions (e.g., memory and learning) based on MRI structural imaging and mouse brain atlas. We found that young mice exhibited an 82% increase in CBF in the hippocampus ($p < 0.001$, Fig. 3F), compared to the old mice.

7.4.4   Compromised Cognition and Increased Anxiety with Age

The old mice spent significantly longer time in the closed arms compared to the young mice in the EPM test (Fig. 4A; 132% increase, $p < 0.0001$), indicating higher anxiety. In the NOR test, the old mice showed a significantly lower D_2 value compared to the young group, suggesting reduced recognition memory (Fig. 4B, -74% decrease, $p < 0.0001$). In the RAWM test, the old group made significantly more errors in the learning phase (Block 3; 46% increase, $p < 0.01$) and the initial recall phase (Block 4; 43% increase, $p < 0.01$), compared to the young group (Fig. 4C).

7.5   Discussion

In this study, we demonstrated the age-dependent changes in brain metabolism, gut microbiome, vascular functions, memory and anxiety.

Specifically, aged mice had enhanced proinflammatory, increased ratio of Firmicutes to Bacteroidetes, increased bacterial alpha diversity, and body weight, impaired BBB and CBF, compromised learning and long-term memory, and increased anxiety. These deleterious changes in aging have the potential to increase the risk for neurological disorders and dementia, including AD.

We found several amino acid increased in the old mice that are highly associated with AD, including spermidine, phenylalanine, creatine citrate, and methionine-related metabolites. First, spermidine levels have been found to be higher in the temporal cortex with a trending elevation in hippocampus and frontal cortex in AD patients, potentially as a response to brain injury [269]. Excess spermidine could exacerbate neurodegeneration as it positively modulates N-methyl-D-aspartate (NMDA) glutamate receptor function and disrupt calcium homeostasis. Second, high phenylalanine levels are also found in AD patients, associated with immune activation [268]. Phenylalanine disturbs neopterin and tryptophan metabolism, which is correlated with cognitive impairment [276, 277]. Third, old mice had higher creatine deposits in the brain, consistent with literature that creatine metabolism malfunction plays an important role in AD [237, 271]. Fourth, old mice had increased levels of citrate in the brain suggesting increased usage of fatty acid synthesis for membrane remodeling associated with aging due to the increased stress and inflammation that damage neuronal membranes [278]. Finally, the old mice had altered methionine-associated metabolism, including increased methionine, cystathionine, cysteine, and cysteine-glutathione disulfide. Excessive methionine has been considered to

be accountable for increased mitochondrial ROS production, which in turn enhances oxidative stress and inflammation [277, 279, 280]. Interestingly, previous studies have shown that methionine restriction can lead to increased longevity by decreasing mitochondrial complex IV activity and accumulation of ROS [281, 282].

Accumulation of lipids in the brain is another hallmark of AD [283]. In the present study, we also found AD-associated fatty acids increased in the aged mice. First, 24(S)-hydroxycholesterol, an oxidized product of cholesterol produced in the brain, has been demonstrated to be elevated in AD patients and is hypothesized to be an early marker for distorted cholesterol status [266]. Second, phosphocholine has been revealed to be increased in rats during the early stages of AD during lesion-induced neuronal sprouting in the hippocampus [272]. This indicates that sprouting may occur early on in AD with phosphocholine as a marker. In addition, sprouting may also lead to a decline in energy metabolism due to energy being used for sprouting, consistent with the evidence of glucose metabolism decline in AD. Third, mead acid (20:3n9), an omega-9 fatty acid, has been demonstrated to be increased in the mid-frontal cortex, temporal cortex, and hippocampus of AD patients [267]. Fourth, docosapentaenoate (n6 DPA), an omega-6 fatty acid, has been inversely correlated with learning [270]. This is consistent with previous findings that oleic acid-enriched triglycerides were found in the brain of a triple transgenic mice model of AD (3xTg-AD); but when the triglycerides were inhibited, proper brain function was restored [284]. Further, prostaglandin D2 and E2, produced from

arachidonate, are generators of an inflammatory response and present in increased amounts in such an event, were also elevated in the old group [285]. Specifically, in one study, prostaglandin E2 was associated with neuronal oxidative damage after activation by lipopolysaccharide (LPS)[286]. LPS also can activate iNOS, which is consistent with our finding that old mice had significantly increased iNOS expression in the brain. In contrast, the aged mice showed reduced levels of CDP-choline, which has shown to alleviate AD symptoms by increasing CBF and brain electrical activity and reducing serum cytokine IL-1β levels [273]. Old mice also had dramatically decreased levels of glycerophopshorylcholine (GPC), which has been used to treat patients with cognitive impairment and AD [287]. Collectively, old mice exhibited a myriad of markers associated with inflammation and AD.

The enhanced inflammation with age may have also occurred in the gut. We found that 3-indoxyl sulfate and phenol sulfate, which originate from the gut microbiota, were significantly elevated in the aged mice's brains after meals. Significant increases of indoxyl sulfate have shown to enhance neurological toxicity, increase oxidative stress and ROS, and induce endothelial dysfunction by inhibiting endothelial proliferation and migration *in vitro* [288, 289]. In addition, phenol sulfate is derived from bacterial metabolism of phenylalanine, a marker for AD, as mentioned above. Next, we found a modest increase in older mice in the relative abundance of sequences from bacteria of the phylum *Firmicutes*, with a concomitant decrease in the relative abundance of sequences from bacteria of the phylum *Bacteroidetes*. Although neither change was statistically significant,

the overall change, leading to an increased *Firmicutes/Bacteroidetes* (F/B) ratio in older mice, was significant. As bacteria from the *Firmicutes* have been associated with weight-gain and those within the *Bacteroidetes* with weight-loss, this increased F/B ratio may promote body weight gain in old mice [49]. Further, this increased F/B ratio may lead to excessive low-grade inflammation and a substantial increase in energy harvesting and food intake [43, 290]. As a result, the F/B ratio has become a well-known marker for obesity and T2DM (Type 2 Diabetes Mellitus) [291]. Interestingly, AD has been called Type 3 diabetes due to the overlapping symptoms observed in T2DM, e.g. insulin resistance and increased inflammation in the brain [292], along with an increased risk of dementia [293]. Thus, the increased F/B ratio may be indicative of an increased risk for AD.

Short-chain fatty acids (SCFAs), including butyrate and propionate that are produced by certain bacterial species, have a dramatic impact on brain function. For example, butyrate has been demonstrated to prevent inflammatory responses via NFκB inhibition in microglia and hippocampal slice cultures [81]. Also, indole-3-proprionic acid (IPA), another metabolite produced by the gut microbiome, was demonstrated to inhibit Aβ fibril formation in neurons and neuroblastoma cells [85]. On the contrary, increased *Firmicutes* may enhance trimethylamine (TMA) and its co-metabolites trimethylamine N-oxide (TMAO) [294]. TMAO level predicts risk for atherosclerosis and directly induces cardiovascular disease [80, 295-297].

Reduced SCFAs has been shown to induce BBB permeability [72]. This is consistent with our findings that BBB function was compromised in the old mice. Specifically, we found the old mice had a significantly lower quantity of P-gp transporters in BBB, which are responsible for Aβ clearance from the brain to blood, indicative of an increased risk of developing AD [298]. BBB breakdown has been caused by elevated neuroinflammation [20] and is associated with CBF reduction. In line with this, we found decreased CBF in old mice. In particular, old mice had significantly decreased CBF in the hippocampus, the brain region that modulates cognitive function. Further, the old mice performed worse in the RAWM and NOR behavior tests than the young animals. Specifically, the old group performed worse in Block 3 and 4 of the RAWM compared to the young group, exhibiting inhibited spatial learning and long-term memory formation, consistent with our previous findings [129, 133]. In the NOR test, the old group had a worse D_2 score compared to the young group, indicating a worse recognition memory. Taken together, our findings are consistent with the literature where impaired neurovascular integrity plays a critical role in determining cognitive functions [299].

Higher anxiety levels were shown in old mice compared to young mice, which may be also associated with brain vascular and metabolic dysfunctions [258-260]. Interestingly, the gut microbiome has been linked with anxiety [141]. Indeed, the gut and brain are connected via the enteric nervous system and have bi-directional communication, impacting behavior [300]. Certain bacterial species such as *L. rhamnosus* have been demonstrated to decrease anxiety like

symptoms and stress induced hormones [88]. Studies using oral administration of food-borne pathogens showed evidence that bacteria residing in the gastrointestinal tract can activate stress circuits through activation of vagal pathways [301, 302]. Exposure to a subpathogenic infection of *C. jejuni* increased anxiety-like behavioral measure in the EPM two days after infection [303]. These studies clearly demonstrated that inflammatory state could have strong influences on behavior and mental health. Conversely, treating mice with probiotics has been shown to reduce anxiety-like behavior; the probiotic-treated group showed increased entries into the open arms of the EPM compared to the control group [304]. Further confirming the importance of the gut microbiome in relation to stress, one study demonstrated germ-free mice to have an excessive release of stress hormones. However, when these mice were colonized with *Bifidobacterium infantis,* this response was alleviated [305]. Similar observations were also made in clinical trials in patients with chronic fatigue, showing that anxiety-like symptoms were alleviated by probiotics [306]. The study findings may be applicable to AD as increased anxiety levels and depression are commonly found preceding the onset of AD [225]. Modulating the gut microbiome may thus be important for reducing risk or preventing AD and other neurodegenerative disorders [307-310].

We summarize our findings with Figure 5. It shows that advancing age drives deleterious modifications in metabolism, gut microbiome, neurovascular integrity, cognition, and mental health, which may significantly enhance the risk for AD. Our study implies that inflammation may play a critical role in the

remodeling process. This is consistent with the concept of inflammaging, the phenomenon where innate immunity is activated, coupled with the rise of proinflammation with advancing age [311]. We suggest that, based on our results, the inflammatory responses with age are systematic; they may be originated from the CNS as well as the peripheral systems, e.g., from the gut. To promote healthy aging and prevent AD, it will thus be critical to manage low-grade, chronic proinflammation over time.

In future studies, it is important to determine mechanisms linking the brain and gut in the context of brain aging, including pathways involved in SCFAs, neurotransmitters, vagus nerve activity, and immune system function. As well as, to identify potential nutritional interventions that can promote brain-gut interactions, such as probiotics and prebiotics.

We have recently shown that dietary interventions can delay brain aging (e.g., caloric restriction and rapamycin) and thus, it will be crucial in the future to determine if these dietary interventions also have a significant impact on the brain-gut axis [129, 133, 312]. In addition, it will be imperative to develop surrogate biomarkers using neuroimaging. In the present study, we used MRI to measure in vivo CBF, but we have also developed imaging methods to determine brain metabolic and anatomical integrity [313, 314]. Further, we will also use this state-of-the-art technology to study brain-gut axis and make our research strategy translatable to clinical applications.

In conclusion, we found the inflammation-associated impact on brain metabolism, gut microbiome, neurovascular functions, memory, and anxiety in

aging mice. However, additional research needs to be conducted on the gut microbiome and mechanisms of the gut-brain axis. Understanding brain aging is imperative to identify risks, and intervention thereof, for AD. A comprehensive and integrative characterization of brain aging, including its crosstalk with peripheral systems and factors, will help to define the mechanisms underlying the shift from normal aging to pathological processes in the etiology of AD [309, 310].

Table 7-1 Enhanced proinflammatory metabolism with age

Classification	Metabolite	P	Young	Old
Amino Acids	creatine	0.003	0.990 ± 0.022	1.101 ± 0.017
	cystathionine	0.026	0.943 ± 0.072	1.316 ± 0.174
	cysteine	0.007	1.023 ± 0.138	1.873 ± 0.262
	cysteine-glutathione disulfide	0.013	1.008 ± 0.132	1.736 ± 0.267
	methionine	0.001	0.915 ± 0.047	1.204 ± 0.015
	phenylalanine	0.002	0.917 ± 0.042	1.255 ± 0.085
	spermidine	0.016	0.910 ± 0.059	1.436 ± 0.238
Cofactors & Vitamins	citrate	0.008	0.867 ± 0.099	1.860 ± 0.381
Lipids	24(S)-hydroxycholesterol	0.025	0.939 ± 0.027	1.135 ± 0.098
	CDP-choline	0.037	1.002 ± 0.014	0.944 ± 0.028
	docosapentaenoate (n6 DPA; 22:5n6)	0.007	0.994 ± 0.019	1.215 ± 0.085
	mead acid (20:3n9)	0.025	1.070 ± 0.068	1.367 ± 0.122
	phosphocholine	0.024	1.076 ±0.029	1.206 ± 0.054
	prostaglandin D2	0.009	0.682 ± 0.087	1.238 ± 0.193
	prostaglandin E2	0.007	0.746 ± 0.076	1.341 ± 0.207

Table 7-1 Enhanced proinflammatory metabolism with age

Metabolomic profiling of brain metabolites. Representative data, shown in scaled intensity, of the young and old groups. Data are mean ± SEM.

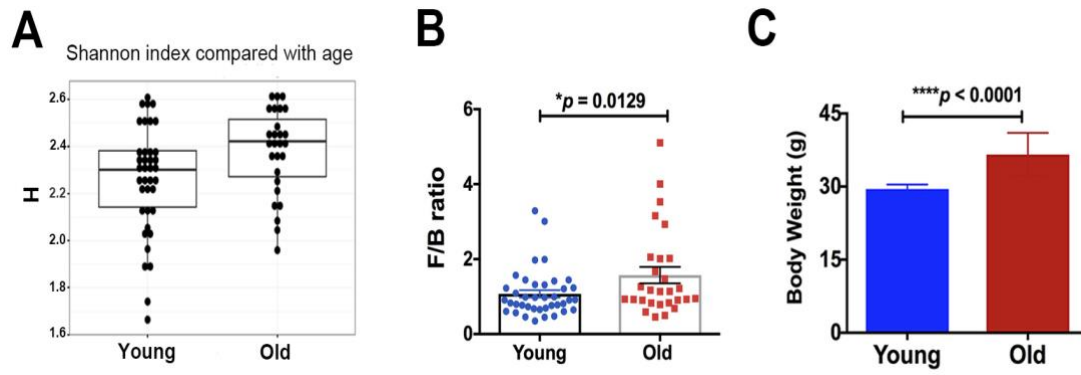**Figure 7-1** Altered gut microbiome and increased body weight with age

Figure 7-1 Altered gut microbiome and increased body weight with age

(A) The old mice showed a higher alpha-diversity, as indicated by the Shannon index, than the young mice (p = 0.02). Compared with the young mice, the old mice had significantly increased **(B)** *Firmicutes/Bacteroidetes* ratio and **(C)** body weight. N= 39 and 28 for young and old mice, respectively. Data are presented as mean ± SEM.

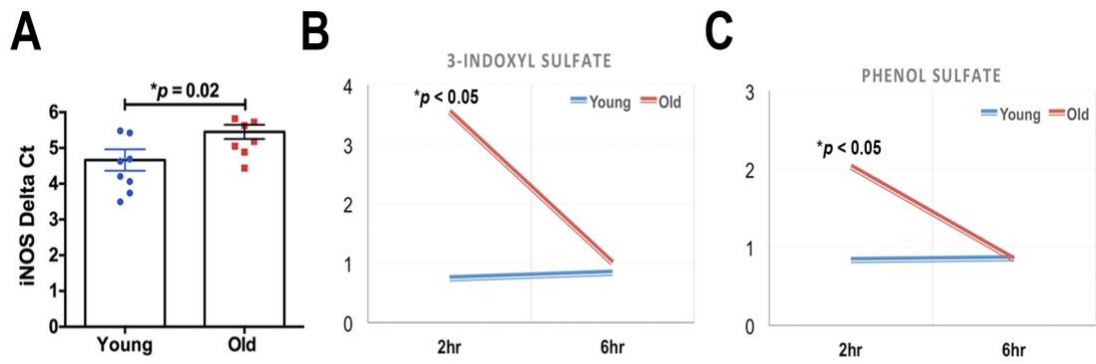**Figure 7-2** Age increases inducible nitric oxide synthase (iNOS)

Figure 7-2 Age increases inducible nitric oxide synthase (iNOS)

(A) The old mice had a significant increase in iNOS in the brain compared to the young mice (N = 7-8 per group). The old mice had acute elevations (2 hours after feeding) in **(B)** 3-indoxyl sulfate and **(C)** phenol sulfate; those levels returned to baseline in 4 hours (N = 6 and 4 for young and old mice, respectively).

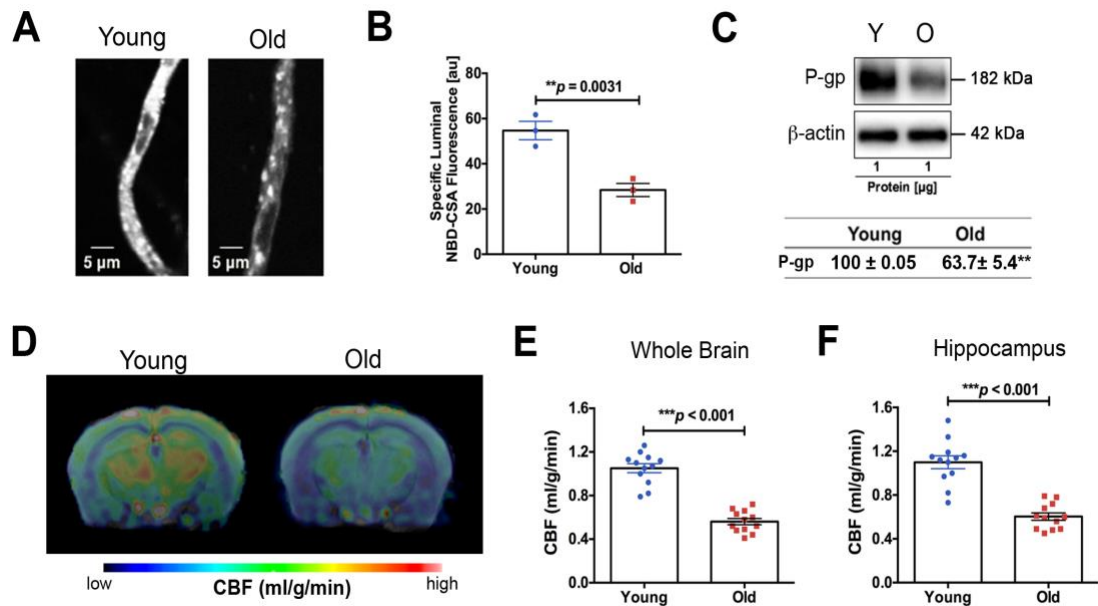**Figure 7-3** Impaired neurovascular functions with age

Figure 7-3 Impaired neurovascular functions with age

(A) Representative confocal images showing decreased luminal accumulation of NBD-CSA fluorescence (green) in brain capillaries isolated from the old mice compared to young mice, indicating reduced P-gp activity. **(B)** Corresponding quantitative fluorescence data; images are shown in arbitrary fluorescence units (scale 0-255). Data are mean ± SEM for 10 capillaries from one preparation of 10 mice. **(C)** Western blotting (WB) for P-gp from the cortical vasculature, β-Actin was used as loading control (top); corresponding values are shown in the table (bottom). The WB data from the old mice were normalized to β-Actin and compared to the young mice (100%), **$p < 0.01$. **(D)** CBF maps superimposed on structural images; the color code indicates the level of CBF in a linear scale. Quantitative CBF (ml/g/min) obtained from **(E)** the whole brain and **(F)** hippocampus (N = 12 per group). Data are mean ± SEM.

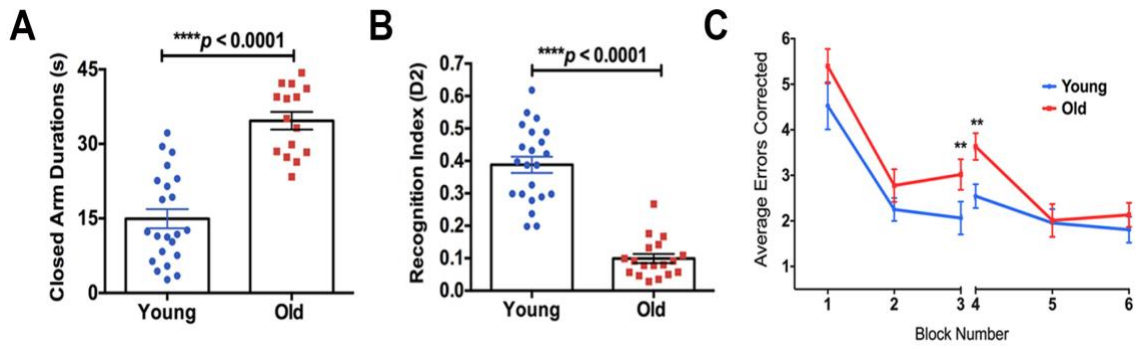**Figure 7-4** Compromised cognition and increased anxiety with age

Figure 7-4 Compromised cognition and increased anxiety with age

(A) The elevated plus maze found the old mice to have a significantly higher closed arm duration compared to the young group. **(B)** The novel object recognition test found the old group had a significantly lower recognition index, or D$_2$, than the young group. **(C)** The average errors made by the young and old mice during the radial arm water maze split into 6 blocks. The significant difference between the two groups in average errors corrected showing in Block 3 (p = 0.0307) and Block 4 (p = 0.0045). N = 22 and 18 for young and old mice, respectively. Data are presented as mean ± SEM.

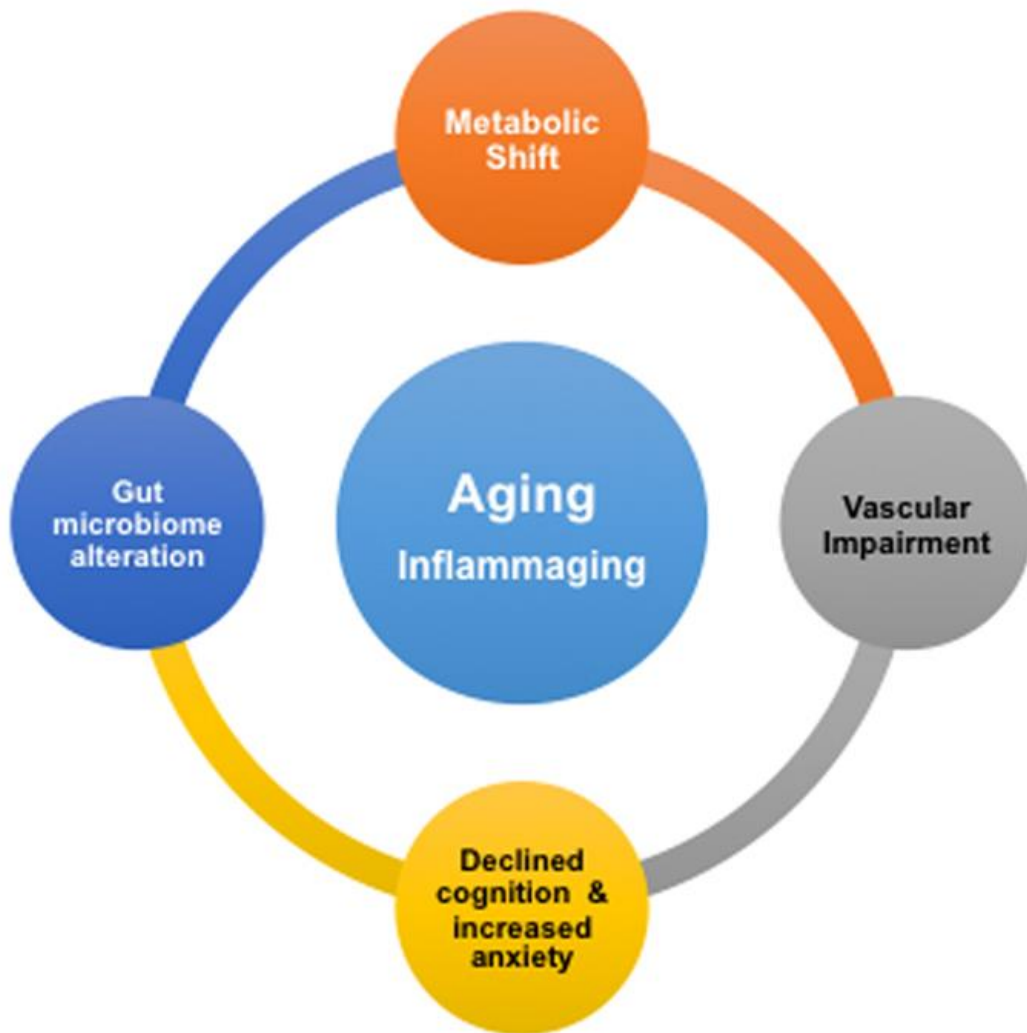**Figure 7-5** Association of age-dependent changes

Figure 7-5 Association of age-dependent changes

Proposed associations of age-dependent changes in brain metabolism, vascular integrity, gut microbiome, cognition and anxiety levels. Inflammation in aging, or inflammaging, might play a critical role in be a driving the deleterious changes in the brain and gut.

References

1. Masters, C.L., et al., *Alzheimer's disease.* Nat Rev Dis Primers, 2015. **1**: p. 15056.

2. Guerreiro, R. and J. Bras, *The age factor in Alzheimer's disease.* Genome Med, 2015. **7**: p. 106.

3. Hebert, L.E., et al., *Alzheimer disease in the United States (2010-2050) estimated using the 2010 census.* Neurology, 2013. **80**(19): p. 1778-83.

4. Corrada, M.M., et al., *Dementia incidence continues to increase with age in the oldest old: the 90+ study.* Ann Neurol, 2010. **67**(1): p. 114-21.

5. Becker, R.E., N.H. Greig, and E. Giacobini, *Why do so many drugs for Alzheimer's disease fail in development? Time for new methods and new practices?* J Alzheimers Dis, 2008. **15**(2): p. 303-25.

6. Kivipelto, M., et al., *The Finnish Geriatric Intervention Study to Prevent Cognitive Impairment and Disability (FINGER): study design and progress.* Alzheimers Dement, 2013. **9**(6): p. 657-65.

7. Serrano-Pozo, A., et al., *Neuropathological alterations in Alzheimer disease.* Cold Spring Harb Perspect Med, 2011. **1**(1): p. a006189.

8. Riedel, B.C., P.M. Thompson, and R.D. Brinton, *Age, APOE and sex: Triad of risk of Alzheimer's disease.* J Steroid Biochem Mol Biol, 2016. **160**: p. 134-47.

9. Bird, T.D., *Genetic aspects of Alzheimer disease.* Genet Med, 2008. **10**(4): p. 231-9.

10. Duering, M., et al., *Mean age of onset in familial Alzheimer's disease is determined by amyloid beta 42.* Neurobiol Aging, 2005. **26**(6): p. 785-8.

11. Huang, Y. and R.W. Mahley, *Apolipoprotein E: structure and function in lipid metabolism, neurobiology, and Alzheimer's diseases.* Neurobiol Dis, 2014. **72 Pt A**: p. 3-12.

12. Bu, G., *Apolipoprotein E and its receptors in Alzheimer's disease: pathways, pathogenesis and therapy.* Nat Rev Neurosci, 2009. **10**(5): p. 333-44.

13. Chang, S., et al., *Lipid- and receptor-binding regions of apolipoprotein E4 fragments act in concert to cause mitochondrial dysfunction and neurotoxicity.* Proc Natl Acad Sci U S A, 2005. **102**(51): p. 18694-9.

14. Moir, R.D., et al., *Differential effects of apolipoprotein E isoforms on metal-induced aggregation of A beta using physiological concentrations.* Biochemistry, 1999. **38**(14): p. 4595-603.

15. Zhong, N. and K.H. Weisgraber, *Understanding the association of apolipoprotein E4 with Alzheimer disease: clues from its structure.* J Biol Chem, 2009. **284**(10): p. 6027-31.

16. Tai, L.M., et al., *Soluble apoE/Abeta complex: mechanism and therapeutic target for APOE4-induced AD risk.* Mol Neurodegener, 2014. **9**: p. 2.

17. Brecht, W.J., et al., *Neuron-specific apolipoprotein e4 proteolysis is associated with increased tau phosphorylation in brains of transgenic mice.* J Neurosci, 2004. **24**(10): p. 2527-34.

18. Lin, A.L., et al., *Chronic rapamycin restores brain vascular integrity and function through NO synthase activation and improves memory in symptomatic mice modeling Alzheimer's disease.* J Cereb Blood Flow Metab, 2013. **33**(9): p. 1412-21.

19. Thambisetty, M., et al., *APOE epsilon4 genotype and longitudinal changes in cerebral blood flow in normal aging.* Arch Neurol, 2010. **67**(1): p. 93-8.

20. Bell, R.D., et al., *Apolipoprotein E controls cerebrovascular integrity via cyclophilin A.* Nature, 2012. **485**(7399): p. 512-6.

21. Rasmussen, K.L., *Plasma levels of apolipoprotein E, APOE genotype and risk of dementia and ischemic heart disease: A review.* Atherosclerosis, 2016. **255**: p. 145-155.

22. Bennet, A.M., et al., *Association of apolipoprotein E genotypes with lipid levels and coronary risk.* JAMA, 2007. **298**(11): p. 1300-11.

23. Reiman, E.M., et al., *Functional brain abnormalities in young adults at genetic risk for late-onset Alzheimer's dementia.* Proc Natl Acad Sci U S A, 2004. **101**(1): p. 284-9.

24. Hauptmann, S., et al., *Mitochondrial dysfunction: an early event in Alzheimer pathology accumulates with age in AD transgenic mice.* Neurobiol Aging, 2009. **30**(10): p. 1574-86.

25. Chan, E.S., et al., *ApoE4 expression accelerates hippocampus-dependent cognitive deficits by enhancing Abeta impairment of insulin signaling in an Alzheimer's disease mouse model.* Sci Rep, 2016. **6**: p. 26119.

26. Chan, E.S., et al., *Differential interaction of Apolipoprotein-E isoforms with insulin receptors modulates brain insulin signaling in mutant human amyloid precursor protein transgenic mice.* Sci Rep, 2015. **5**: p. 13842.

27. Johnson, L.A., et al., *Apolipoprotein E4 and Insulin Resistance Interact to Impair Cognition and Alter the Epigenome and Metabolome.* Sci Rep, 2017. **7**: p. 43701.

28. Tai, L.M., et al., *Introducing Human APOE into Abeta Transgenic Mouse Models.* Int J Alzheimers Dis, 2011. **2011**: p. 810981.

29. Youmans, K.L., et al., *APOE4-specific changes in Abeta accumulation in a new transgenic mouse model of Alzheimer disease.* J Biol Chem, 2012. **287**(50): p. 41774-86.

30. Oakley, H., et al., *Intraneuronal beta-amyloid aggregates, neurodegeneration, and neuron loss in transgenic mice with five familial Alzheimer's disease mutations: potential factors in amyloid plaque formation.* J Neurosci, 2006. **26**(40): p. 10129-40.

31. Bales, K.R., et al., *Human APOE isoform-dependent effects on brain beta-amyloid levels in PDAPP transgenic mice.* J Neurosci, 2009. **29**(21): p. 6771-9.

32.   Rodriguez, G.A., et al., *Human APOE4 increases microglia reactivity at Abeta plaques in a mouse model of Abeta deposition.* J Neuroinflammation, 2014. **11**: p. 111.

33.   Liu, D.S., et al., *APOE4 enhances age-dependent decline in cognitive function by down-regulating an NMDA receptor pathway in EFAD-Tg mice.* Mol Neurodegener, 2015. **10**: p. 7.

34.   Cacciottolo, M., et al., *The APOE4 allele shows opposite sex bias in microbleeds and Alzheimer's disease of humans and mice.* Neurobiol Aging, 2016. **37**: p. 47-57.

35.   Zhou, M., et al., *APOE4 Induces Site-Specific Tau Phosphorylation Through Calpain-CDK5 Signaling Pathway in EFAD-Tg Mice.* Curr Alzheimer Res, 2016. **13**(9): p. 1048-55.

36.   Teter, B., et al., *Apolipoprotein E isotype-dependent modulation of microRNA-146a in plasma and brain.* Neuroreport, 2016. **27**(11): p. 791-5.

37.   Thomas, R., et al., *Epidermal growth factor prevents APOE4 and amyloid-beta-induced cognitive and cerebrovascular deficits in female mice.* Acta Neuropathol Commun, 2016. **4**(1): p. 111.

38.   Abdullah, L., et al., *APOE epsilon4 specific imbalance of arachidonic acid and docosahexaenoic acid in serum phospholipids identifies individuals with preclinical Mild Cognitive Impairment/Alzheimer's Disease.* Aging (Albany NY), 2017.

39.   Oria, R.B., et al., *Role of apolipoprotein E4 in protecting children against early childhood diarrhea outcomes and implications for later development.* Med Hypotheses, 2007. **68**(5): p. 1099-107.

40.   Puig, K.L., et al., *Overexpression of mutant amyloid-beta protein precursor and presenilin 1 modulates enteric nervous system.* J Alzheimers Dis, 2015. **44**(4): p. 1263-78.

41.   Harach, T., et al., *Reduction of Abeta amyloid pathology in APPPS1 transgenic mice in the absence of gut microbiota.* Sci Rep, 2017. **7**: p. 41802.

42.	Jandhyala, S.M., et al., *Role of the normal gut microbiota.* World J Gastroenterol, 2015. **21**(29): p. 8787-803.

43.	Cani, P.D., et al., *Involvement of gut microbiota in the development of low-grade inflammation and type 2 diabetes associated with obesity.* Gut Microbes, 2012. **3**(4): p. 279-88.

44.	Sokol, H., et al., *Low counts of Faecalibacterium prausnitzii in colitis microbiota.* Inflamm Bowel Dis, 2009. **15**(8): p. 1183-9.

45.	Rajilic-Stojanovic, M., et al., *Global and deep molecular analysis of microbiota signatures in fecal samples from patients with irritable bowel syndrome.* Gastroenterology, 2011. **141**(5): p. 1792-801.

46.	Mariat, D., et al., *The Firmicutes/Bacteroidetes ratio of the human microbiota changes with age.* BMC Microbiol, 2009. **9**: p. 123.

47.	Zhao, S., et al., *Akkermansia muciniphila improves metabolic profiles by reducing inflammation in chow diet-fed mice.* J Mol Endocrinol, 2017. **58**(1): p. 1-14.

48.	Jump, R.L., *Clostridium difficile infection in older adults.* Aging health, 2013. **9**(4): p. 403-414.

49.	Turnbaugh, P.J., et al., *An obesity-associated gut microbiome with increased capacity for energy harvest.* Nature, 2006. **444**(7122): p. 1027-31.

50.	Piya, M.K., P.G. McTernan, and S. Kumar, *Adipokine inflammation and insulin resistance: the role of glucose, lipids and endotoxin.* J Endocrinol, 2013. **216**(1): p. T1-T15.

51.	Backhed, F., et al., *The gut microbiota as an environmental factor that regulates fat storage.* Proc Natl Acad Sci U S A, 2004. **101**(44): p. 15718-23.

52.	Abrams, G.D. and J.E. Bishop, *Effect of the normal microbial flora on gastrointestinal motility.* Proc Soc Exp Biol Med, 1967. **126**(1): p. 301-4.

53.   Musso, G., R. Gambino, and M. Cassader, *Interactions between gut microbiota and host metabolism predisposing to obesity and diabetes.* Annu Rev Med, 2011. **62**: p. 361-80.

54.   Vrieze, A., et al., *Transfer of intestinal microbiota from lean donors increases insulin sensitivity in individuals with metabolic syndrome.* Gastroenterology, 2012. **143**(4): p. 913-6 e7.

55.   Neves, A.L., et al., *The microbiome and its pharmacological targets: therapeutic avenues in cardiometabolic diseases.* Curr Opin Pharmacol, 2015. **25**: p. 36-44.

56.   Dumoulin, V., et al., *Peptide YY, glucagon-like peptide-1, and neurotensin responses to luminal factors in the isolated vascularly perfused rat ileum.* Endocrinology, 1998. **139**(9): p. 3780-6.

57.   Ronveaux, C.C., D. Tome, and H.E. Raybould, *Glucagon-like peptide 1 interacts with ghrelin and leptin to regulate glucose metabolism and food intake through vagal afferent neuron signaling.* J Nutr, 2015. **145**(4): p. 672-80.

58.   Manning, S. and R.L. Batterham, *The role of gut hormone peptide YY in energy and glucose homeostasis: twelve years on.* Annu Rev Physiol, 2014. **76**: p. 585-608.

59.   De Silva, A. and S.R. Bloom, *Gut Hormones and Appetite Control: A Focus on PYY and GLP-1 as Therapeutic Targets in Obesity.* Gut Liver, 2012. **6**(1): p. 10-20.

60.   Wahlstrom, A., et al., *Intestinal Crosstalk between Bile Acids and Microbiota and Its Impact on Host Metabolism.* Cell Metab, 2016. **24**(1): p. 41-50.

61.   Joyce, S.A., et al., *Regulation of host weight gain and lipid metabolism by bacterial bile acid modification in the gut.* Proc Natl Acad Sci U S A, 2014. **111**(20): p. 7421-6.

62.   Haeusler, R.A., et al., *Human insulin resistance is associated with increased plasma levels of 12alpha-hydroxylated bile acids.* Diabetes, 2013. **62**(12): p. 4184-91.

63.   Kuipers, F., V.W. Bloks, and A.K. Groen, *Beyond intestinal soap--bile acids in metabolic control.* Nat Rev Endocrinol, 2014. **10**(8): p. 488-98.

64.   Sinal, C.J., et al., *Targeted disruption of the nuclear receptor FXR/BAR impairs bile acid and lipid homeostasis.* Cell, 2000. **102**(6): p. 731-44.

65.   Parseus, A., et al., *Microbiota-induced obesity requires farnesoid X receptor.* Gut, 2017. **66**(3): p. 429-437.

66.   Fang, S., et al., *Intestinal FXR agonism promotes adipose tissue browning and reduces obesity and insulin resistance.* Nat Med, 2015. **21**(2): p. 159-65.

67.   Inagaki, T., et al., *Regulation of antibacterial defense in the small intestine by the nuclear bile acid receptor.* Proc Natl Acad Sci U S A, 2006. **103**(10): p. 3920-5.

68.   Smith, P.M., et al., *The microbial metabolites, short-chain fatty acids, regulate colonic Treg cell homeostasis.* Science, 2013. **341**(6145): p. 569-73.

69.   Park, J., et al., *Short-chain fatty acids induce both effector and regulatory T cells by suppression of histone deacetylases and regulation of the mTOR-S6K pathway.* Mucosal Immunol, 2015. **8**(1): p. 80-93.

70.   Vinolo, M.A., et al., *SCFAs induce mouse neutrophil chemotaxis through the GPR43 receptor.* PLoS One, 2011. **6**(6): p. e21205.

71.   Nastasi, C., et al., *The effect of short-chain fatty acids on human monocyte-derived dendritic cells.* Sci Rep, 2015. **5**: p. 16148.

72.   Braniste, V., et al., *The gut microbiota influences blood-brain barrier permeability in mice.* Sci Transl Med, 2014. **6**(263): p. 263ra158.

73.   Erny, D., et al., *Host microbiota constantly control maturation and function of microglia in the CNS.* Nat Neurosci, 2015. **18**(7): p. 965-77.

74.   Venkatesh, M., et al., *Symbiotic bacterial metabolites regulate gastrointestinal barrier function via the xenobiotic sensor PXR and Toll-like receptor 4.* Immunity, 2014. **41**(2): p. 296-310.

75.   Andrade, M.E., et al., *The role of immunomodulators on intestinal barrier homeostasis in experimental models.* Clin Nutr, 2015. **34**(6): p. 1080-7.

76.   Neal, M.D., et al., *Enterocyte TLR4 mediates phagocytosis and translocation of bacteria across the intestinal barrier.* J Immunol, 2006. **176**(5): p. 3070-9.

77.   Ghanim, H., et al., *Increase in plasma endotoxin concentrations and the expression of Toll-like receptors and suppressor of cytokine signaling-3 in mononuclear cells after a high-fat, high-carbohydrate meal: implications for insulin resistance.* Diabetes Care, 2009. **32**(12): p. 2281-7.

78.   Cani, P.D., et al., *Metabolic endotoxemia initiates obesity and insulin resistance.* Diabetes, 2007. **56**(7): p. 1761-72.

79.   Qin, L., et al., *Systemic LPS causes chronic neuroinflammation and progressive neurodegeneration.* Glia, 2007. **55**(5): p. 453-62.

80.   Zhang, L.S. and S.S. Davies, *Microbial metabolism of dietary components to bioactive metabolites: opportunities for new therapeutic interventions.* Genome Med, 2016. **8**(1): p. 46.

81.   Huuskonen, J., et al., *Regulation of microglial inflammatory response by sodium butyrate and short-chain fatty acids.* Br J Pharmacol, 2004. **141**(5): p. 874-80.

82.   Yin, L., G. Laevsky, and C. Giardina, *Butyrate suppression of colonocyte NF-kappa B activation and cellular proteasome activity.* J Biol Chem, 2001. **276**(48): p. 44641-6.

83.   De Vadder, F., et al., *Microbiota-generated metabolites promote metabolic benefits via gut-brain neural circuits.* Cell, 2014. **156**(1-2): p. 84-96.

84.   Perry, R.J., et al., *Acetate mediates a microbiome-brain-beta-cell axis to promote metabolic syndrome.* Nature, 2016. **534**(7606): p. 213-7.

85.	Chyan, Y.J., et al., *Potent neuroprotective properties against the Alzheimer beta-amyloid by an endogenous melatonin-related indole structure, indole-3-propionic acid.* J Biol Chem, 1999. **274**(31): p. 21937-42.

86.	Foster, J.A., L. Rinaman, and J.F. Cryan, *Stress & the gut-brain axis: Regulation by the microbiome.* Neurobiol Stress, 2017. **7**: p. 124-136.

87.	Costedio, M.M., N. Hyman, and G.M. Mawe, *Serotonin and its role in colonic function and in gastrointestinal disorders.* Dis Colon Rectum, 2007. **50**(3): p. 376-88.

88.	Bravo, J.A., et al., *Ingestion of Lactobacillus strain regulates emotional behavior and central GABA receptor expression in a mouse via the vagus nerve.* Proc Natl Acad Sci U S A, 2011. **108**(38): p. 16050-5.

89.	Bercik, P., et al., *The anxiolytic effect of Bifidobacterium longum NCC3001 involves vagal pathways for gut-brain communication.* Neurogastroenterol Motil, 2011. **23**(12): p. 1132-9.

90.	Cani, P.D., A. Everard, and T. Duparc, *Gut microbiota, enteroendocrine functions and metabolism.* Curr Opin Pharmacol, 2013. **13**(6): p. 935-40.

91.	El Aidy, S., T.G. Dinan, and J.F. Cryan, *Immune modulation of the brain-gut-microbe axis.* Front Microbiol, 2014. **5**: p. 146.

92.	Bilbo, S.D. and J.M. Schwarz, *The immune system and developmental programming of brain and behavior.* Front Neuroendocrinol, 2012. **33**(3): p. 267-86.

93.	Macpherson, A.J. and T. Uhr, *Gut flora--mechanisms of regulation.* Eur J Surg Suppl, 2002(587): p. 53-7.

94.	Lowry, C.A., et al., *Identification of an immune-responsive mesolimbocortical serotonergic system: potential role in regulation of emotional behavior.* Neuroscience, 2007. **146**(2): p. 756-72.

95.   Bindels, L.B., et al., *Non Digestible Oligosaccharides Modulate the Gut Microbiota to Control the Development of Leukemia and Associated Cachexia in Mice.* PLoS One, 2015. **10**(6): p. e0131009.

96.   Slavin, J., *Fiber and prebiotics: mechanisms and health benefits.* Nutrients, 2013. **5**(4): p. 1417-35.

97.   Pandey, K.R., S.R. Naik, and B.V. Vakil, *Probiotics, prebiotics and synbiotics- a review.* J Food Sci Technol, 2015. **52**(12): p. 7577-87.

98.   O'Bryant, S.E., et al., *Brain-derived neurotrophic factor levels in Alzheimer's disease.* J Alzheimers Dis, 2009. **17**(2): p. 337-41.

99.   Savignac, H.M., et al., *Prebiotic feeding elevates central brain derived neurotrophic factor, N-methyl-D-aspartate receptor subunits and D-serine.* Neurochem Int, 2013. **63**(8): p. 756-64.

100.   Schmidt, K., et al., *Prebiotic intake reduces the waking cortisol response and alters emotional bias in healthy volunteers.* Psychopharmacology (Berl), 2015. **232**(10): p. 1793-801.

101.   Kelly, G., *Inulin-type prebiotics--a review: part 1.* Altern Med Rev, 2008. **13**(4): p. 315-29.

102.   van Loo, J., et al., *On the presence of inulin and oligofructose as natural ingredients in the western diet.* Crit Rev Food Sci Nutr, 1995. **35**(6): p. 525-52.

103.   Kelly, G., *Inulin-type prebiotics: a review. (Part 2).* Altern Med Rev, 2009. **14**(1): p. 36-55.

104.   Riviere, A., et al., *Bifidobacteria and Butyrate-Producing Colon Bacteria: Importance and Strategies for Their Stimulation in the Human Gut.* Front Microbiol, 2016. **7**: p. 979.

105.   Vandeputte, D., et al., *Prebiotic inulin-type fructans induce specific changes in the human gut microbiota.* Gut, 2017.

106. Kleessen, B., et al., *Effects of inulin and lactose on fecal microflora, microbial activity, and bowel habit in elderly constipated persons.* Am J Clin Nutr, 1997. **65**(5): p. 1397-402.

107. Balcazar-Munoz, B.R., E. Martinez-Abundis, and M. Gonzalez-Ortiz, *[Effect of oral inulin administration on lipid profile and insulin sensitivity in subjects with obesity and dyslipidemia].* Rev Med Chil, 2003. **131**(6): p. 597-604.

108. Rivera-Huerta, M., et al., *Functional Effects of Prebiotic Fructans in Colon Cancer and Calcium Metabolism in Animal Models.* Biomed Res Int, 2017. **2017**: p. 9758982.

109. Parnell, J.A. and R.A. Reimer, *Effect of prebiotic fibre supplementation on hepatic gene expression and serum lipids: a dose-response study in JCR:LA-cp rats.* Br J Nutr, 2010. **103**(11): p. 1577-84.

110. Hess, M.W., et al., *Dietary Inulin Fibers Prevent Proton-Pump Inhibitor (PPI)-Induced Hypocalcemia in Mice.* PLoS One, 2015. **10**(9): p. e0138881.

111. Coudray, C., et al., *Effect of soluble or partly soluble dietary fibres supplementation on absorption and balance of calcium, magnesium, iron and zinc in healthy young men.* Eur J Clin Nutr, 1997. **51**(6): p. 375-80.

112. Weitkunat, K., et al., *Effects of dietary inulin on bacterial growth, short-chain fatty acid production and hepatic lipid metabolism in gnotobiotic mice.* J Nutr Biochem, 2015. **26**(9): p. 929-37.

113. Laukens, D., et al., *Heterogeneity of the gut microbiome in mice: guidelines for optimizing experimental design.* FEMS Microbiol Rev, 2016. **40**(1): p. 117-32.

114. Walters, W., et al., *Improved Bacterial 16S rRNA Gene (V4 and V4-5) and Fungal Internal Transcribed Spacer Marker Gene Primers for Microbial Community Surveys.* mSystems, 2016. **1**(1).

115. Bybee, S.M., et al., *Targeted amplicon sequencing (TAS): a scalable next-gen approach to multilocus, multitaxa phylogenetics.* Genome Biol Evol, 2011. **3**: p. 1312-23.

116. Green, S.J., R. Venkatramanan, and A. Naqib, *Deconstructing the polymerase chain reaction: understanding and correcting bias associated with primer degeneracies and primer-template mismatches.* PLoS One, 2015. **10**(5): p. e0128122.

117. Zhang, J., et al., *PEAR: a fast and accurate Illumina Paired-End reAd mergeR.* Bioinformatics, 2014. **30**(5): p. 614-20.

118. Caporaso, J.G., et al., *QIIME allows analysis of high-throughput community sequencing data.* Nat Methods, 2010. **7**(5): p. 335-6.

119. Edgar, R.C., *Search and clustering orders of magnitude faster than BLAST.* Bioinformatics, 2010. **26**(19): p. 2460-1.

120. McDonald, D., et al., *An improved Greengenes taxonomy with explicit ranks for ecological and evolutionary analyses of bacteria and archaea.* ISME J, 2012. **6**(3): p. 610-8.

121. R-Core-Team, *R: A language and environment for statistical computing.* 2015.

122. Oksanen, J., F.G. Blanchet, and F.e.a. Friendly *Vegan: Community ecology package.* 2016.

123. Hadley, W., *Ggplot2.* 2016, New York, NY: Springer Science+Business Media, LLC. pages cm.

124. Evans, A.M., et al., *Integrated, nontargeted ultrahigh performance liquid chromatography/electrospray ionization tandem mass spectrometry platform for the identification and relative quantification of the small-molecule complement of biological systems.* Anal Chem, 2009. **81**(16): p. 6656-67.

125. Weiner, J., 3rd, et al., *Biomarkers of inflammation, immunosuppression and stress with active disease are revealed by metabolomic profiling of tuberculosis patients.* PLoS One, 2012. **7**(7): p. e40221.

126. Sha, W., et al., *Metabolomic profiling can predict which humans will develop liver dysfunction when deprived of dietary choline.* FASEB J, 2010. **24**(8): p. 2962-75.

127. Ohta, T., et al., *Untargeted metabolomic profiling as an evaluative tool of fenofibrate-induced toxicology in Fischer 344 male rats.* Toxicol Pathol, 2009. **37**(4): p. 521-35.

128. Dehaven, C.D., et al., *Organization of GC/MS and LC/MS metabolomics data into chemical libraries.* J Cheminform, 2010. **2**(1): p. 9.

129. Parikh, I., et al., *Caloric restriction preserves memory and reduces anxiety of aging mice with early enhancement of neurovascular functions.* Aging (Albany NY), 2016. **8**(11): p. 2814-2826.

130. Hong, X., et al., *Evaluation of EPI distortion correction methods for quantitative MRI of the brain at high magnetic field.* Magn Reson Imaging, 2015. **33**(9): p. 1098-105.

131. Alsop, D.C., et al., *Recommended implementation of arterial spin-labeled perfusion MRI for clinical applications: A consensus of the ISMRM perfusion study group and the European consortium for ASL in dementia.* Magn Reson Med, 2014.

132. Buonocore, M.H. and R.J. Maddock, *Magnetic resonance spectroscopy of the brain: a review of physical principles and technical methods.* Rev Neurosci, 2015. **26**(6): p. 609-32.

133. Guo, J., V. Bakshi, and A.L. Lin, *Early Shifts of Brain Metabolism by Caloric Restriction Preserve White Matter Integrity and Long-Term Memory in Aging Mice.* Front Aging Neurosci, 2015. **7**: p. 213.

134. Bachstetter, A.D., et al., *Generation and behavior characterization of CaMKIIbeta knockout mice.* PLoS One, 2014. **9**(8): p. e105191.

135. Prut, L. and C. Belzung, *The open field as a paradigm to measure the effects of drugs on anxiety-like behaviors: a review.* Eur J Pharmacol, 2003. **463**(1-3): p. 3-33.

136. Lin, A.L., et al., *Decreased in vitro mitochondrial function is associated with enhanced brain metabolism, blood flow, and memory in Surf1-deficient mice.* J Cereb Blood Flow Metab, 2013. **33**(10): p. 1605-11.

137. Sood, A., et al., *The effects of JWB1-84-1 on memory-related task performance by amyloid Abeta transgenic mice and by young and aged monkeys.* Neuropharmacology, 2007. **53**(5): p. 588-600.

138. Arendash, G.W., et al., *Progressive, age-related behavioral impairments in transgenic mice carrying both mutant amyloid precursor protein and presenilin-1 transgenes.* Brain Res, 2001. **891**(1-2): p. 42-53.

139. Clemente, J.C., et al., *The impact of the gut microbiota on human health: an integrative view.* Cell, 2012. **148**(6): p. 1258-70.

140. Carabotti, M., et al., *The gut-brain axis: interactions between enteric microbiota, central and enteric nervous systems.* Ann Gastroenterol, 2015. **28**(2): p. 203-209.

141. Foster, J.A. and K.A. McVey Neufeld, *Gut-brain axis: how the microbiome influences anxiety and depression.* Trends Neurosci, 2013. **36**(5): p. 305-12.

142. Jiang, C., et al., *The Gut Microbiota and Alzheimer's Disease.* J Alzheimers Dis, 2017. **58**(1): p. 1-15.

143. Vogt, N.M., et al., *Gut microbiome alterations in Alzheimer's disease.* Sci Rep, 2017. **7**(1): p. 13537.

144. Shen, L., L. Liu, and H.F. Ji, *Alzheimer's Disease Histological and Behavioral Manifestations in Transgenic Mice Correlate with Specific Gut Microbiome State.* J Alzheimers Dis, 2017. **56**(1): p. 385-390.

145. Patrick, P.D., et al., *Limitations in verbal fluency following heavy burdens of early childhood diarrhea in Brazilian shantytown children.* Child Neuropsychol, 2005. **11**(3): p. 233-44.

146. Roberfroid, M., *Prebiotics: the concept revisited.* J Nutr, 2007. **137**(3 Suppl 2): p. 830S-7S.

147. Gibson, G.R., et al., *Dietary modulation of the human colonic microbiota: updating the concept of prebiotics.* Nutr Res Rev, 2004. **17**(2): p. 259-75.

148. Bourassa, M.W., et al., *Butyrate, neuroepigenetics and the gut microbiome: Can a high fiber diet improve brain health?* Neurosci Lett, 2016. **625**: p. 56-63.

149. Michel, L. and A. Prat, *One more role for the gut: microbiota and blood brain barrier.* Ann Transl Med, 2016. **4**(1): p. 15.

150. Yasuda, K., et al., *Cecum is the major degradation site of ingested inulin in young pigs.* J Nutr, 2007. **137**(11): p. 2399-404.

151. Nyman, M., *Fermentation and bulking capacity of indigestible carbohydrates: the case of inulin and oligofructose.* Br J Nutr, 2002. **87 Suppl 2**: p. S163-8.

152. Kuo, S.M., P.M. Merhige, and L.R. Hagey, *The effect of dietary prebiotics and probiotics on body weight, large intestine indices, and fecal bile acid profile in wild type and IL10-/- mice.* PLoS One, 2013. **8**(3): p. e60270.

153. Wang, Y., et al., *Fructo-oligosaccharides enhance the mineral absorption and counteract the adverse effects of phytic acid in mice.* Nutrition, 2010. **26**(3): p. 305-11.

154. den Besten, G., et al., *The role of short-chain fatty acids in the interplay between diet, gut microbiota, and host energy metabolism.* J Lipid Res, 2013. **54**(9): p. 2325-40.

155. Tanaka, K., et al., *A new-generation of Bacillus subtilis cell factory for further elevated scyllo-inositol production.* Microb Cell Fact, 2017. **16**(1): p. 67.

156. Clements, R.S., Jr. and B. Darnell, *Myo-inositol content of common foods: development of a high-myo-inositol diet.* Am J Clin Nutr, 1980. **33**(9): p. 1954-67.

157. Duan, Y., et al., *Multiple univariate data analysis reveals the inulin effects on the high-fat-diet induced metabolic alterations in rat myocardium and testicles in the preobesity state.* J Proteome Res, 2013. **12**(7): p. 3480-95.

158. Michaelis, T., et al., *Identification of Scyllo-inositol in proton NMR spectra of human brain in vivo.* NMR Biomed, 1993. **6**(1): p. 105-9.

159. Fenili, D., et al., *Properties of scyllo-inositol as a therapeutic treatment of AD-like pathology.* J Mol Med (Berl), 2007. **85**(6): p. 603-11.

160. Kaiser, L.G., et al., *Scyllo-inositol in normal aging human brain: 1H magnetic resonance spectroscopy study at 4 Tesla.* NMR Biomed, 2005. **18**(1): p. 51-5.

161. Yamashita, Y., et al., *Detection of orally administered inositol stereoisomers in mouse blood plasma and their effects on translocation of glucose transporter 4 in skeletal muscle cells.* J Agric Food Chem, 2013. **61**(20): p. 4850-4.

162. Viola, A., et al., *High cerebral scyllo-inositol: a new marker of brain metabolism disturbances induced by chronic alcoholism.* MAGMA, 2004. **17**(1): p. 47-61.

163. Griffith, H.R., et al., *Elevated brain scyllo-inositol concentrations in patients with Alzheimer's disease.* NMR Biomed, 2007. **20**(8): p. 709-16.

164. Li, G. and R. Pomes, *Binding mechanism of inositol stereoisomers to monomers and aggregates of Abeta(16-22).* J Phys Chem B, 2013. **117**(22): p. 6603-13.

165. McLaurin, J., et al., *Cyclohexanehexol inhibitors of Abeta aggregation prevent and reverse Alzheimer phenotype in a mouse model.* Nat Med, 2006. **12**(7): p. 801-8.

166. Townsend, M., et al., *Orally available compound prevents deficits in memory caused by the Alzheimer amyloid-beta oligomers.* Ann Neurol, 2006. **60**(6): p. 668-76.

167.	Sun, Y., et al., *Synthesis of scyllo-inositol derivatives and their effects on amyloid beta peptide aggregation.* Bioorg Med Chem, 2008. **16**(15): p. 7177-84.

168.	Li, G., et al., *Binding of inositol stereoisomers to model amyloidogenic peptides.* J Phys Chem B, 2012. **116**(3): p. 1111-9.

169.	Salloway, S., et al., *A phase 2 randomized trial of ELND005, scyllo-inositol, in mild to moderate Alzheimer disease.* Neurology, 2011. **77**(13): p. 1253-62.

170.	Larsen, O.F.A. and E. Claassen, *The mechanistic link between health and gut microbiota diversity.* Sci Rep, 2018. **8**(1): p. 2183.

171.	Hoffman, J.D., et al., *Age Drives Distortion of Brain Metabolic, Vascular and Cognitive Functions, and the Gut Microbiome.* Front Aging Neurosci, 2017. **9**: p. 298.

172.	Uronis, J.M., et al., *Gut microbial diversity is reduced by the probiotic VSL#3 and correlates with decreased TNBS-induced colitis.* Inflamm Bowel Dis, 2011. **17**(1): p. 289-97.

173.	Zhang, Q., et al., *Inulin-type fructan improves diabetic phenotype and gut microbiota profiles in rats.* PeerJ, 2018. **6**: p. e4446.

174.	Sarkar, A. and S. Mandal, *Bifidobacteria-Insight into clinical outcomes and mechanisms of its probiotic action.* Microbiol Res, 2016. **192**: p. 159-71.

175.	Kovatcheva-Datchary, P., et al., *Dietary Fiber-Induced Improvement in Glucose Metabolism Is Associated with Increased Abundance of Prevotella.* Cell Metab, 2015. **22**(6): p. 971-82.

176.	Wexler, H.M., *Bacteroides: the good, the bad, and the nitty-gritty.* Clin Microbiol Rev, 2007. **20**(4): p. 593-621.

177.	Zhou, P., et al., *Microbial Mechanistic Insight into the Role of Inulin in Improving Maternal Health in a Pregnant Sow Model.* Front Microbiol, 2017. **8**: p. 2242.

178. Turnbaugh, P.J., et al., *A core gut microbiome in obese and lean twins.* Nature, 2009. **457**(7228): p. 480-4.

179. Cani, P.D. and W.M. de Vos, *Next-Generation Beneficial Microbes: The Case of Akkermansia muciniphila.* Front Microbiol, 2017. **8**: p. 1765.

180. Carlson, J.L., et al., *Prebiotic Dietary Fiber and Gut Health: Comparing the in Vitro Fermentations of Beta-Glucan, Inulin and Xylooligosaccharide.* Nutrients, 2017. **9**(12).

181. Wolever, T.M. and J.L. Chiasson, *Acarbose raises serum butyrate in human subjects with impaired glucose tolerance.* Br J Nutr, 2000. **84**(1): p. 57-61.

182. Shokryazdan, P., et al., *Effects of prebiotics on immune system and cytokine expression.* Med Microbiol Immunol, 2017. **206**(1): p. 1-9.

183. Correa-Oliveira, R., et al., *Regulation of immune cell function by short-chain fatty acids.* Clin Transl Immunology, 2016. **5**(4): p. e73.

184. Sherry, C.L., et al., *Sickness behavior induced by endotoxin can be mitigated by the dietary soluble fiber, pectin, through up-regulation of IL-4 and Th2 polarization.* Brain Behav Immun, 2010. **24**(4): p. 631-40.

185. Khan, N.A., et al., *Dietary fiber is positively associated with cognitive control among prepubertal children.* J Nutr, 2015. **145**(1): p. 143-9.

186. Kennedy, P.J., et al., *Kynurenine pathway metabolism and the microbiota-gut-brain axis.* Neuropharmacology, 2017. **112**(Pt B): p. 399-412.

187. Hwang, I.K., et al., *Indole-3-propionic acid attenuates neuronal damage and oxidative stress in the ischemic hippocampus.* J Neurosci Res, 2009. **87**(9): p. 2126-37.

188. Perkins, M., et al., *Altered Energy Metabolism Pathways in the Posterior Cingulate in Young Adult Apolipoprotein E varepsilon4 Carriers.* J Alzheimers Dis, 2016. **53**(1): p. 95-106.

189. Reiman, E.M. and W.J. Jagust, *Brain imaging in the study of Alzheimer's disease.* Neuroimage, 2012. **61**(2): p. 505-16.

190. Swerdlow, R.H., J.M. Burns, and S.M. Khan, *The Alzheimer's disease mitochondrial cascade hypothesis: progress and perspectives.* Biochim Biophys Acta, 2014. **1842**(8): p. 1219-31.

191. Wolf, A.B., et al., *Apolipoprotein E as a beta-amyloid-independent factor in Alzheimer's disease.* Alzheimers Res Ther, 2013. **5**(5): p. 38.

192. Maruszak, A. and S. Thuret, *Why looking at the whole hippocampus is not enough-a critical role for anteroposterior axis, subfield and activation analyses to enhance predictive value of hippocampal changes for Alzheimer's disease diagnosis.* Front Cell Neurosci, 2014. **8**: p. 95.

193. O'Mahony, S.M., et al., *Serotonin, tryptophan metabolism and the brain-gut-microbiome axis.* Behav Brain Res, 2015. **277**: p. 32-48.

194. Agus, A., J. Planchais, and H. Sokol, *Gut Microbiota Regulation of Tryptophan Metabolism in Health and Disease.* Cell Host Microbe, 2018. **23**(6): p. 716-724.

195. He, B., et al., *Transmissible microbial and metabolomic remodeling by soluble dietary fiber improves metabolic homeostasis.* Sci Rep, 2015. **5**: p. 10604.

196. Nicholson, J.K., et al., *Host-gut microbiota metabolic interactions.* Science, 2012. **336**(6086): p. 1262-7.

197. Mardinoglu, A., et al., *The gut microbiota modulates host amino acid and glutathione metabolism in mice.* Mol Syst Biol, 2015. **11**(10): p. 834.

198. Voevodskaya, O., et al., *Myo-inositol changes precede amyloid pathology and relate to APOE genotype in Alzheimer disease.* Neurology, 2016. **86**(19): p. 1754-61.

199. Rafii, M.S., et al., *A Randomized, Double-Blind, Placebo-Controlled, Phase II Study of Oral ELND005 (scyllo-Inositol) in Young Adults with*

Down Syndrome without Dementia. J Alzheimers Dis, 2017. **58**(2): p. 401-411.

200.	Wang, Z., et al., *Advanced glycation end-product Nepsilon-carboxymethyl-Lysine accelerates progression of atherosclerotic calcification in diabetes.* Atherosclerosis, 2012. **221**(2): p. 387-96.

201.	Gold, C.A. and A.E. Budson, *Memory loss in Alzheimer's disease: implications for development of therapeutics.* Expert Rev Neurother, 2008. **8**(12): p. 1879-91.

202.	Mazza, M., et al., *Primary cerebral blood flow deficiency and Alzheimer's disease: shadows and lights.* J Alzheimers Dis, 2011. **23**(3): p. 375-89.

203.	Wang, J., et al., *A systemic view of Alzheimer disease - insights from amyloid-beta metabolism beyond the brain.* Nat Rev Neurol, 2017. **13**(11): p. 703.

204.	Hashimoto, T., et al., *Apolipoprotein E, especially apolipoprotein E4, increases the oligomerization of amyloid beta peptide.* J Neurosci, 2012. **32**(43): p. 15181-92.

205.	Liu, C.C., et al., *ApoE4 Accelerates Early Seeding of Amyloid Pathology.* Neuron, 2017. **96**(5): p. 1024-1032 e3.

206.	Ophir, G., et al., *Apolipoprotein E4 enhances brain inflammation by modulation of the NF-kappaB signaling cascade.* Neurobiol Dis, 2005. **20**(3): p. 709-18.

207.	Meraz-Rios, M.A., et al., *Inflammatory process in Alzheimer's Disease.* Front Integr Neurosci, 2013. **7**: p. 59.

208.	Haghikia, A., et al., *Dietary Fatty Acids Directly Impact Central Nervous System Autoimmunity via the Small Intestine.* Immunity, 2016. **44**(4): p. 951-3.

209.	Arpaia, N., et al., *Metabolites produced by commensal bacteria promote peripheral regulatory T-cell generation.* Nature, 2013. **504**(7480): p. 451-5.

210. Adcock, I.M., *HDAC inhibitors as anti-inflammatory agents.* Br J Pharmacol, 2007. **150**(7): p. 829-31.

211. Govindarajan, N., et al., *Sodium butyrate improves memory function in an Alzheimer's disease mouse model when administered at an advanced stage of disease progression.* J Alzheimers Dis, 2011. **26**(1): p. 187-97.

212. Melamed, E., et al., *Reduction in regional cerebral blood flow during normal aging in man.* Stroke, 1980. **11**(1): p. 31-5.

213. Kisler, K., et al., *Cerebral blood flow regulation and neurovascular dysfunction in Alzheimer disease.* Nat Rev Neurosci, 2017. **18**(7): p. 419-434.

214. Lopez-Gonzalez, I., et al., *Neuroinflammatory signals in Alzheimer disease and APP/PS1 transgenic mice: correlations with plaques, tangles, and oligomeric species.* J Neuropathol Exp Neurol, 2015. **74**(4): p. 319-44.

215. Zhu, M., et al., *Age-related brain expression and regulation of the chemokine CCL4/MIP-1beta in APP/PS1 double-transgenic mice.* J Neuropathol Exp Neurol, 2014. **73**(4): p. 362-74.

216. Caberlotto, L., et al., *Integration of transcriptomic and genomic data suggests candidate mechanisms for APOE4-mediated pathogenic action in Alzheimer's disease.* Sci Rep, 2016. **6**: p. 32583.

217. Gonzalez-Pena, D., et al., *Microglia Transcriptome Changes in a Model of Depressive Behavior after Immune Challenge.* PLoS One, 2016. **11**(3): p. e0150858.

218. Fuller, J.P., J.B. Stavenhagen, and J.L. Teeling, *New roles for Fc receptors in neurodegeneration-the impact on Immunotherapy for Alzheimer's Disease.* Front Neurosci, 2014. **8**: p. 235.

219. Krauthausen, M., et al., *CXCR3 promotes plaque formation and behavioral deficits in an Alzheimer's disease model.* J Clin Invest, 2015. **125**(1): p. 365-78.

220. Xia, M.Q., et al., *Expression of the chemokine receptor CXCR3 on neurons and the elevated expression of its ligand IP-10 in reactive astrocytes: in vitro ERK1/2 activation and role in Alzheimer's disease.* J Neuroimmunol, 2000. **108**(1-2): p. 227-35.

221. Galimberti, D., et al., *Intrathecal chemokine synthesis in mild cognitive impairment and Alzheimer disease.* Arch Neurol, 2006. **63**(4): p. 538-43.

222. Hansen, D.V., J.E. Hanson, and M. Sheng, *Microglia in Alzheimer's disease.* J Cell Biol, 2018. **217**(2): p. 459-472.

223. Keren-Shaul, H., et al., *A Unique Microglia Type Associated with Restricting Development of Alzheimer's Disease.* Cell, 2017. **169**(7): p. 1276-1290 e17.

224. Wyss-Coray, T. and J. Rogers, *Inflammation in Alzheimer disease-a brief review of the basic science and clinical literature.* Cold Spring Harb Perspect Med, 2012. **2**(1): p. a006346.

225. Ferretti, L., et al., *Anxiety and Alzheimer's disease.* J Geriatr Psychiatry Neurol, 2001. **14**(1): p. 52-8.

226. Guerrant, R.L., et al., *Malnutrition as an enteric infectious disease with long-term effects on child development.* Nutr Rev, 2008. **66**(9): p. 487-505.

227. Alexander, D.M., et al., *The contribution of apolipoprotein E alleles on cognitive performance and dynamic neural activity over six decades.* Biol Psychol, 2007. **75**(3): p. 229-38.

228. Mosconi, L., A. Pupi, and M.J. De Leon, *Brain glucose hypometabolism and oxidative stress in preclinical Alzheimer's disease.* Ann N Y Acad Sci, 2008. **1147**: p. 180-95.

229. LaFerla, F.M. and K.N. Green, *Animal models of Alzheimer disease.* Cold Spring Harb Perspect Med, 2012. **2**(11).

230. Rintala, A., et al., *Gut Microbiota Analysis Results Are Highly Dependent on the 16S rRNA Gene Target Region, Whereas the Impact of DNA Extraction Is Minor.* J Biomol Tech, 2017. **28**(1): p. 19-30.

231. Ericsson, A.C. and C.L. Franklin, *Manipulating the Gut Microbiota: Methods and Challenges.* ILAR J, 2015. **56**(2): p. 205-17.

232. Morris, G.P., I.A. Clark, and B. Vissel, *Inconsistencies and controversies surrounding the amyloid hypothesis of Alzheimer's disease.* Acta Neuropathol Commun, 2014. **2**: p. 135.

233. Selkoe, D.J., *Resolving controversies on the path to Alzheimer's therapeutics.* Nat Med, 2011. **17**(9): p. 1060-5.

234. Kametani, F. and M. Hasegawa, *Reconsideration of Amyloid Hypothesis and Tau Hypothesis in Alzheimer's Disease.* Front Neurosci, 2018. **12**: p. 25.

235. Reitz, C., C. Brayne, and R. Mayeux, *Epidemiology of Alzheimer disease.* Nat Rev Neurol, 2011. **7**(3): p. 137-52.

236. Bangen, K.J., et al., *APOE genotype modifies the relationship between midlife vascular risk factors and later cognitive decline.* J Stroke Cerebrovasc Dis, 2013. **22**(8): p. 1361-9.

237. Zlokovic, B.V., *Neurovascular pathways to neurodegeneration in Alzheimer's disease and other disorders.* Nat Rev Neurosci, 2011. **12**(12): p. 723-38.

238. Wallace, D.C., *Bioenergetic origins of complexity and disease.* Cold Spring Harb Symp Quant Biol, 2011. **76**: p. 1-16.

239. Petit-Taboue, M.C., et al., *Effects of healthy aging on the regional cerebral metabolic rate of glucose assessed with statistical parametric mapping.* Neuroimage, 1998. **7**(3): p. 176-84.

240. Ivanisevic, J., et al., *Metabolic drift in the aging brain.* Aging (Albany NY), 2016. **8**(5): p. 1000-20.

241. Everson-Rose, S.A. and J.P. Ryan, *Diabetes, Obesity, and the Brain: New Developments in Biobehavioral Medicine.* Psychosom Med, 2015. **77**(6): p. 612-5.

242. O'Neill, L.A., R.J. Kishton, and J. Rathmell, *A guide to immunometabolism for immunologists.* Nat Rev Immunol, 2016. **16**(9): p. 553-65.

243. Ron-Harel, N., et al., *Mitochondrial Biogenesis and Proteome Remodeling Promote One-Carbon Metabolism for T Cell Activation.* Cell Metab, 2016. **24**(1): p. 104-17.

244. Lynch, A.M., et al., *The impact of glial activation in the aging brain.* Aging Dis, 2010. **1**(3): p. 262-78.

245. Boumezbeur, F., et al., *Altered brain mitochondrial metabolism in healthy aging as assessed by in vivo magnetic resonance spectroscopy.* J Cereb Blood Flow Metab, 2010. **30**(1): p. 211-21.

246. Wong, M.L., et al., *Inducible nitric oxide synthase gene expression in the brain during systemic inflammation.* Nat Med, 1996. **2**(5): p. 581-4.

247. Kau, A.L., et al., *Human nutrition, the gut microbiome and the immune system.* Nature, 2011. **474**(7351): p. 327-36.

248. Verbeke, K.A., L. Boesmans, and E. Boets, *Modulating the microbiota in inflammatory bowel diseases: prebiotics, probiotics or faecal transplantation?* Proc Nutr Soc, 2014. **73**(4): p. 490-7.

249. Biagi, E., et al., *Through ageing, and beyond: gut microbiota and inflammatory status in seniors and centenarians.* PLoS One, 2010. **5**(5): p. e10667.

250. Claesson, M.J., et al., *Composition, variability, and temporal stability of the intestinal microbiota of the elderly.* Proc Natl Acad Sci U S A, 2011. **108 Suppl 1**: p. 4586-91.

251. Langille, M.G., et al., *Microbial shifts in the aging mouse gut.* Microbiome, 2014. **2**(1): p. 50.

252. Verdam, F.J., et al., *Human intestinal microbiota composition is associated with local and systemic inflammation in obesity.* Obesity (Silver Spring), 2013. **21**(12): p. E607-15.

253. Al-Asmakh, M. and L. Hedin, *Microbiota and the control of blood-tissue barriers.* Tissue Barriers, 2015. **3**(3): p. e1039691.

254. Dinan, T.G. and J.F. Cryan, *Melancholic microbes: a link between gut microbiota and depression?* Neurogastroenterol Motil, 2013. **25**(9): p. 713-9.

255. Foster, J.A., *Gut Microbiome and Behavior: Focus on Neuroimmune Interactions.* Int Rev Neurobiol, 2016. **131**: p. 49-65.

256. Sharon, G., et al., *The Central Nervous System and the Gut Microbiome.* Cell, 2016. **167**(4): p. 915-932.

257. Erickson, M.A. and W.A. Banks, *Blood-brain barrier dysfunction as a cause and consequence of Alzheimer's disease.* J Cereb Blood Flow Metab, 2013. **33**(10): p. 1500-13.

258. Ebmeier, K.P., et al., *Cerebral perfusion correlates of depressed mood.* Br J Psychiatry, 1997. **170**: p. 77-81.

259. Gur, R.C., et al., *The effect of anxiety on cortical cerebral blood flow and metabolism.* J Cereb Blood Flow Metab, 1987. **7**(2): p. 173-7.

260. Park, J. and B. Moghaddam, *Impact of anxiety on prefrontal cortex encoding of cognitive flexibility.* Neuroscience, 2016.

261. Hartz, A.M., D.S. Miller, and B. Bauer, *Restoring blood-brain barrier P-glycoprotein reduces brain amyloid-beta in a mouse model of Alzheimer's disease.* Mol Pharmacol, 2010. **77**(5): p. 715-23.

262. Hartz, A.M., et al., *Abeta40 Reduces P-Glycoprotein at the Blood-Brain Barrier through the Ubiquitin-Proteasome Pathway.* J Neurosci, 2016. **36**(6): p. 1930-41.

263. Hartz, A.M., et al., *Amyloid-beta contributes to blood-brain barrier leakage in transgenic human amyloid precursor protein mice and in humans with cerebral amyloid angiopathy.* Stroke, 2012. **43**(2): p. 514-23.

264. Miller, D.S., B. Bauer, and A.M. Hartz, *Modulation of P-glycoprotein at the blood-brain barrier: opportunities to improve central nervous system pharmacotherapy.* Pharmacol Rev, 2008. **60**(2): p. 196-209.

265. Pamplona, R. and G. Barja, *Mitochondrial oxidative stress, aging and caloric restriction: the protein and methionine connection.* Biochim Biophys Acta, 2006. **1757**(5-6): p. 496-508.

266. Lutjohann, D., et al., *Plasma 24S-hydroxycholesterol (cerebrosterol) is increased in Alzheimer and vascular demented patients.* J Lipid Res, 2000. **41**(2): p. 195-8.

267. Astarita, G., et al., *Elevated stearoyl-CoA desaturase in brains of patients with Alzheimer's disease.* PLoS One, 2011. **6**(10): p. e24777.

268. Wissmann, P., et al., *Immune activation in patients with Alzheimer's disease is associated with high serum phenylalanine concentrations.* J Neurol Sci, 2013. **329**(1-2): p. 29-33.

269. Morrison, L.D. and S.J. Kish, *Brain polyamine levels are altered in Alzheimer's disease.* Neurosci Lett, 1995. **197**(1): p. 5-8.

270. Garcia-Calatayud, S., et al., *Brain docosahexaenoic acid status and learning in young rats submitted to dietary long-chain polyunsaturated fatty acid deficiency and supplementation limited to lactation.* Pediatr Res, 2005. **57**(5 Pt 1): p. 719-23.

271. Gallant, M., et al., *Focally elevated creatine detected in amyloid precursor protein (APP) transgenic mice and Alzheimer disease brain tissue.* J Biol Chem, 2006. **281**(1): p. 5-8.

272. Geddes, J.W., et al., *Elevated phosphocholine and phosphatidylcholine following rat entorhinal cortex lesions.* Neurobiol Aging, 1997. **18**(3): p. 305-8.

273. Alvarez, X.A., et al., *Double-blind placebo-controlled study with citicoline in APOE genotyped Alzheimer's disease patients. Effects on cognitive performance, brain bioelectrical activity and cerebral perfusion.* Methods Find Exp Clin Pharmacol, 1999. **21**(9): p. 633-44.

274. Zgoda-Pols, J.R., et al., *Metabolomics analysis reveals elevation of 3-indoxyl sulfate in plasma and brain during chemically-induced acute kidney injury in mice: investigation of nicotinic acid receptor agonists.* Toxicol Appl Pharmacol, 2011. **255**(1): p. 48-56.

275. Weber, D., et al., *Low urinary indoxyl sulfate levels early after transplantation reflect a disrupted microbiome and are associated with poor outcome.* Blood, 2015. **126**(14): p. 1723-8.

276. Keegan, M.R., et al., *Tryptophan Metabolism and Its Relationship with Depression and Cognitive Impairment Among HIV-infected Individuals.* Int J Tryptophan Res, 2016. **9**: p. 79-88.

277. Palermo, L., et al., *Cognitive outcomes in early-treated adults with phenylketonuria (PKU): A comprehensive picture across domains.* Neuropsychology, 2017. **31**(3): p. 255-267.

278. Curi, R., et al., *A past and present overview of macrophage metabolism and functional outcomes.* Clin Sci (Lond), 2017. **131**(12): p. 1329-1342.

279. Jaeschke, H., *Reactive oxygen and mechanisms of inflammatory liver injury: Present concepts.* J Gastroenterol Hepatol, 2011. **26 Suppl 1**: p. 173-9.

280. Schweinberger, B.M. and A.T. Wyse, *Mechanistic basis of hypermethioninemia.* Amino Acids, 2016. **48**(11): p. 2479-2489.

281. Koziel, R., et al., *Methionine restriction slows down senescence in human diploid fibroblasts.* Aging Cell, 2014. **13**(6): p. 1038-48.

282. Brown-Borg, H.M., *Reduced growth hormone signaling and methionine restriction: interventions that improve metabolic health and extend life span.* Ann N Y Acad Sci, 2016. **1363**: p. 40-9.

283. Alzheimer, A., et al., *An English translation of Alzheimer's 1907 paper, "Uber eine eigenartige Erkankung der Hirnrinde".* Clin Anat, 1995. **8**(6): p. 429-31.

284. Hamilton, L.K., et al., *Aberrant Lipid Metabolism in the Forebrain Niche Suppresses Adult Neural Stem Cell Proliferation in an Animal Model of Alzheimer's Disease.* Cell Stem Cell, 2015.

285. Ricciotti, E. and G.A. FitzGerald, *Prostaglandins and inflammation.* Arterioscler Thromb Vasc Biol, 2011. **31**(5): p. 986-1000.

286. Montine, T.J., et al., *Neuronal oxidative damage from activated innate immunity is EP2 receptor-dependent.* J Neurochem, 2002. **83**(2): p. 463-70.

287. Parnetti, L., et al., *Cholinergic precursors in the treatment of cognitive impairment of vascular origin: ineffective approaches or need for re-evaluation?* J Neurol Sci, 2007. **257**(1-2): p. 264-9.

288. Brunet, P., et al., *Protein-bound uremic retention solutes.* Adv Ren Replace Ther, 2003. **10**(4): p. 310-20.

289. Dou, L., et al., *The uremic solute indoxyl sulfate induces oxidative stress in endothelial cells.* J Thromb Haemost, 2007. **5**(6): p. 1302-8.

290. Harris, K., et al., *Is the gut microbiota a new factor contributing to obesity and its metabolic disorders?* J Obes, 2012. **2012**: p. 879151.

291. Walters, W.A., Z. Xu, and R. Knight, *Meta-analyses of human gut microbes associated with obesity and IBD.* FEBS Lett, 2014. **588**(22): p. 4223-33.

292. de la Monte, S.M. and J.R. Wands, *Alzheimer's disease is type 3 diabetes-evidence reviewed.* J Diabetes Sci Technol, 2008. **2**(6): p. 1101-13.

293. Vagelatos, N.T. and G.D. Eslick, *Type 2 diabetes as a risk factor for Alzheimer's disease: the confounders, interactions, and neuropathology associated with this relationship.* Epidemiol Rev, 2013. **35**: p. 152-60.

294. Martinez-del Campo, A., et al., *Characterization and detection of a widely distributed gene cluster that predicts anaerobic choline utilization by human gut bacteria.* MBio, 2015. **6**(2).

295. Bennett, B.J., et al., *Trimethylamine-N-oxide, a metabolite associated with atherosclerosis, exhibits complex genetic and dietary regulation.* Cell Metab, 2013. **17**(1): p. 49-60.

296. Wang, Z., et al., *Gut flora metabolism of phosphatidylcholine promotes cardiovascular disease.* Nature, 2011. **472**(7341): p. 57-63.

297. Wang, Z., et al., *Prognostic value of choline and betaine depends on intestinal microbiota-generated metabolite trimethylamine-N-oxide.* Eur Heart J, 2014. **35**(14): p. 904-10.

298. Cirrito, J.R., et al., *P-glycoprotein deficiency at the blood-brain barrier increases amyloid-beta deposition in an Alzheimer disease mouse model.* J Clin Invest, 2005. **115**(11): p. 3285-90.

299. Birdsill, A.C., et al., *Low cerebral blood flow is associated with lower memory function in metabolic syndrome.* Obesity (Silver Spring), 2013. **21**(7): p. 1313-20.

300. Schnorr, S.L. and H.A. Bachner, *Integrative Therapies in Anxiety Treatment with Special Emphasis on the Gut Microbiome.* Yale J Biol Med, 2016. **89**(3): p. 397-422.

301. Goehler, L.E., et al., *Campylobacter jejuni infection increases anxiety-like behavior in the holeboard: possible anatomical substrates for viscerosensory modulation of exploratory behavior.* Brain Behav Immun, 2008. **22**(3): p. 354-66.

302. Lyte, M., et al., *Induction of anxiety-like behavior in mice during the initial stages of infection with the agent of murine colonic hyperplasia Citrobacter rodentium.* Physiol Behav, 2006. **89**(3): p. 350-7.

303. Lyte, M., J.J. Varcoe, and M.T. Bailey, *Anxiogenic effect of subclinical bacterial infection in mice in the absence of overt immune activation.* Physiol Behav, 1998. **65**(1): p. 63-8.

304. Casey, B.J., et al., *Behavioral and neural correlates of delay of gratification 40 years later: Proc. Natl. Acad. Sci. U.S.A. 2011, Vol 108 No. 36:14998-5003.* Ann Neurosci, 2012. **19**(1): p. 27-8.

305. Sudo, N., et al., *Postnatal microbial colonization programs the hypothalamic-pituitary-adrenal system for stress response in mice.* J Physiol, 2004. **558**(Pt 1): p. 263-75.

306. Rao, A.V., et al., *A randomized, double-blind, placebo-controlled pilot study of a probiotic in emotional symptoms of chronic fatigue syndrome.* Gut Pathog, 2009. **1**(1): p. 6.

307. Hu, X., T. Wang, and F. Jin, *Alzheimer's disease and gut microbiota.* Sci China Life Sci, 2016. **59**(10): p. 1006-1023.

308. Tremlett, H., et al., *The gut microbiome in human neurological disease: A review.* Ann Neurol, 2017. **81**(3): p. 369-382.

309. Fung, T.C., C.A. Olson, and E.Y. Hsiao, *Interactions between the microbiota, immune and nervous systems in health and disease.* Nat Neurosci, 2017. **20**(2): p. 145-155.

310. Hill, J.M., et al., *Pathogenic microbes, the microbiome, and Alzheimer's disease (AD).* Front Aging Neurosci, 2014. **6**: p. 127.

311. Xia, S., et al., *An Update on Inflamm-Aging: Mechanisms, Prevention, and Treatment.* J Immunol Res, 2016. **2016**: p. 8426874.

312. Lin, A.L., et al., *Rapamycin rescues vascular, metabolic and learning deficits in apolipoprotein E4 transgenic mice with pre-symptomatic Alzheimer's disease.* J Cereb Blood Flow Metab, 2017. **37**(1): p. 217-226.

313. Lin, A.L., et al., *Caloric restriction impedes age-related decline of mitochondrial function and neuronal activity.* J Cereb Blood Flow Metab, 2014. **34**(9): p. 1440-3.

314. Lin, A.L., et al., *Caloric restriction increases ketone bodies metabolism and preserves blood flow in aging brain.* Neurobiol Aging, 2015. **36**(7): p. 2296-303.

Vita

Jared David Hoffman

Education

2009-2013   Truman State University, Kirksville, MO
               Bachelor of Science in Biology
2013-2015   The University of North Carolina at Greensboro,
               Greensboro, North Carolina
               Master of Science in Nutrition

Professional Positions Held

2013-2014   Lab Assistant, The University of North Carolina at
               Greensboro
               Mentor: Dr. George Loo, Department of Nutrition
2013-2015   Nutrition Consultant, The Fit Station, Greensboro, North
               Carolina
2013-2015   Assistant Tennis Pro, Sherwood Swim & Racquet Club,
               Greensboro, North Carolina
2014-2015   Lab Assistant, The University of North Carolina at
               Greensboro
               Mentor: Dr. Keith Erikson and Dr. Lenka Shriver, Department
               of Nutrition

Scholastic and Professional Honors

2009   A + Recognition Award
2010-2012   Truman Service Scholarship
2014   Nell Wilborn Thayer and Mildred B. Davis Scholarship, The
               University of North Carolina at Greensboro
2015   NIH LabTV Interview
2015   Graduate School Academic Year Fellowship, University of
               Kentucky
2015   First Place Poster Award, ACN 2015 Conference, Orlando,
               FL
2016   Graduate School Academic Year Fellowship, University of
               Kentucky
2016   AAAS/Science Program for Excellence in Science Free
               Membership Award
2016   Kentucky Opportunity Fellowship Award, University of
               Kentucky
2016-2017   NIH T32 Training Fellowship, University of Kentucky
2017   Travel Bursary Award, BRAIN 2017 Conference
2017   Keystone Symposia (X3) Scholarship Award

| 2018 | Keystone Symposia (X3) Invited Oral Presenter |

Publications

2015	**Hoffman JD**, Ward WM, Loo G. Effect of antioxidants on the genotoxicity of phenethyl isothiocyanate. *Mutagenesis* 2015; 30(3): 421-30.
2015	**Hoffman JD**, Ward WM, Loo G. Genotoxic effect of ethacrynic acid and impact of antioxidants. Toxicol Appl Pharmacol 2015; 286(1): 17-26.
2016	Parikh I, Guo J, Chuang K, Zhong Y, Rempe R, **Hoffman JD**, Armstrong R, Bauer B, Hartz AM, Lin AL. Caloric Restriction Preserves Memory and Reduces Anxiety of Aging Mice with Early Enhancement of Neurovascular Functions. *AGING* 2016.
2016	Lin AL, Parikh I, **Hoffman JD**, Ma D. Neuroimaging Biomarkers of Caloric Restriction on Brain Metabolic and Vascular Functions. *Springer* 2017.
2017	**Hoffman JD**, Parikh I, Green SJ, Chlipala G, Mohney RP, Keaton M, Bauer B, Hartz AMS, Lin AL. Age Drives Distortion of Brain Metabolic, Vascular, and Cognitive Functions, and the Gut Microbiome. *Front. Aging Neurosci*. 2017.
2018	Lee J, Yanckello L, Ma D, **Hoffman JD**, Parikh I, Thalman S, Bauer B, Hartz AMS, Hyder F, Lin AL. Neuroimaging Biomarkers of mTOR Inhibition on Vascular and Metabolic Function in Aging Brain and Alzheimer's Disease. *Front. Aging Neurosci*. 2018.

Abstracts

2015	**Hoffman JD**, Lin AL, Zhang W, Gao X, Watts L. Caloric Restriction Increases Ketone Bodies Metabolism and Preserves Blood Flow in Aging. American Society for Nutrition 2015. Orlando, FL. *Won First Place Poster Award*
2015	**Hoffman JD**, Bakshi V, Parikh I, Guo J, Armstrong R, Estus S, Lin AL. Aging Increases Markers of Inflammation and Alters Brain-Gut Interactions: Implications Towards Alzheimer's Disease. Experimental Biology 2016:6340. San Diego, CA.
2016	**Hoffman JD**, Bakshi V, Parikh I, Guo J, Armstrong R, Estus S, Lin AL. Aging Increases Markers of Inflammation and Alters Brain-Gut Interactions: Implications Towards Alzheimer's Disease. Proc. Intl. Soc. Mag. Reson. Med. 2016. Singapore.

2016	**Hoffman JD**, Bakshi V, Parikh I, Guo J, Armstrong R, Estus S, Lin AL. Aging Increases Markers of Inflammation and Alters Brain-Gut Interactions: Implications Towards Alzheimer's Disease. University of Kentucky Center for Clinical and Translational Science (CCTS) Spring Conference. 2016. Lexington, KY.
2016	Wang AC, Ma D, Bakshi V, **Hoffman JD**, Armstrong R, Guo J, Parikh I, Lin AL. A low-carbohydrate ketogenic diet restores brain functions in type 2 diabetes mellitus patients: an assessment of neuroimaging. Experimental Biology 2016:6340. San Diego, CA.
2016	**Hoffman JD**, Bakshi V, Parikh I, Guo J, Armstrong R, Green S, Lin AL. Age Drives the Distortion of Brain Vascular, Metabolic, and Cognitive Functions and the Gut Microbiome. Markesbery Symposium on Aging and Dementia, 2016.
2017	**Hoffman JD**, Bakshi V, Parikh I, Guo J, Armstrong R, Green S, Lin AL. The Effects of Age on the Gut and Brain: Insights into the Gut-Brain Axis. Experimental Biology (EB), 2017.
2017	**Hoffman JD**, Bakshi V, Parikh I, Guo J, Armstrong R, Green S, Lin AL. Age Drives the Distortion of Brain Vascular, Metabolic, and Cognitive Functions and the Gut Microbiome. BRAIN, 2017.
2017	**Hoffman JD,** Parikh I, Hoffman JB, Green S, Lin AL. Prebiotics for the Gut Microbiota as an Intervention for Alzheimer's Disease Prevention in APOE4 Carriers. Markesbery Symposium on Aging and Dementia, 2017.
2017	**Hoffman JD,** Parikh I, Hoffman JB, Green S, Lin AL. Prebiotics for the Gut Microbiota as an Intervention for Alzheimer's Disease Prevention in APOE4 Carriers. Keystone Symposia – Manipulation of the Gut Microbiota for Metabolic Health (X3), 2017.
2017	**Hoffman JD,** Parikh I, Hoffman JB, Green S, Lin AL. Prebiotics for the Gut Microbiota as an Intervention for Alzheimer's Disease Prevention in APOE4 Carriers. American Society of Nutrition (ASN), 2017.
2017	Parikh I, Ma D, **Hoffman JD**, Wang A, Lin AL. Rapamycin treatment increases cerebral blood flow and attenuates anxiety in APOE4. 7th Markesbery Symposium on Aging and Dementia, Lexington, KY 2017.
2018	Parikh I, Ma D, **Hoffman JD**, Wang A, Lin AL. Rapamycin treatment increases cerebral blood flow and attenuates anxiety in pre-symptomatic APOE4 mice: effects of sex and APP transgene. Proc. Intl. Soc. Mag. Reson. Med. 2018.
2018	Parikh I, Ma D, **Hoffman JD**, Wang A, Thalman S, Green SJ, Lin AL. Rapamycin Treatment Increases Cerebral Blood Flow and Gut Microbiome Diversity in EFAD Mice.

	Alzheimer's Association International Conference, Chicago, IL 2018.
2018	**Hoffman JD,** Parikh I, Hoffman JB, Green S, Lin AL. Prebiotics for the Gut Microbiota as an Intervention for Alzheimer's Disease Prevention in APOE4 Carriers. Alzheimer's Association International Conference (AAIC), 2018.
2018	**Hoffman JD**, Rice BB, Tan K, Wise JTF, Police S. Fighting Depression. Health & Wellness Magazine. February 2018.